ESTCP Project 199902 – Tyndall AFB Site Demo:

Data Processing Results for UXO Classification using UWB Full-Polarization GPR System

M. Higgins, C.-C. Chen, and K. O'Neill

March 2001

US Army Corps of Engineers
Research and Development Center (ERDC)
Cold Regions Research
and Engineering Laboratory (CRREL)
72 Lyme Road
Hanover, NH 03755

Report Documentation Page

Form Approved
OMB No. 0704-0188

1. REPORT DATE	2. REPORT TYPE	3. DATES COVERED
MAR 2001		**00-00-2001 to 00-00-2001**

4. TITLE AND SUBTITLE	5a. CONTRACT NUMBER
Data Processing Results for UXO Classification using UWB Full-Polarization GPR System	5b. GRANT NUMBER
	5c. PROGRAM ELEMENT NUMBER
6. AUTHOR(S)	5d. PROJECT NUMBER
	5e. TASK NUMBER
	5f. WORK UNIT NUMBER
7. PERFORMING ORGANIZATION NAME(S) AND ADDRESS(ES) **U.S. Army Engineer Research and Development Center (ERDC),Cold Regions Research and Engineering Laboratory (CRREL),72 Lyme Road,hanover,NH,03755**	8. PERFORMING ORGANIZATION REPORT NUMBER
9. SPONSORING/MONITORING AGENCY NAME(S) AND ADDRESS(ES)	10. SPONSOR/MONITOR'S ACRONYM(S)
	11. SPONSOR/MONITOR'S REPORT NUMBER(S)

12. DISTRIBUTION/AVAILABILITY STATEMENT
Approved for public release; distribution unlimited

13. SUPPLEMENTARY NOTES

14. ABSTRACT

15. SUBJECT TERMS

16. SECURITY CLASSIFICATION OF:			17. LIMITATION OF ABSTRACT	18. NUMBER OF PAGES	19a. NAME OF RESPONSIBLE PERSON
a. REPORT **unclassified**	b. ABSTRACT **unclassified**	c. THIS PAGE **unclassified**	**Same as Report (SAR)**	**98**	

Table of Contents

DATA PROCESSING RESULTS FOR UXO CLASSIFICATION USING UWB FULL-POLARIZATION GPR SYSTEM

List of Figures

List of Tables

List of Symbols

CNR	Complex Natural Resonance
CRREL	Cold Regions Research and Engineering Laboratory
DEN	Density of Estimated Angles
DEP	Depth of Estimated Angles
DR	Detection Rate
ELF	Estimated Linearity Factor
$\mathbf{ELF_t}$	Estimated Linearity Factor from Time Domain Data
$\mathbf{ELF_f}$	Estimated Linearity Factor from Frequency Domain Data
ESL	ElectroScience Laboratory
ETO	Estimated Target Orientation
ETL	Estimated Target Length
FAR	False Alarm Rate
FFT	Fast Fourier Transform
GPR	Ground Penetrating Radar
GPS	Global Positioning System
L/D	Length-to-Diameter Ratio
OSU	Ohio State University
ROC	Receiver Observation Characteristics
SCR	Signal-to-Clutter Ratio
SNR	Signal-to-Noise Ratio
STD	Standard Deviation
TLS-Prony	Total-Least-Square Error Prony Method
UXO	Unexploded Ordnance
UWB	Ultra-Wide Bandwidth
UWBFP	Ultra-Wide Bandwidth Full-Polarization

1 Introduction

UXO characterization is an important and yet challenging task for the reduction of UXO clearance cost due to the large number of false targets that often appear at UXO sites. Only metallic false targets are considered here since non-metallic objects could be easily screened out with advanced magnetic sensors which have been applied effectively in detecting UXO's up to 1~2 meter depth.

Previous attempts from various groups in applying GPR systems for UXO classification were not satisfactory due to excessive clutter resulting either from site characteristics or inadequate antenna designs. The use of surface-based full-polarimetric GPR for UXO characterization was almost non-existent. Most UXO's have elongated bodies that generate strong electromagnetic resonance and unique polarimetric scattering properties compared to most false-alarm targets. Theoretical aspects of using these two signatures for UXO classification have been discussed in the 1999 UXO Forum [1]. Although the resonance concept has been demonstrated to be quite feasible in a previous effort supported by NAVEODTECHDIV [2], the use of the polarization signature has not been demonstrated from field data. Therefore a UXO test site was setup at Tyndall AFB, Florida, in 1999 for this purpose under the support of ESTCP program. This site contains only metallic objects at known locations to simulate a field pre-surveyed by advanced magnetic sensors. Many UXO and non-UXO objects were buried at various depth and orientations. Initial measurements were conducted in January 2000, by the CRREL-OSU team using an ultra-wide bandwidth full-polarization (UWBFP) GPR system developed at OSU.

Electromagnetic complex natural resonances (CNR) are excited on a conducting object when illuminated by a broad bandwidth radar signal. Here "complex" is used in the mathematical sense, indicating a number with real and imaginary parts. This is tantamount to saying that the signal possesses distinct, characteristic oscillatory modes, each of which fades at a characteristic rate. The induced surface currents flowing around the body cause these resonant modes. During the resonance period, electromagnetic fields are radiated by the target. This usually occurs after the initial reflections and thus is referred to as the "late-time" region. The late-time resonance signals can then be picked up by a sensor (or receiving antenna) and processed to infer the target's dimension. A larger target would resonate at lower frequencies since it takes time for the surface currents to flow around the body. For targets with large length-to-diameter ratios like most UXO's, the resonant length (one half of the resonant wavelength) of the fundamental mode is directly related to the nose-to-tail distance along the UXO body surface. Although circumferential (transverse) resonant modes do exist, they are highly damped because their resonant frequencies are usually too high to have any practice importance. Therefore, in the late-time region, the re-radiated fields from the target are mainly polarized in the direction of the UXO's axis. For metallic fragments that do not have elongated bodies, they either don't have strong resonance or they have resonant fields polarized in multiple directions. For small bullets, their resonant frequencies are beyond the operational frequency range and, therefore, are non-resonant. In principle the UXO orientation does not change the resonance signatures (resonant frequency and damping rate) however it will affect the resonance strength. Strongest resonances are excited when the incident radar signals is at normal incidence to the UXO from the side. Also, both resonant frequency and damping rate are functions of the soil electrical properties [3]. An accurate UXO length estimation requires a good estimate of the soil properties. Although a UXO may have different resonant frequencies in different soils, its electric fields are almost always polarized in the direction of the UXO axis.

2 System Description

The OSU/ESL GPR system consists of a step-frequency radar source, an ultra-wideband fully polarimetric (UWBFP) antenna and a portable computer for radar control, data collection and on-site data processing. The UWBFP antenna consists of two linearly polarized horn-fed dipole elements [4] arranged in orthogonal directions. Each element can be operated in the transmitting or receiving mode. If a radar signal is transmitted and received from the same element, "co-polarized" data is obtained. If the signal is transmitted from one antenna element and received on the other, perpendicular elements, the "cross-polarized" data is obtained. By recording amplitude and phase of both co-polarized and cross-polarized data, complete radar information about the target's scattering properties is obtained. Such properties are then used to extract features associated with the target's geometry, depth and orientation. Given the fully polarimetric data from any particular antenna rotation, we can synthesize the response from any other rotation from a weighted combination of responses to the original orientation. Figure 1 and Figure 2 show the sketches of the OSU/ESL UWBFP GPR antenna used for Tyndall AFB UXO site measurements. The four antenna wings are made of tapered resistive films to reduce the antenna ringing. Figure 3 shows the radar equipment including (1) a RF network analyzer for reflection and transmission measurement form 10 MHz to 810 MHz at 20 MHz step (2) a laptop computer for measurement control, data storage and data processing.

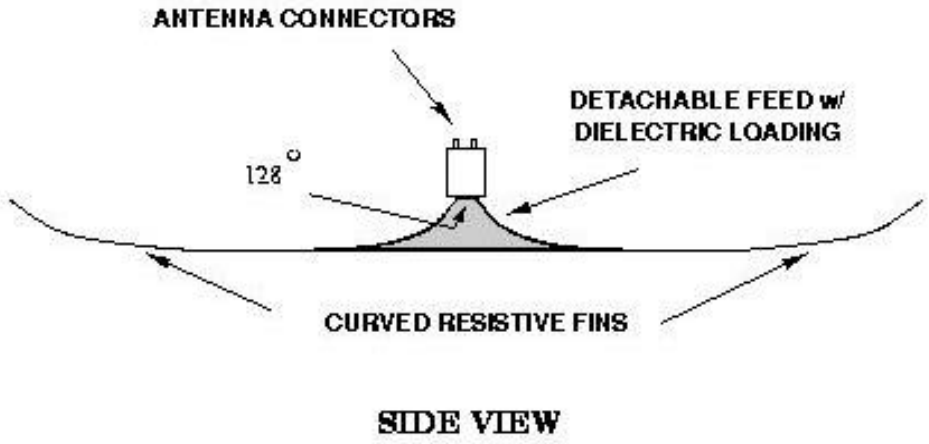

Figure 1 Sketch of the side-view OSU/ESL ultra-wide bandwidth full-polarization GPR antenna.

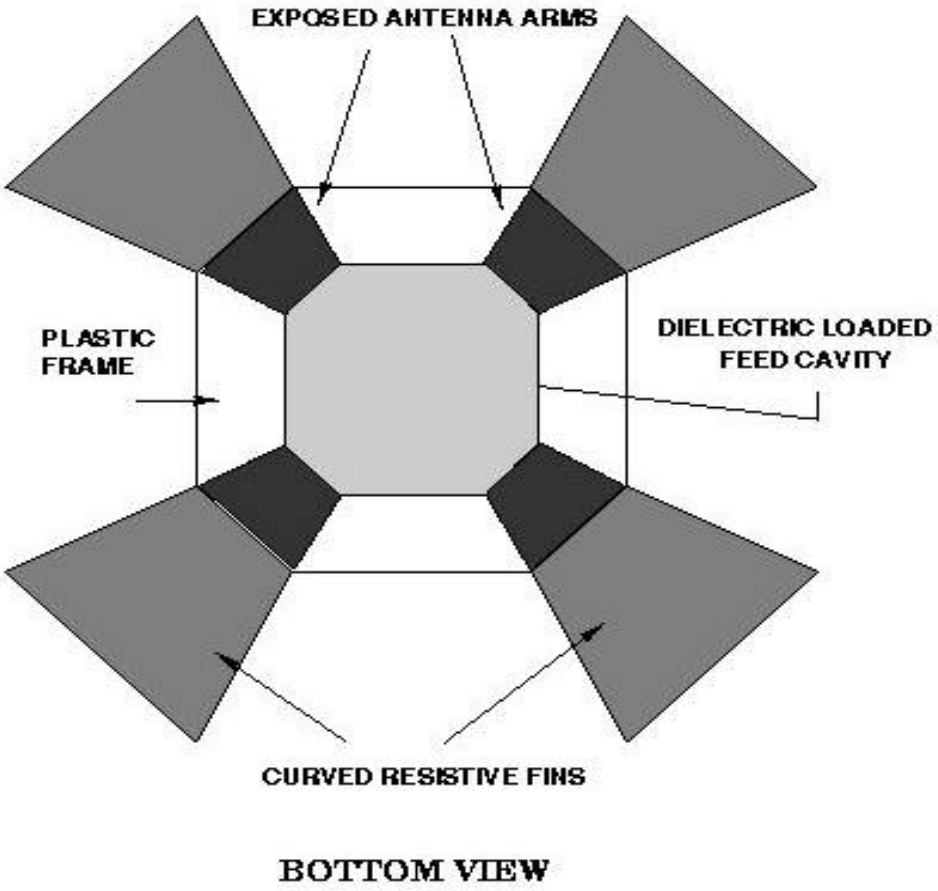

Figure 2 Sketch of the bottom-view OSU/ESL ultra-wide bandwidth full-polarization GPR antenna.

Figure 3 Photo of the radar (microwave network analyzer) and the laptop computer mounted on an all-terrain vehicle (ATV).

Figure 4 Photo of the OSU/ESL UWBFP GPR antenna mounted on an ATV in raised position.

3 Measurement Approaches

For each target location, a broad-bandwidth (10 MHz - 810 MHz) full-polarization radar data set was recorded at multiple positions along a straight line, the midpoint of which as at the presumed target location. This set of measurements produces different look angles at the subsurface target. The data collected at the largest distance position could also provide a local background data. During the initial measurement, the UXO orientation was unknown and the orientation of the straight line was chosen arbitrarily. If the on-site processing results indicated the existence of a linearly-shaped target or ambiguous linearity, two additional second-run measurements were performed along two straight lines oriented parallel and perpendicular to the estimated target orientation. Among the 152 targets measured, 63 targets were selected for the second-run measurement. During these second-run measurements, data were collected at five equally spaced positions along each line that had a length of 2-meter or 4-meter long, depending on the previously estimated target depth. For deeper targets, a 4-meter line was selected. Figure 5 shows the radar system during a measurement in Tyndall AFB UXO site. A long stick ruler was laid on the ground for antenna positioning.

Throughout the two-week measurement period, the radar system functioned without any major problems. Upon arriving at the site, it was found that the target locations were not marked by the contractor or centered in each cell as originally planned, though GPS location data were available. CRREL and OSU personnel then used both a GPS and a handheld magnetometer to verify each target location and emplace plastic markers. This required extra effort and results in a position uncertainty of about $\pm$20 cm.

The original plan was to take a background measurement at a single or a couple of known no-target cells on the two grids. This background data would then be subtracted out of all target-measurement data to remove system and antenna clutter. However, it was found that the surface roughness caused by the tracks of vehicles and human activity created undesired early-time clutter, which made the background measurements from a just a few cells insufficiently representative. Considerable effort was then devoted to smoothing the surface in advance of the antenna as it proceeded along measurement lines. This was done manually by pulling a long, heavy bar along the surface prior to the radar measurement. During the second week, a rental tractor was used.

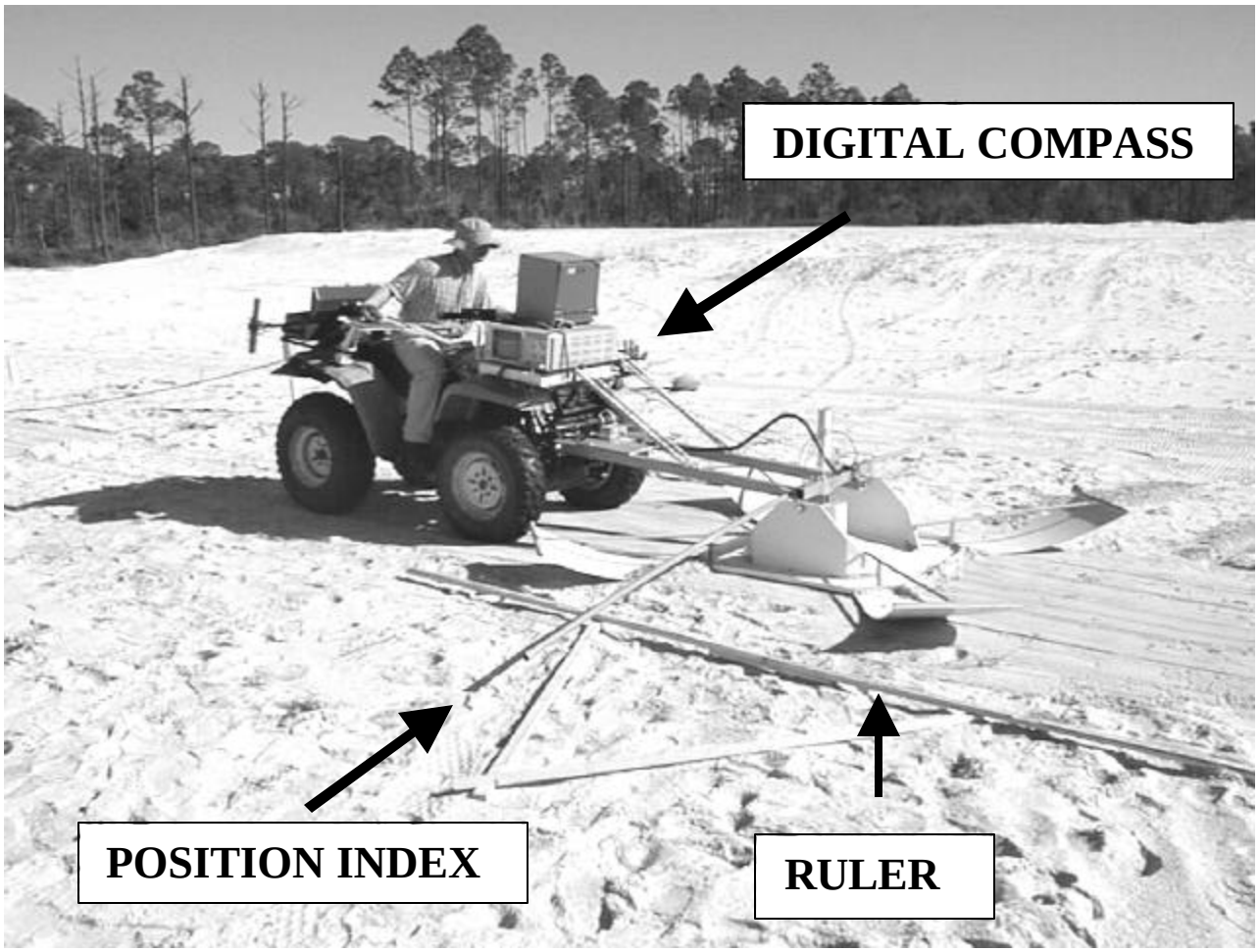

Figure 5 OSU/ESL full-polarization GPR in Tyndall AFB UXO site.

4 Feature Extraction Procedure

The current processing algorithm was designed to make use of the late-time resonance and polarization signatures discussed in the previous section. Measured frequency-domain data were first transformed into time-domain responses. A late-time region was then selected based on the damped resonance feature observed in the time responses. For instance, Figure 6 plots the measured responses of a 105mm UXO buried horizontally at the depth of 24cm in Tyndall site (see Target #5 in the Appendix). The co-polarized (S_{11} and S_{22}) and cross-polarized (S_{21}) responses at each time instant in the late-time region were combined into a full scattering matrix associated with that time instant.

In general, the full scattering matrix of a radar target can be expressed as

$$\begin{bmatrix} S_{11} & S_{21} \\ S_{21} & S_{22} \end{bmatrix} = \mathbf{M}^{-1} \begin{bmatrix} S_{//,//} & S_{//,\perp} \\ S_{\perp,//} & S_{\perp\perp} \end{bmatrix} \mathbf{M} ,$$

where the "S_{21}" indicates the fields are transmitted and received from polarization 1 and 2, respectively, in the antenna coordinate system. The directions "1" and "2" are orthogonal to each other. The subscripts "//" indicates the field component that is parallel to the UXO axis. The unitary matrix, **M**, rotates the antenna coordinate system into the target coordinate system. For UXO type of target, its scattering matrix has the following form

$$\begin{bmatrix} S_{//,//} & S_{//,\perp} \\ S_{\perp,//} & S_{\perp\perp} \end{bmatrix} = \begin{bmatrix} \lambda_{//} & \rho \\ \rho & \lambda_{\perp} \end{bmatrix} \quad , \rho \ll \lambda_{\perp} \ll \lambda_{//} .$$

The off-diagonal components are often negligible and the diagonal components are the eigenvalues of the target's scattering matrix. Since the eigenvalues would not be affected by the coordinate transformation, **M**, these eigenvalues can be obtained from the any antenna orientation. Note that the above discussion focus only on the fields projected onto the plane parallel to the antenna plane. When the antenna is placed on the air-ground interface, the UXO has been projected to the horizontal plane parallel to the air-ground interface. Therefore, for a horizontal UXO, the LDR can be estimated from the ratio of the eigenvalues. Such polarization signatures can also be used to discriminate UXO's from many other false alarms that do not have elongated bodies.

Two eigenvalues, $\lambda_{//}$ and $\lambda_{\perp}$, were then solved from each scattering matrix. $\lambda_{//}$ and $\lambda_{\perp}$ correspond to the parallel and transverse components of re-radiated resonant field intensity. For an UXO-like target, these correspond to the field components parallel and transverse to the target axis. As discussed earlier, $\lambda_{\perp}$ would be negligible for such a target, in late time. This leads to an *estimated linearity factor* (ELF) close to unity. In the current processing, the final ELF is defined by the average of both time-domain and frequency domain linearity factors corresponding to the late-time region and resonance peak, respectively. They are defined explicitly below.

$$ELF_t \equiv mean\left(\frac{\left\| l_{//}(t)\right| - \left| l_{\perp}(t)\right\|}{\left\| l_{//}(t)\right| + \left| l_{\perp}(t)\right\|}\right), \ t \in late-time ;$$

$$ELF_f \equiv mean\left(\frac{\left\| l_{//}(t)\right| - \left| l(t)_{\perp}\right\|}{\left\| l_{//}(t)\right| + \left| l(t)_{\perp}\right\|}\right),\ f = f_{CNR} - \Delta f,\ f_{CNR},\ f_{CNR} + \Delta f,\ \Delta f = 3\ MHz;$$

$$ELF = \frac{ELF_t + ELF_f}{2}.$$

Further improvement in ELF estimation was also obtained by introducing the "resonant-frequency ELF," using an estimated resonant frequency f_{CNR}. This improvement was achieved by clutter reduction via the frequency filtering process. First a range gate is applied to the time domain data and then the late-time portion is transformed into the frequency domain. A band-pass filter with a center frequency at the estimated resonant frequency is applied. The co-polarized and cross-polarized data near the estimated resonant frequency were used to calculate the frequency ELF. The final ELF was calculated from the average of the time and frequency ELF's. The filtered frequency-domain data is then transformed back to obtain the filtered time-domain data for feature extraction.

Notice that, for a rotationally symmetric target, ELF=0 since $\lambda_{//} = \lambda_{\perp}$. Of course, real data always contain a certain degree of random noise and undesired responses, i.e. clutter. The estimated ELF from measured data from an elongated object would not be ideal, namely unity, but would be affected by the signal-to-noise ratio (SNR) and signal-to-clutter ratio (SCR). Figure 7 plots the estimated ELF for an ideally linear target ($\lambda_{//} = 1$, $\lambda_{\perp} = 0$) with random noise added to the scattering matrix. The level of the noise is specified by the SNR as shown by the horizontal scale. Figure 8 plots the effect of additional clutter added to the scattering matrix. As one can see, when SNR or SCR is less than 6dB (or a factor of 2), the estimated ELF decreases quickly.

While we solve for the eigenvalues of the scattering matrix, the corresponding eigenfunctions are also obtained. Such eigenfunctions can be used to rotate the electromagnetic fields from the antenna coordinates to the target coordinates. The magnitude of the eigenvalue itself indicates the signal strength of each principal direction, including the stronger direction along the target's long axis. We consider that the direction of the strongest signal overall indicates the axis direction of an elongated target.

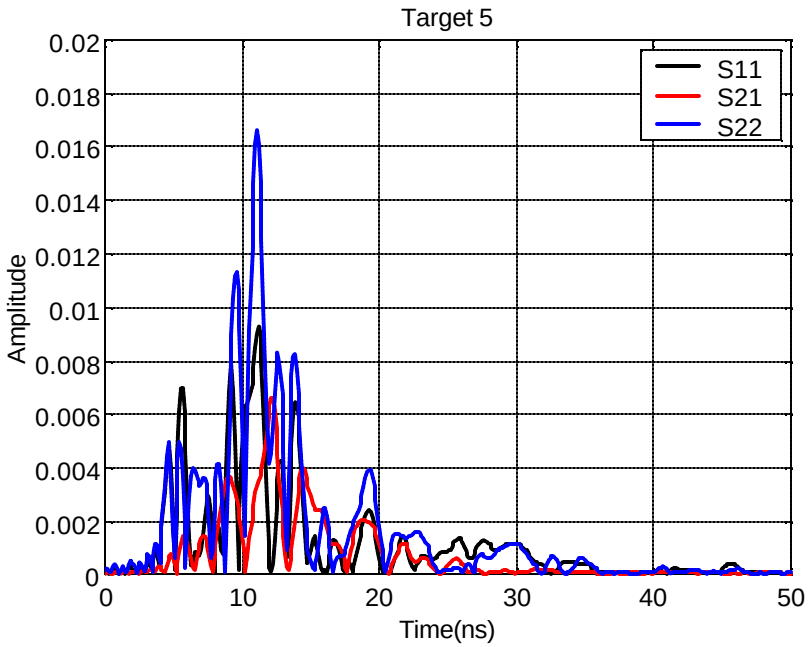

(a) Background removed time responses of Target #5

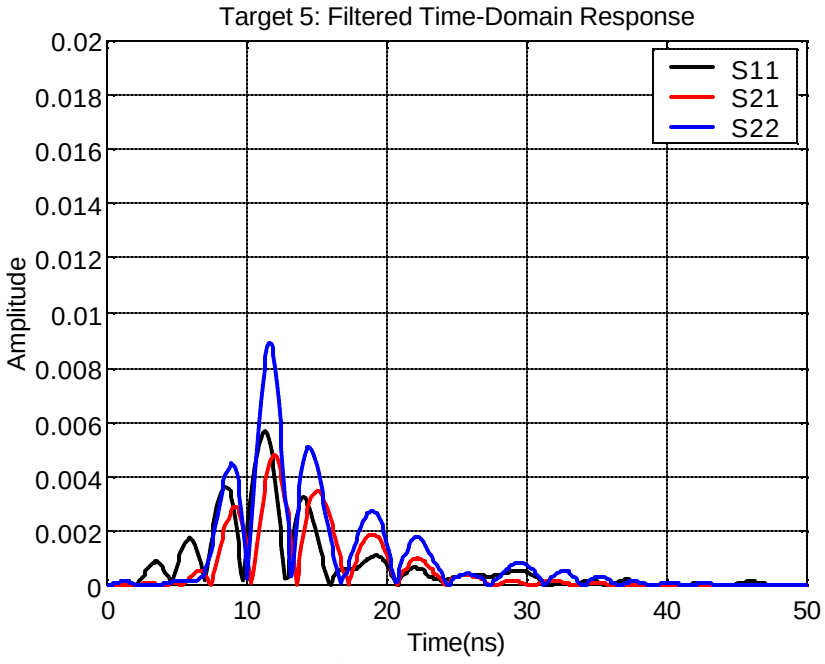

(b) filtered time responses

Figure 6 Measured time-domain responses of Target #5 before (a) and after (b) applying bandpass filter centered at the resonant frequency determined from its late-time spectrum (c).

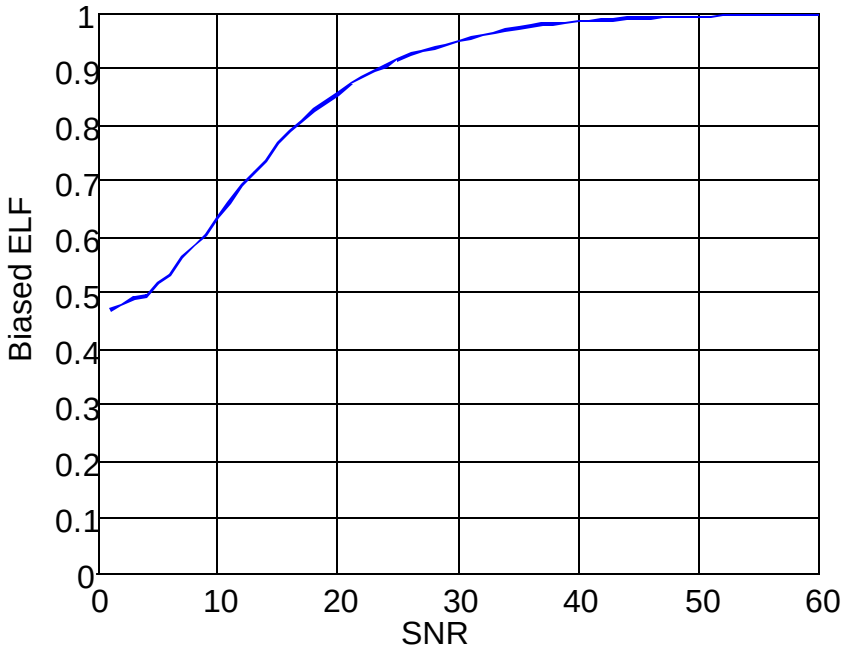

Figure 7 Estimated Linearity Factor (ELF) vs. signal-to-noise ratio (SNR) using Monte-Carlo simulation.

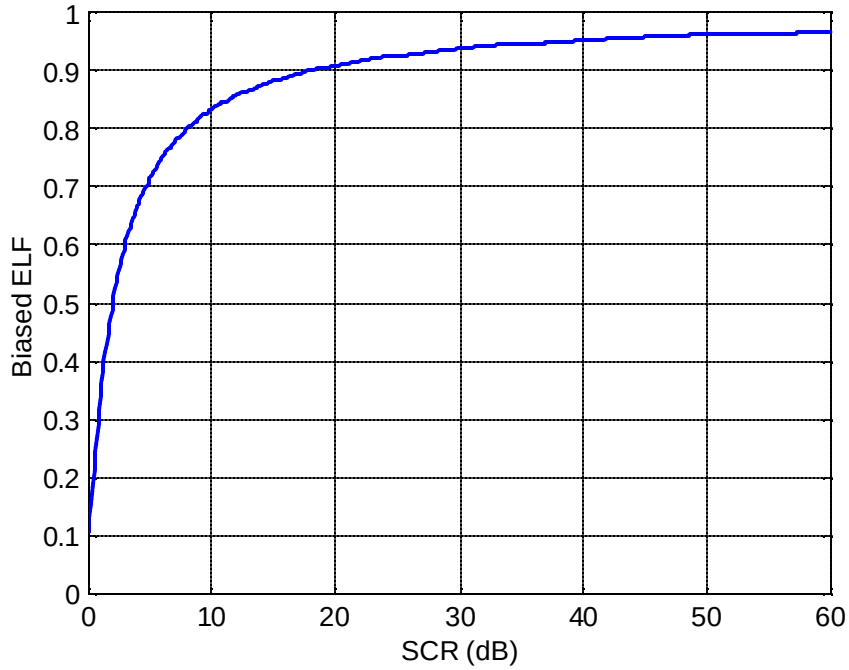

Figure 8 Estimated Linearity Factor (ELF) vs. signal-to-clutter ratio (SCR).

In terms of our data processing: the target orientation can also be calculated from the eigenfunctions. At each time position in the late-time region, an orientation estimation is obtained. For an UXO-like target, the estimated orientations in the late-time region should cluster closely together as demonstrated in

Figure 9 calculated from measured data for Tyndall Target #5. The radial length at each point (or time instant) corresponds to the parallel-component eigenvalue and hence indicates the field intensity. The *Estimated Target Orientation* (ETO) is then defined to be the angle associated with the maximum eigenvalue. For instance, Figure 9 indicates the target orientation to be about $32^{o} \pm 180^{o}$. Such 180^{o} alias always exists due to the backscattering measurement. This agrees very well with the true orientation, 30 degrees. For a non-elongated target, the calculated orientations tend to point randomly in all directions as demonstrated in Figure 10 calculated from data collected at an empty cell in Tyndall site. A measure of the consistency or density of the orientation information around the ETO direction is obtained by summing the eigenvalues within a $\mathrm{ETO} \pm 10^{o}$ range and comparing it to the sum over all angles. This gives the definition of the angle density (DEN), the degree of angle concentration, defined to be the weighted probability of the calculated orientations near the ETO direction,

$$\mathrm{DEN} = \sum_{ETO-10}^{ETO+10} | l_i(t) | q_i(t) \; / \; \sum_{-180}^{180} | l_i(t) | q_i(t)$$

where $|\lambda_i|$ is the magnitude of the principal scattering component associated with the estimated orientation. Such angle density can also be used as an indicator of target linearity.

In addition to the ELF, ETO and DEN, the *estimate target length* (ETL) was also obtained from the resonant frequency extracted from the late-time response using the advanced Prony method [2]. The target depth (DEP) was also estimated from the time delay of the target echo. Depending on the UXO orientation, multiple echoes may be received from different body parts of the UXO. In practice, the earliest detectable response is usually selected to determine the target depth by considering the time delay and wave velocity in the soil. Since the earliest detectable response of a target depends on the target geometry as well as its orientation, uncertainty of the target depth is inevitable. Both ETL and DEP estimations require a proper estimation of soil electrical property that was measured using a soil probe at limited locations. The variation of the soil property at different sites can also cause errors in the estimation of the above feature parameters.

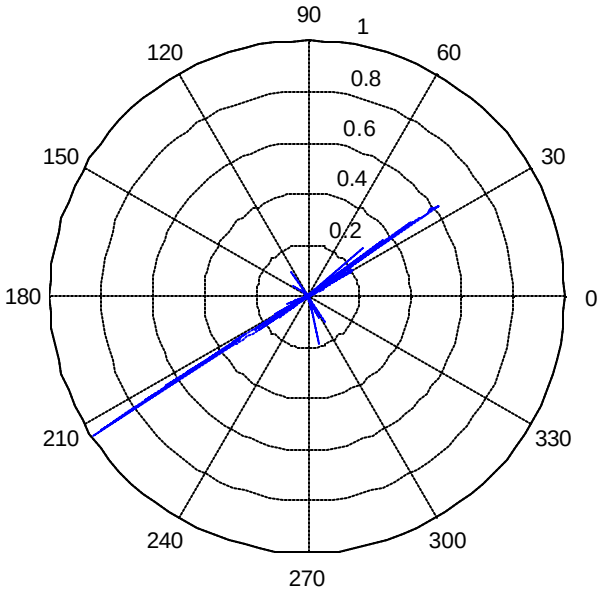

Figure 9 Example of the calculated orientations for target (Tyndall #5) with a good linearity.

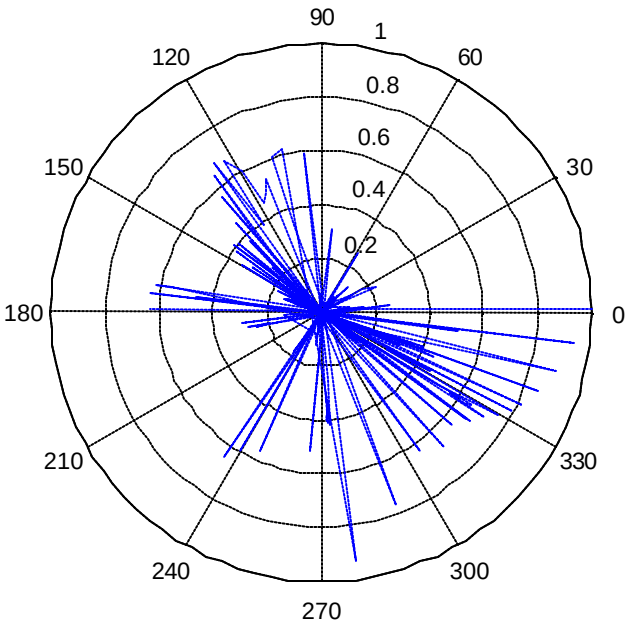

Figure 10 Example of calculated orientation with poor linearity for data collected at an empty cell.

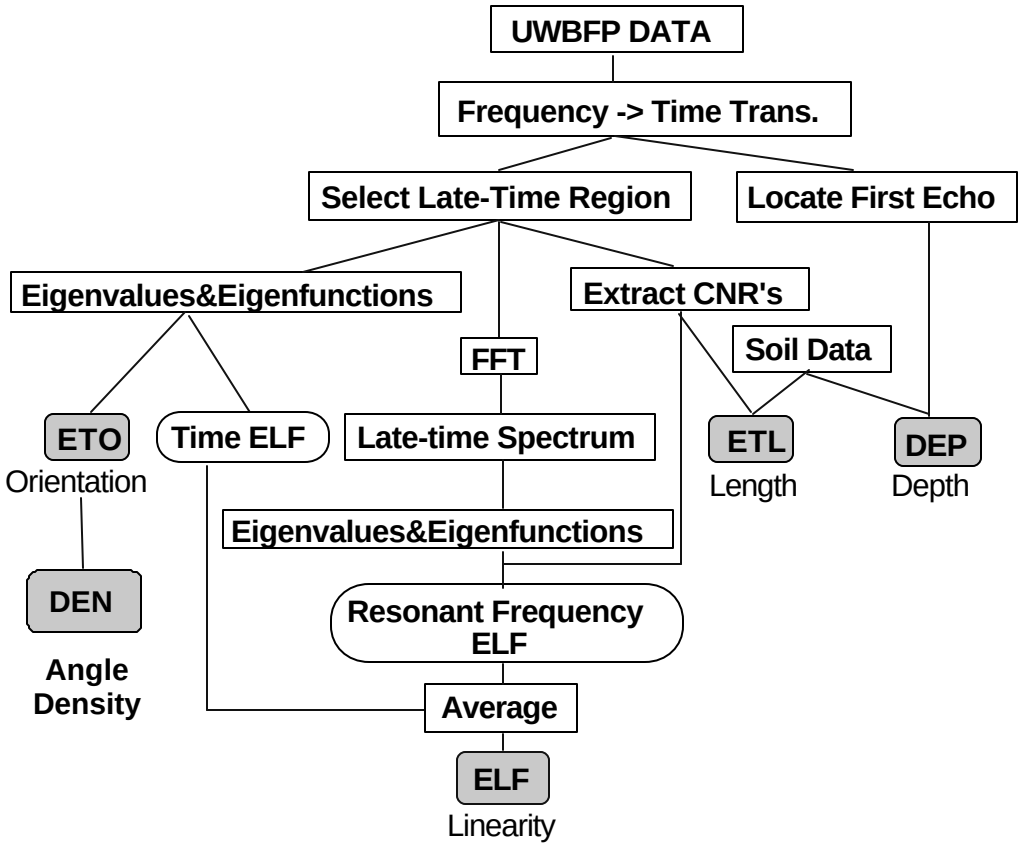

Figure 11 Flow chart of the current UXO feature extraction algorithm for UWBFP GPR data.

5 Tyndall GPR Data Feature Extraction Results

5.1 Feature Extraction for Known Targets

The processed results for known targets emplaced at the Tyndall site are shown in the Table 1. The estimated ELF_t and ELF_f for linear objects are greater than 0.7. This is a indication of good linearity. The two spheres, on the other hand, show relative low ELF values as expected. Notice that the ELF estimated for the empty cell is 0.5544 in the time domain but only 0.2302 in the frequency domain. Unlike a true linear target, both ELF_t and ELF_f tend to be high. This motivated the use of the average value between the time-domain and frequency-domain ELF. The angle density also shows good discrimination capability between linear and non-linear objects. Figure 12 also plots the DEN and average ELF for the known targets. Their values are indicated by the right scale. The ETL's are also compared with true lengths by plotting the ratio of (True Length/ETL) in Figure 12. As shown by the left scale, the ETL's are on an average 25% longer than the true lengths. Figure 13 compares the actual depths with the estimated depths and shows a reasonable agreement for most targets. Figure 14 also compares the estimated orientations with the true orientations. The largest error was observed to be 35 degrees. Some estimation errors due to the presence of random noise and rotationally symmetric clutter will be discussed in the next section.

Table 1 Extracted Features for Known Targets.

type	location	ELF_t	ELF_f	ETL (m)	True L	DEP (m)	True Dep.	ETO	True Oren.	DE
sphere	148	0.4329	0.3543	0.9305	0.1500	0.3114	0.3050	3	N.A.	0.0895
sphere	149	0.3591	0.3028	1.0266	0.1500	0.2015	0.5550	18	N.A.	0.1751
pipe	79	0.8726	0.8510	1.2713	0.9000	0.6598	0.4300	-172	0 or 180	0.8983
pipe	78	0.8471	0.6913	0.7031	0.6000	0.3298	0.2600	-6	0 or 180	0.6412
pipe	77	0.9180	0.8302	0.3921	0.3000	0.5132	0.1200	-173	0 or 180	0.8094
rebar	74	0.8215	0.7170	0.4204	0.3000	0.3481	0.3000	14	0 or 180	0.7721
rebar	75	0.7626	0.9121	0.7058	0.6000	1.1992	1.1000	-19	0 or 180	0.6132
rebar	76	0.7989	0.8279	1.0593	0.9000	1.6317	1.5000	13	0 or 180	0.7067
rebar	EXTRA	0.7730	0.8264	1.1941	1.0200	0.6045	0.5800	151	-30 or 150	0.8972
UXO	151	0.7328	0.6900	0.4525	0.6000	0.8244	0.5000	28	0 or 180	0.7998
pipe	150	0.9239	0.5578	0.6178	0.6000	0.4580	0.5000	-145	0 or 180	0.7430
no target	Upper 9,2	0.5544	0.2302	0.6940		0.4580		135		0.2239

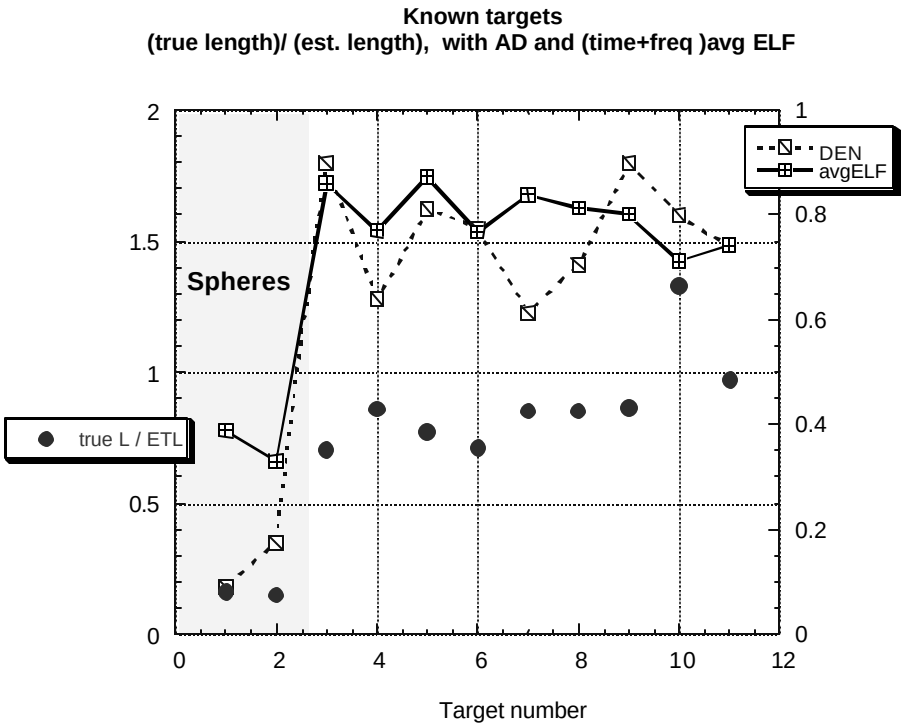

Figure 12 Comparison between the true lengths and the estimated lengths for the known targets (left axis). The DEN and average ELF are also shown using the right axis.

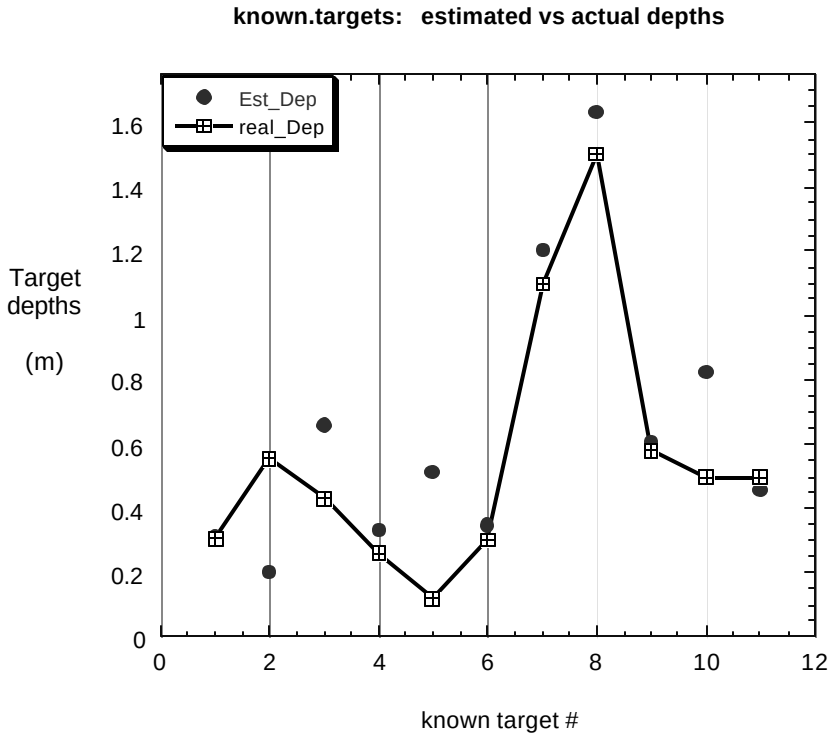

Figure 13 Comparison between the true depths and the estimated depths for the known targets.

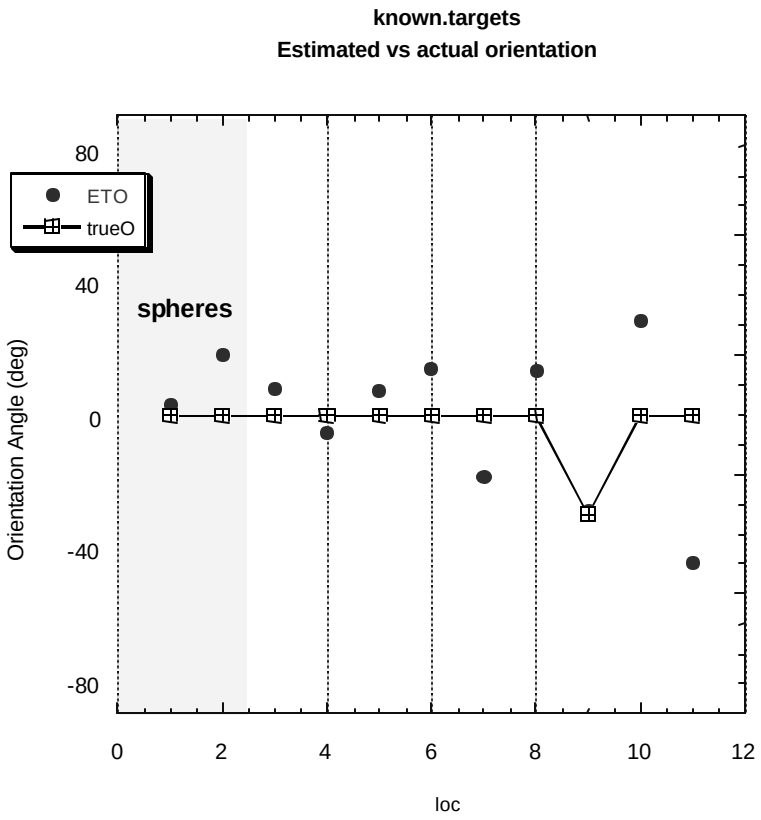

Figure 14 Comparison between the ETO and the true orientations for known targets.

5.2 Uncertainty Analysis of Tyndall GPR Data Feature Extraction

5.2.1 Random Noise Effect

Measured data always contains random noise. A most common type of noise is the Gaussian noise whose amplitude distribution is characterized by a Gaussian distribution. The presence of such random noise may cause different degrees of errors in the estimated parameters depending on its amplitude level with respect to the desired signal level, i.e. signal-to-noise ratio (SNR). The noise level is usually described by its standard deviation (STD). In our application, the desired signal is characterized by a damped sinusoidal function related to target's natural resonance. Since instantaneous signal magnitude decreases as time increases due to the damping nature of the signal, a convenient way to define the signal level is to use the signal magnitude at the beginning of damping where the signal has the strongest magnitude. Eventually, the signal level will be damped such that it is less than the noise level, i.e. instantaneous SNR less than 0 dB. This will result in great error in the estimation of feature parameters. Therefore, in practice, only the segment of data where the SNR is greater than, say 0 dB, is used for feature extraction. Some example waveforms of a damped resonance characterized by a complex pole, 1.2566+0.1 j, in the presence of different noise levels are also provided from Figure 15 to Figure 17.

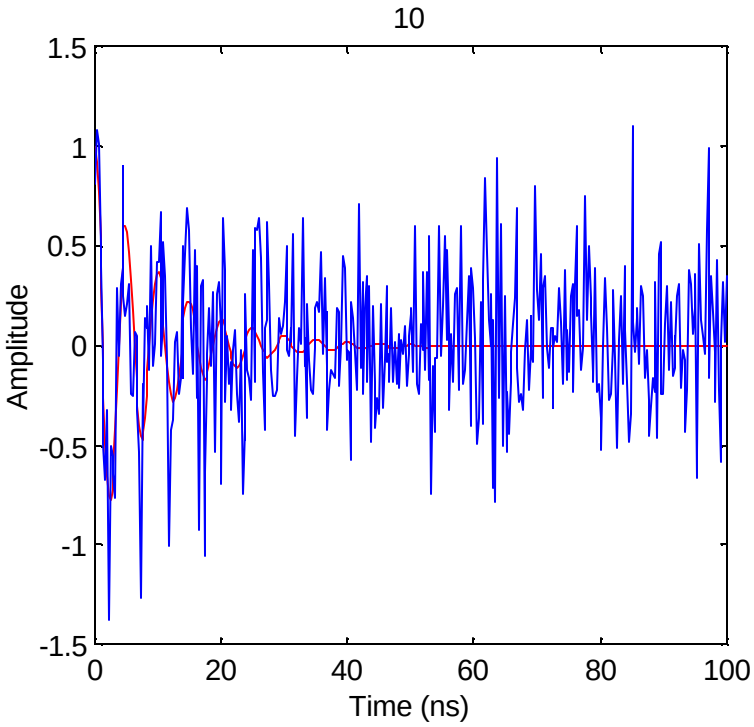

Figure 15 Example of a damped resonance in the presence of random Gaussian with SNR=10 dB. The red curve shows the signal response in the absence of noise.

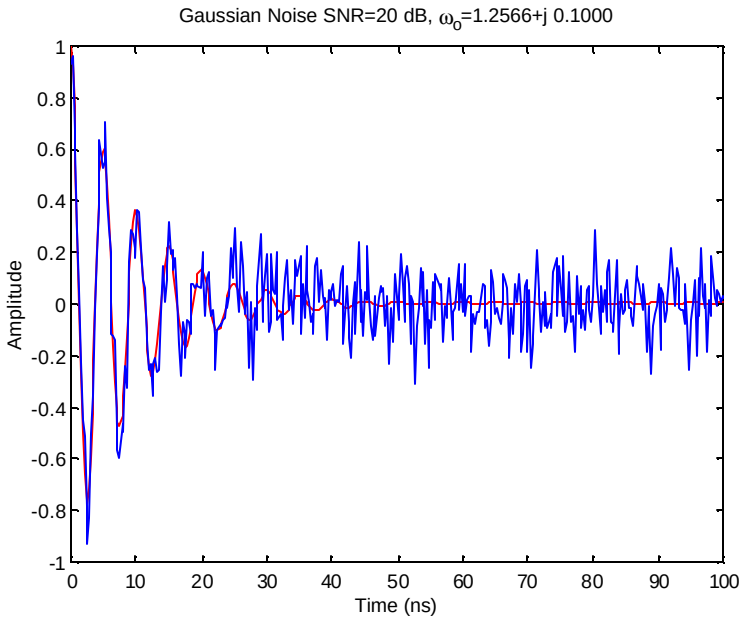

Figure 16 Example of a damped resonance in the presence of random Gaussian with SNR=20 dB. The red curve shows the signal response in the absence of noise.

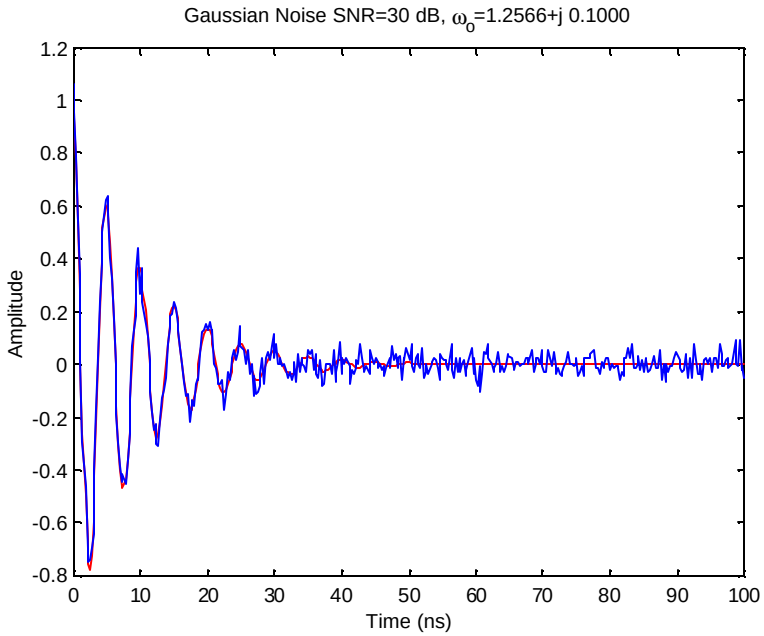

Figure 17 Example of a damped resonance in the presence of random Gaussian with SNR=30 dB. The red curve shows the signal response in the absence of noise.

The presence of random noise during the estimation causes bias and variation to the estimated feature parameter. The bias causes the mean value of an estimated parameter to be different from its true value as illustrated by the Monte-Carlo simulation data shown in Figure 18, Figure 19, and Figure 20 for CNR, ELF and ETO, respectively. In this case, the bias of the CNR estimation is negligible. However, in reality, the bias of the estimation of the soil permittivity results in biased resonant frequency. This in turn causes bias in estimating the target length. From this simulation, it was found that SNR had to be at least 17 dB to obtain an ELF value higher than 0.8, i.e. less than 20% of error. Negligible bias is observed in the ETO estimation when the SNR is greater than 15 dB.

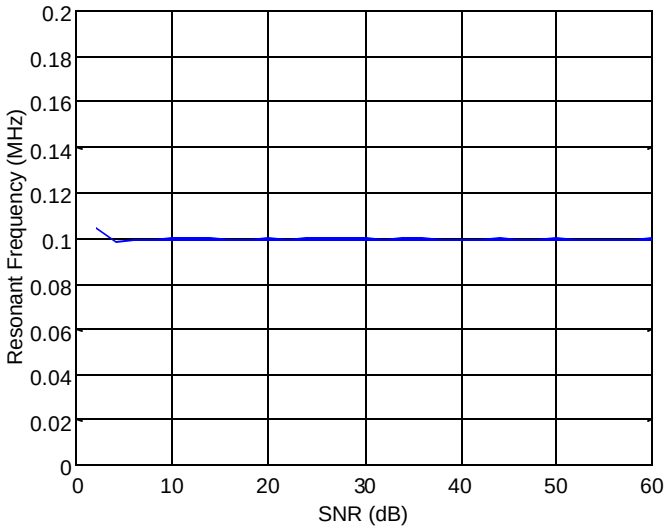

Figure 18 The estimated resonant frequency using TLS-Prony method under the influence of different levels of random Gaussian noise. The true frequency should be 100 MHz.

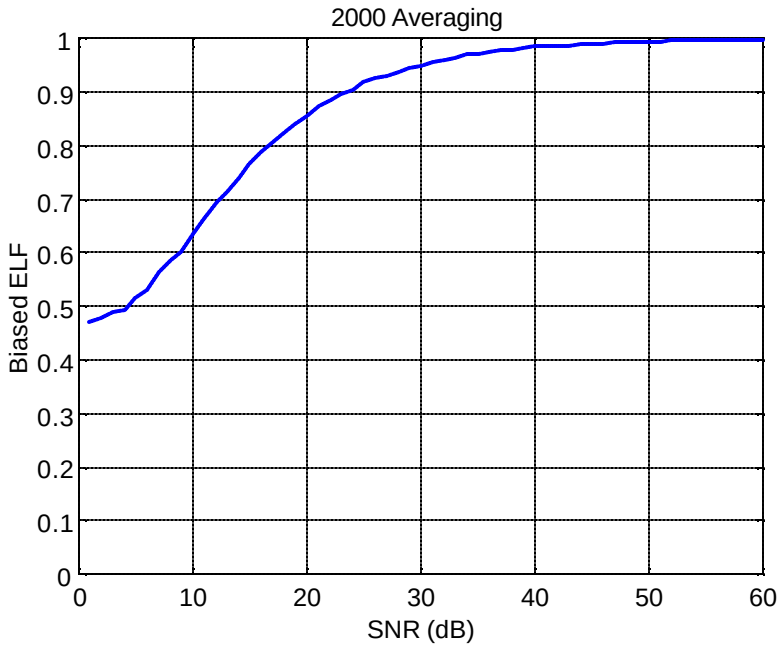

Figure 19 The estimated ELF under the influence of different levels of random Gaussian noise. The true value should be one.

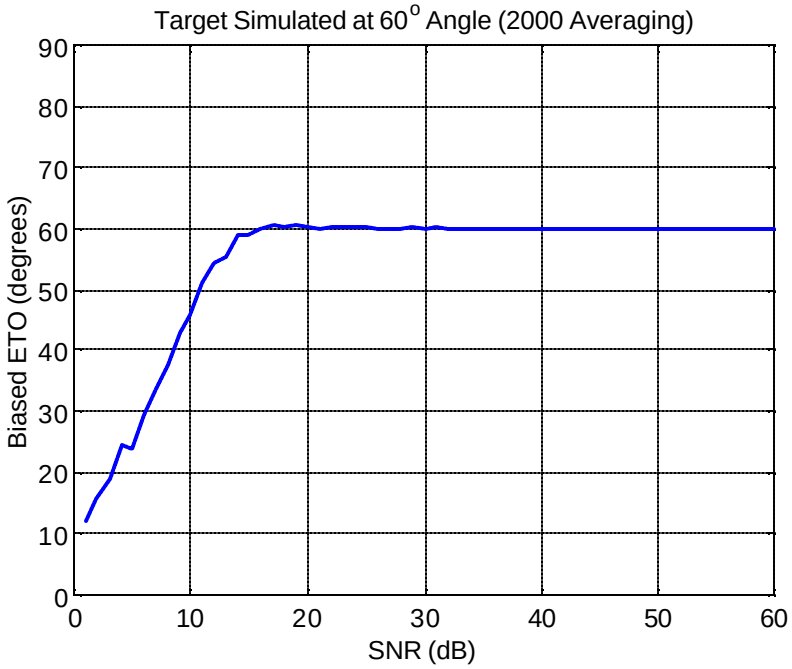

Figure 20 The estimated ETO under the influence of different levels of random Gaussian noise. The true orientation should be 60 degrees.

From actual Tyndall GPR data, samples of noise were obtained from a segment of data in the negative-time region of the measured data since this region contain only noise. The standard deviation of the noise sample was then calculated to represent the noise level for that particular measurement. The signal level was defined to be the maximum eigenvalue extracted from fully-polarimetric data in the

selected late-time region. Recall that fully-polarimetric data at each time position gave a 2-by-2 scattering matrix from which two eigenvalues were extracted. The dominant eigenvalue corresponds to the scattering magnitude of a linear target when the incident fields are polarized in parallel with the axis of the target. Since the target response is in the form of damped resonances in the late-time region, the maximum eigenvalue in the late-time region would be obtained from the beginning of the resonance. Notice that the standard deviation of a Gaussian noise is the same as its eigenvalue extracted from a noise matrix. The signal-to-noise ratio (SNR) is then defined to be the ratio of the above signal level to the noise level.

Figure 21 shows the histogram of calculated SNR's for all targets measured at Tyndall site. The resultant potential biases for the estimation of ELF are indicated by "X" markers in Figure 22. As one can see, other than Targets #77 and #79 which have SNR greater than 20 dB, all other targets have SNR greater than 30 dB. The resultant biases for the CNR and ETO estimation are negligible from Figure 18 and Figure 19 and are not shown. A complete list of uncertainty for the ELF estimation can also be found in Table 2.

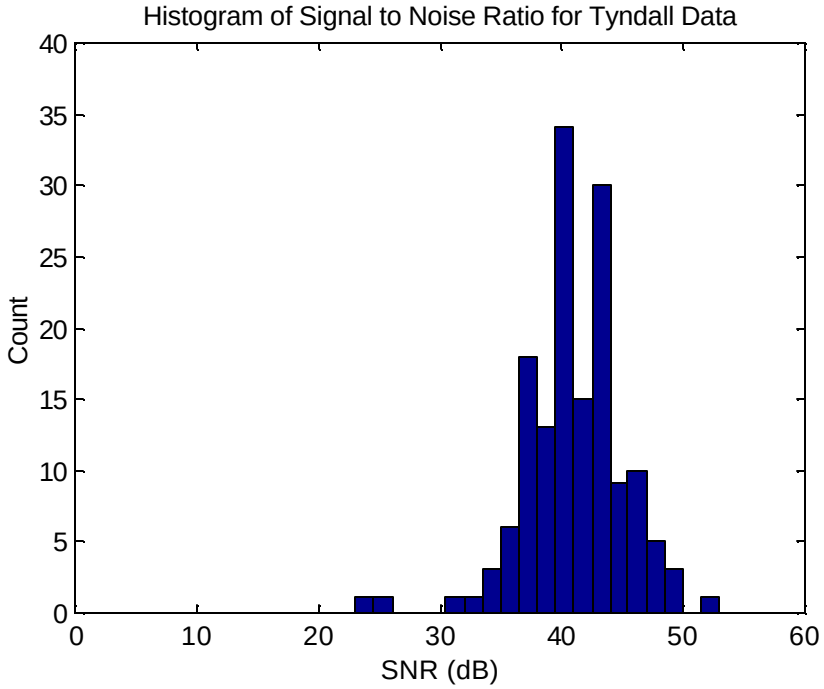

Figure 21 Histogram of the SNR for Tyndall targets.

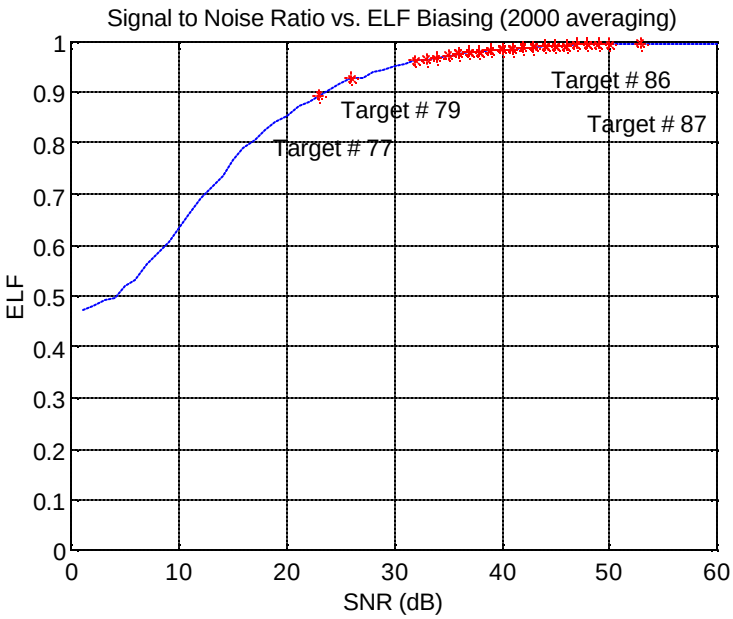

Figure 22 Possible bias of ELF estimation of Tyndall Targets.

The variation of the estimated parameters results in uncertainty due to the randomness of the noise. The standard deviation (STD) is a common measure of such a variation that represents the uncertainty of the estimated parameters. The STD's of the estimated resonant frequency, the ELF and ETO in the presence of different SNR levels are shown in Figure 22, Figure 24 and Figure 25, respectively. When the SNR is greater than 20 dB, the STD's for the CNR, ELF's and ETO's are less than 2 MHz, 0.1 and 4 degrees, respectively. These values are quite acceptable and should not affect the performance of target classification. The STD's of the ELF estimation for Tyndall targets are also indicated by "X" markers in Figure 26. Each marker corresponds to one target in Tyndall. A few target numbers are also indicated in the figure. A complete list is also provided in Table 2.

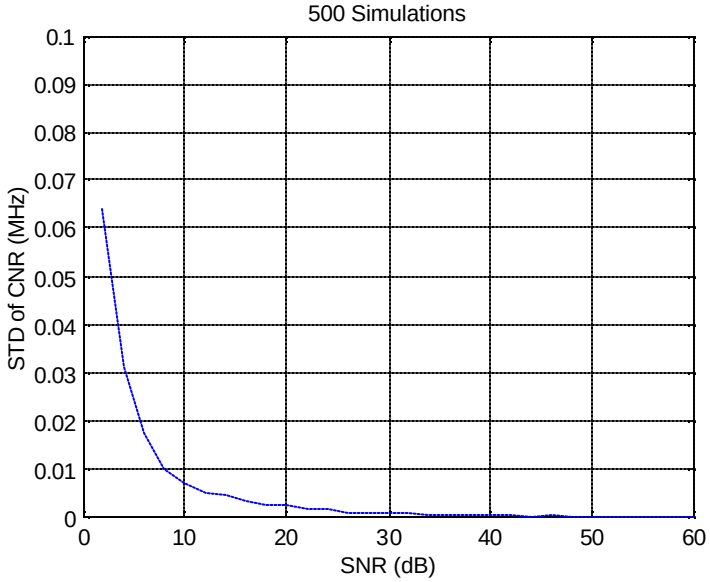

Figure 23 STD of the estimated resonant frequency in random Gaussian noise. 500 noise realizations were used in this simulation.

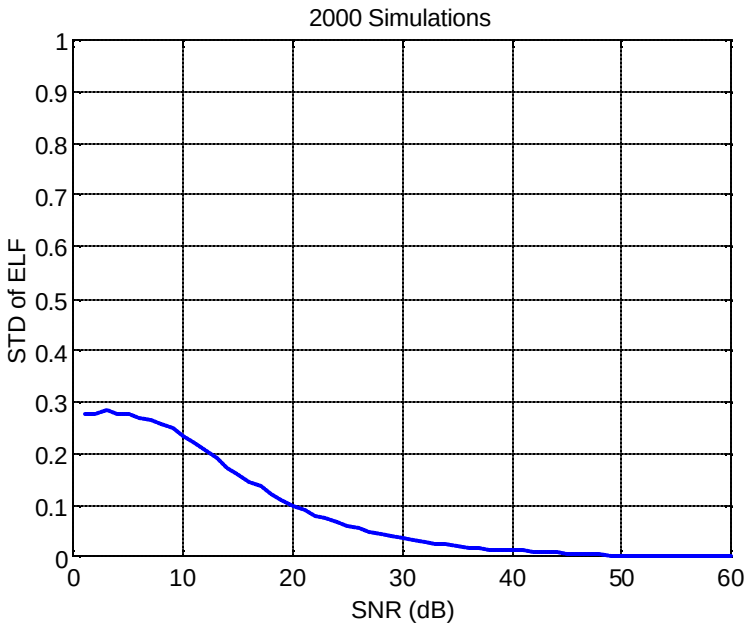

Figure 24 STD of the estimated ELF in random Gaussian noise.

Figure 25 STD of the estimated ETO in random Gaussian noise.

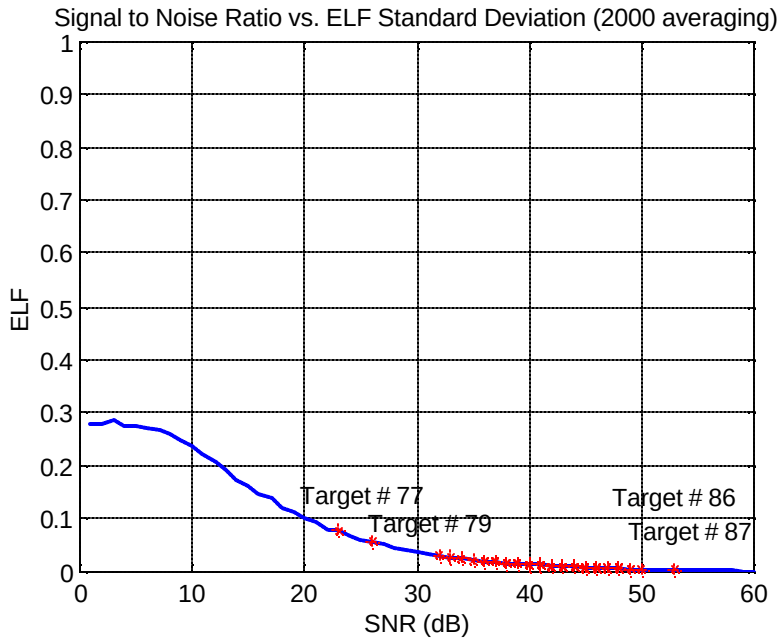

Figure 26 The STD of the estimated ELF due to the presence of different noise levels.

5.2.2 Clutter Issues

A background subtraction process was applied prior to the feature extraction to remove any target unrelated responses, i.e. clutter. These background clutter are mainly caused by reflection and coupling occurring at the feed point (top point of the dielectric loading section of Figure 1), at the junction of exposed antenna arm and the resistive fin shown in Figure 2 and scattering from the ground surface (bottom of the antenna in Figure 1).

Figure 27 plots the raw data collected at an empty site in frequency domain. The solid lines correspond to the co-polarized responses, S_{11} and S_{22}, caused by impedance mismatch between the feeding cables and the input ports of the antenna. The response in the S_{21} channel is caused by the coupling between the two antenna elements. Although the magnitudes of these reflections dominate the data in almost all measurements, they are also very stable and independent of measurements. This stability feature is a result of our special antenna design that reduces the ground-feed interaction. For most GPR antennas, this feed reflection is a function of the ground condition. It should also be noted that such a mismatch level over such a broad frequency range is far more superior to most GPR antennas. A simple background subtraction using a background data collected at an empty site can effectively removed such a feed reflection and coupling. This is demonstrated in Figure 28 by comparing the time-domain responses of the raw data (dashed line) with the background removed data (solid line) for a 105mm UXO (Target #5). After background subtraction, the feed mismatch term started at approximated 2ns position has been effectively removed. The low-frequency components of the feed mismatch term give rise to the long tail observed in the raw data.

The reflections from wing junctions occurring at approximately 9ns are much weaker than the feed reflections and are usually stable and independent of measurements unless excessive mechanical stress is introduced by mechanism vibrations.

The scattering from the ground surface is composed of coherent and incoherent parts. The former is caused by the permittivity difference between the antenna's dielectric filling and the ground. This is less dependent on the antenna position as long as the electromagnetic property of the soil at top layer remains unchanged. The latter is caused by the surface roughness that varies from spot to spot. In practice, the background data should be collected at a location as close to the target location as possible to obtain similar surface responses to achieve maximum ground clutter subtraction. As long as the background data does not contain target responses in it. It our system, the surface scattering occurs approximately at 5ns position as shown in Figure 29. Notice that the cross-polarized response, S_{21}, has much weaker surface clutter as expected. The clutter caused by wing junctions are apparent at about 8~9ns. The majority (coherent part) of the surface reflection was also removed. The residual surface responses correspond to the incoherent scattering caused by the surface roughness change between the two sites. The responses observed at later time are caused by subsurface variation of the soil property.

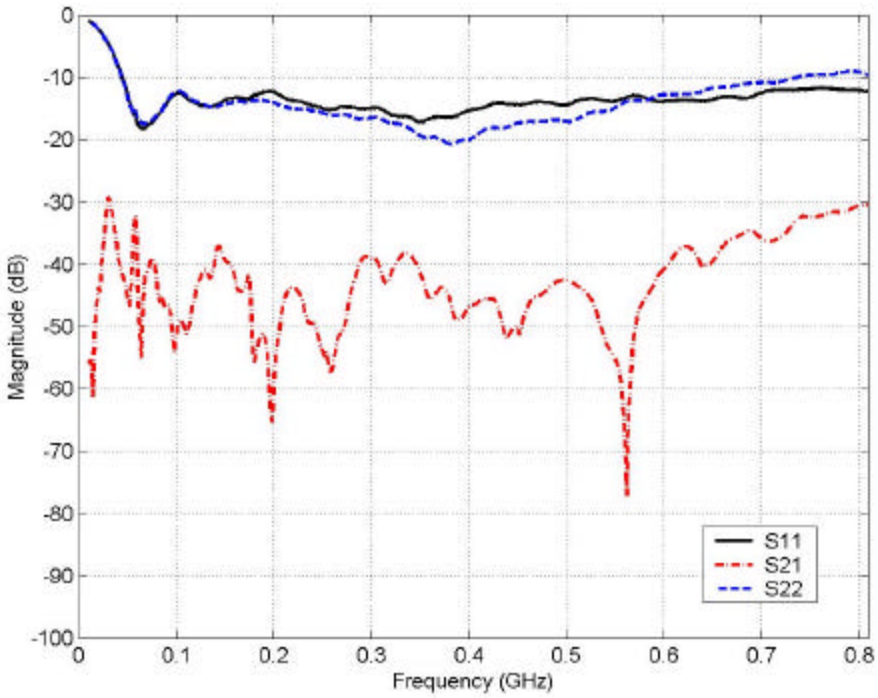

Figure 27 Raw data in frequency domain collected at a empty cell of the Tyndall site.

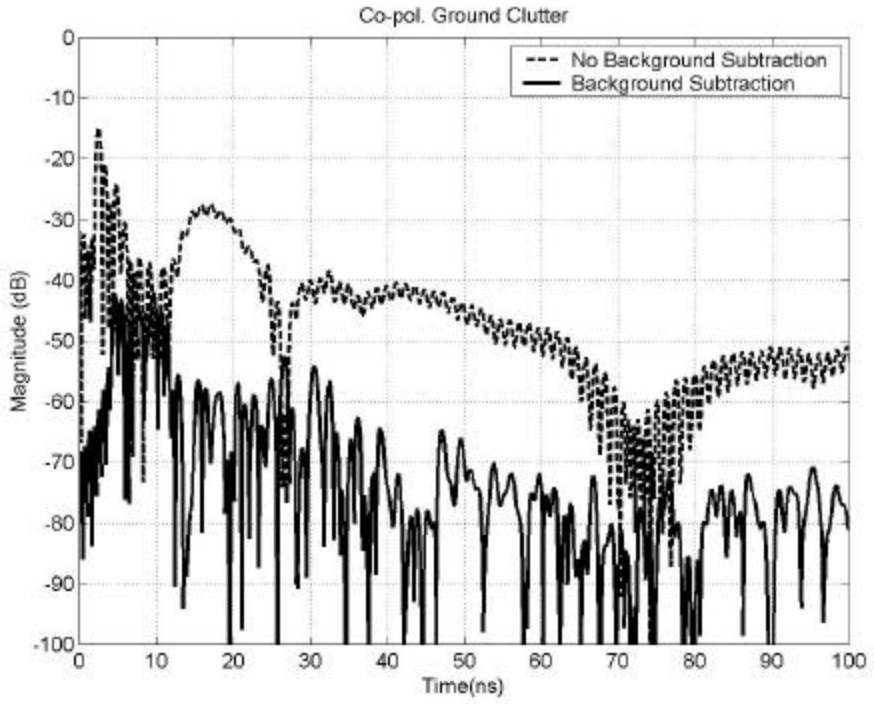

Figure 28 Measured S_{11} response in time domain for Target #5 (105mm) before (dashed line) and after (solid line) background removal.

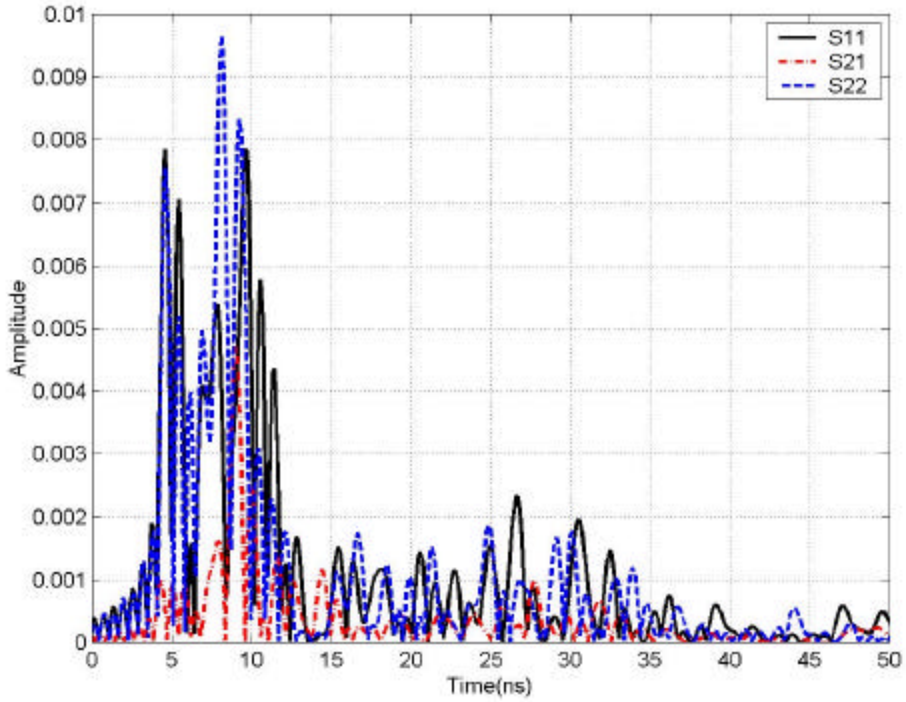

Figure 29 Subtracted results from data collected at two empty spots separated by approximately 4 meters.

It is observed from Figure 29 that the clutter from the ground surface and wing junction are primarily rotationally symmetric. This is obvious by observing that responses of S_{11} and S_{22} have similar magnitudes that are also much stronger than that of S_{21}. The presence of this type of clutter can cause bias to the estimation of ELF and ETO. This is demonstrated by simulated data shown in Figure 30 and Figure 31. The simulated data is composed of a superposition of a scattering matrix for an ideal linear target, i.e. $\begin{bmatrix} 1 & 0 \\ 0 & 0 \end{bmatrix}$ and a clutter matrix, $\begin{bmatrix} c & c/100 \\ c/100 & c \end{bmatrix}$, where c is a positive constant. In this case, the SCR is then equal to $20\log_{10}(1/c)$. Figure 30 shows that the estimated ELF in the presence of rotationally symmetric clutter is biased from its true value, one. Especially when SCR is less than 5 dB, the estimated ELF becomes less than 0.7, more 30% of bias. On the other hand, the estimation of ETO is much less sensitive to the presence of rotationally symmetric clutter. Even when the SCR is 5 dB, the bias is less than 1 degree. It should be noted that the biases of ELF and ETO are functions of the true values of ELF and ETO, the results shown here only serve as examples.

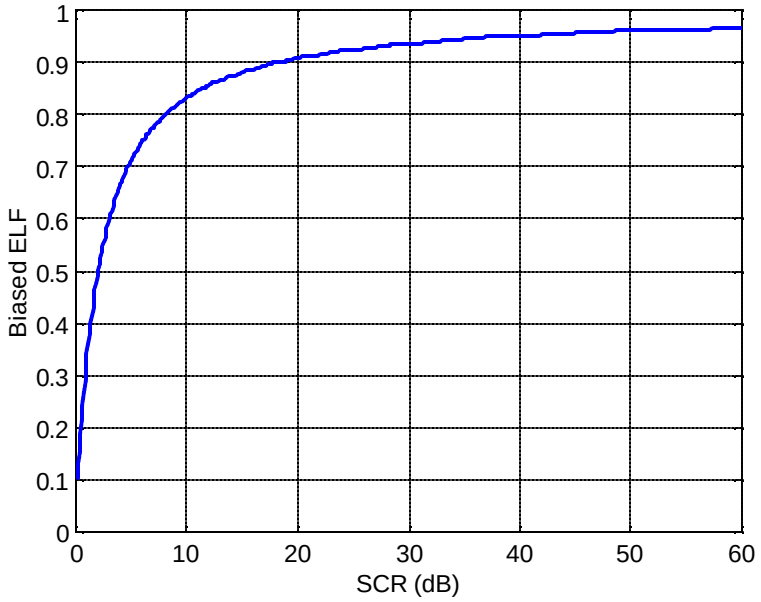

Figure 30 The biasing effect of the ELF estimation in the presence of rotationally symmetric clutter.

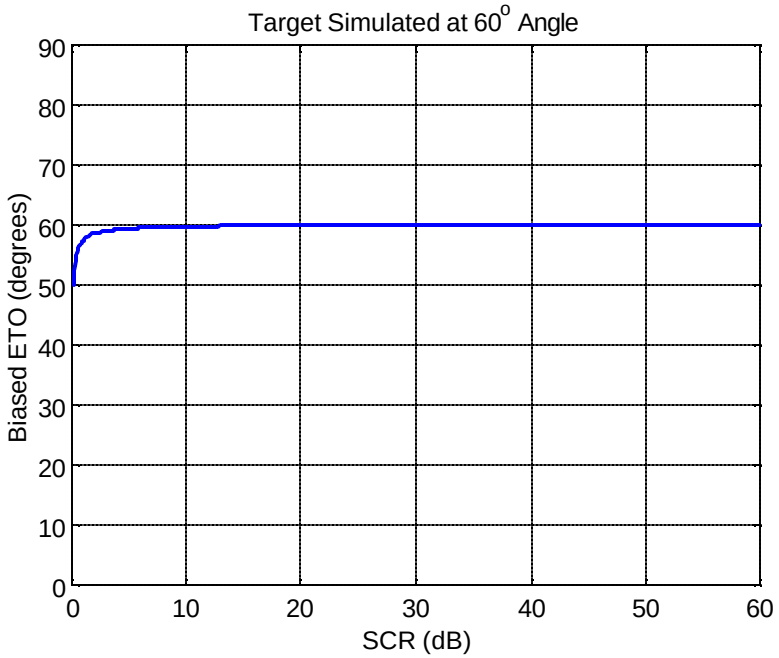

Figure 31 The biasing effect of the ETO estimation in the presence of rotationally symmetric clutter.

Next, the SCR of the Tyndall data are investigated to determine the bias and uncertainty of the estimated parameters. The clutter samples of the Tyndall measurements were obtained from the data collected at an empty cell. Background subtraction was applied to removed measurement independent clutter and coherent ground clutter as discussed previously and shown in Figure 29. The clutter level was determined by calculating the maximum eigenvalue from responses later than 25 ns, as would be done for any other target. The signal level was determined the same way described in the SNR section. The SCR is then defined to the ratio of signal level to the clutter level. Figure 32 shows the histogram of the SCR for all the targets measured at Tyndall site. Most SCR values are around 8~12 dB only. Compared to the SNR histogram shown in Figure 21, one can immediately see that the performance limitation is limited by clutter rather than noise. This conclusion is also true for most GPR applications. Figure 33 shows the potential bias in ELF estimation for Tyndall targets according to their SCR levels. A detailed list of the SCR and biased values for all targets can be found in Table 2.

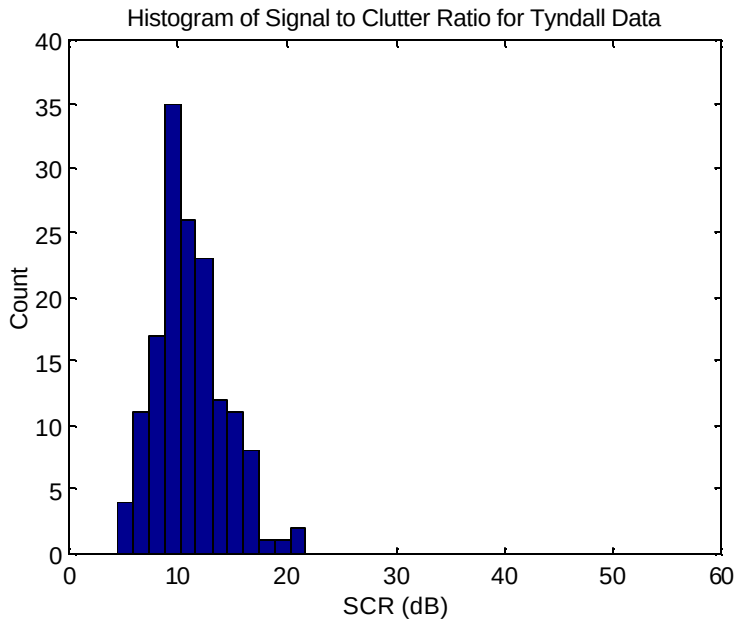

Figure 32 The histogram of the late-time SCR for Tyndall targets.

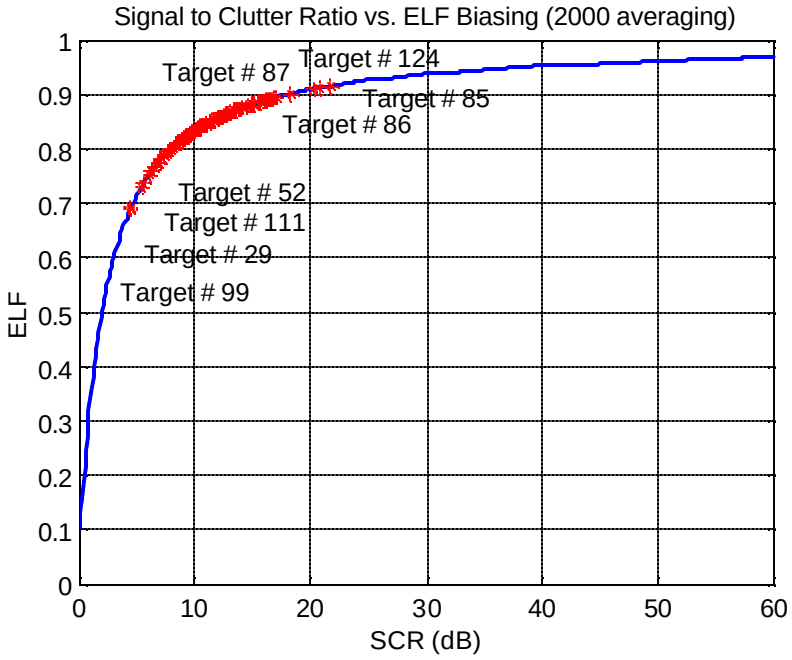

Figure 33 Biased ELF due to the presence of different levels of clutter.

Due to the presence of random noise and rotationally symmetric clutter, the estimation of ELF, ETO and ETL will be biased or have variations. The uncertainty of each estimated parameter is then taken to be the maximum value among the bias and STD caused by both SNR and SCR, i.e. the worst-case scenario. These are listed from Table 2 to Table 4. Take Target #1 in Table 2 as an example, the bias values resulted from SNR and SCR are 0.0128 and 0.1407, respectively. The STD for this target is 0.0094. The uncertainty of the estimated ELF is then 0.1407. Figure 34 also plots the histogram of all the uncertainty values for the ELF estimation. As one can see, a majority of the targets has an uncertainty

value less than 0.2. However, such an uncertainty value may be critical when the estimated ELF is close to the threshold chosen for deciding whether a target should be UXO-like or non-UXO since the uncertainty value could change the ELF value to above or below the threshold.

As one can see, the uncertainty of ETO caused by the noise and rotationally symmetric clutter is negligible. It should also be noted that the uncertainty considers only the effect of random. The major uncertainty is caused by the presence of clutter and the error in estimating soil permittivity. It is rather difficult to study the clutter effect on the resonance extraction that eventually affects the target length estimation. The difficulty arises from the definition of clutter, should it be time domain, frequency domain, early time, late time band-limited, or band-unlimited. Each choice will probably gives different answers to the estimation errors.

Table 2 The SNR, SCR and Uncertainty of the ELF Parameter for Tyndall Targets.

Target #	**ELF**	SNR (dB)	SNR Biased ELF	STD	SCR (dB)	SCR Biased ELF	**Uncertainty**
1	**0.58**	41.74	0.9872	0.0094	12.22	0.8593	**0.1407**
2	**0.60**	45.56	0.9922	0.0058	13.93	0.8743	**0.1257**
3	**0.86**	36.13	0.9760	0.0186	8.72	0.8133	**0.1867**
4	**0.82**	43.70	0.9900	0.0075	9.52	0.8263	**0.1737**
5	**0.83**	45.31	0.9908	0.0066	16.39	0.8914	**0.1086**
6	**0.79**	41.30	0.9860	0.0103	9.76	0.8307	**0.1693**
7	**0.66**	40.20	0.9843	0.0119	10.07	0.8349	**0.1651**
8	**0.54**	41.21	0.9860	0.0103	11.60	0.8531	**0.1469**
9	**0.85**	38.56	0.9826	0.0134	10.07	0.8349	**0.1651**
10	**0.69**	37.42	0.9782	0.0164	15.07	0.8831	**0.1169**
11	**0.69**	37.59	0.9806	0.0147	7.38	0.7875	**0.2125**
12	**0.85**	41.56	0.9872	0.0094	7.75	0.7962	**0.2038**
13	**0.61**	33.24	0.9642	0.0255	8.45	0.8097	**0.1903**
14	**0.74**	44.11	0.9900	0.0075	12.71	0.8641	**0.1359**
15	**0.57**	40.24	0.9843	0.0119	10.95	0.8463	**0.1537**
16	**0.64**	43.06	0.9887	0.0086	14.43	0.8781	**0.1219**
17	**0.81**	43.06	0.9887	0.0086	9.82	0.8307	**0.1693**
18	**0.64**	37.20	0.9782	0.0164	6.78	0.7731	**0.2269**
19	**0.64**	39.70	0.9843	0.0119	6.86	0.7756	**0.2244**
20	**0.49**	39.93	0.9843	0.0119	8.00	0.8002	**0.1998**
21	**0.87**	38.69	0.9826	0.0134	8.90	0.8167	**0.1833**
22	**0.61**	39.59	0.9843	0.0119	8.98	0.8184	**0.1816**
23	**0.75**	47.83	0.9936	0.0049	17.11	0.8953	**0.1047**
24	**0.67**	41.87	0.9872	0.0094	11.00	0.8463	**0.1537**
25	**0.66**	41.45	0.9860	0.0103	9.17	0.8216	**0.1784**
26	**0.68**	42.59	0.9887	0.0086	9.91	0.8321	**0.1679**
27	**0.53**	37.68	0.9806	0.0147	11.02	0.8463	**0.1537**
28	**0.77**	38.79	0.9826	0.0134	8.20	0.8042	**0.1958**
29	**0.57**	37.26	0.9782	0.0164	4.40	0.6882	**0.3118**
30	**0.44**	40.29	0.9843	0.0119	12.99	0.8668	**0.1332**
31	**0.81**	42.45	0.9872	0.0094	16.72	0.8931	**0.1069**
32	**0.44**	41.66	0.9872	0.0094	10.46	0.8402	**0.1598**
33	**0.61**	45.73	0.9922	0.0058	13.53	0.8711	**0.1289**
34	**0.83**	43.22	0.9887	0.0086	12.21	0.8593	**0.1407**
35	**0.66**	40.54	0.9860	0.0103	10.93	0.8451	**0.1549**

36	**0.70**	44.77	0.9908	0.0066	11.33	0.8498	**0.1502**
37	**0.68**	40.23	0.9843	0.0119	16.46	0.8920	**0.1080**
38	**0.80**	41.45	0.9860	0.0103	9.02	0.8184	**0.1816**
39	**0.69**	38.51	0.9826	0.0134	8.95	0.8184	**0.1816**
40	**0.59**	45.50	0.9922	0.0058	12.68	0.8641	**0.1359**
41	**0.59**	38.59	0.9826	0.0134	8.54	0.8097	**0.1903**
42	**0.47**	38.39	0.9806	0.0147	11.97	0.8573	**0.1427**
43	**0.76**	39.33	0.9826	0.0134	7.89	0.7982	**0.2018**
44	**0.66**	41.77	0.9872	0.0094	9.81	0.8307	**0.1693**
45	**0.37**	39.26	0.9826	0.0134	6.87	0.7756	**0.2244**
46	**0.43**	40.28	0.9843	0.0119	9.05	0.8200	**0.1800**
47	**0.67**	44.93	0.9908	0.0066	12.89	0.8659	**0.1341**
48	**0.68**	38.04	0.9806	0.0147	8.67	0.8133	**0.1867**
49	**0.71**	40.13	0.9843	0.0119	10.92	0.8451	**0.1549**
50	**0.57**	41.92	0.9872	0.0094	11.32	0.8498	**0.1502**
51	**0.69**	42.05	0.9872	0.0094	8.28	0.8061	**0.1939**
52	**0.58**	37.23	0.9782	0.0164	5.62	0.7373	**0.2627**
53	**0.40**	34.03	0.9692	0.0231	11.01	0.8463	**0.1537**
54	**0.49**	43.04	0.9887	0.0086	12.81	0.8650	**0.1350**
55	**0.09**	40.68	0.9860	0.0103	9.70	0.8292	**0.1708**
56	**0.28**	39.99	0.9843	0.0119	9.95	0.8335	**0.1665**
57	**0.30**	39.71	0.9843	0.0119	9.26	0.8232	**0.1768**
58	**0.27**	37.22	0.9782	0.0164	10.06	0.8349	**0.1651**
59	**0.46**	41.96	0.9872	0.0094	8.55	0.8115	**0.1885**
60	**0.42**	40.13	0.9843	0.0119	11.64	0.8531	**0.1469**
61	**0.35**	42.20	0.9872	0.0094	12.13	0.8583	**0.1417**
62	**0.22**	44.12	0.9900	0.0075	15.13	0.8831	**0.1169**
63	**0.79**	43.47	0.9887	0.0086	11.33	0.8498	**0.1502**
64	**0.43**	44.15	0.9900	0.0075	10.41	0.8389	**0.1611**
65	**0.72**	43.93	0.9900	0.0075	11.89	0.8562	**0.1438**
66	**0.26**	42.67	0.9887	0.0086	12.59	0.8631	**0.1369**
67	**0.80**	43.07	0.9887	0.0086	9.90	0.8321	**0.1679**
68	**0.62**	48.31	0.9936	0.0049	15.42	0.8851	**0.1149**
69	**0.82**	42.79	0.9887	0.0086	12.57	0.8631	**0.1369**
70	**0.72**	43.63	0.9900	0.0075	14.45	0.8789	**0.1211**
71	**0.63**	40.32	0.9843	0.0119	12.68	0.8641	**0.1359**
72	**0.40**	44.70	0.9908	0.0066	12.94	0.8659	**0.1341**
73	**0.45**	45.26	0.9908	0.0066	13.63	0.8719	**0.1281**
74	**0.77**	46.28	0.9922	0.0058	6.76	0.7731	**0.2269**
75	**0.65**	31.93	0.9610	0.0285	7.96	0.8002	**0.1998**
76	**0.81**	36.74	0.9782	0.0164	7.32	0.7852	**0.2148**
77	**0.87**	23.19	0.8958	0.0750	13.53	0.8711	**0.1289**
78	**0.80**	42.55	0.9887	0.0086	12.09	0.8583	**0.1417**
79	**0.75**	25.79	0.9263	0.0548	12.68	0.8641	**0.1359**
80	**0.76**	47.68	0.9936	0.0049	13.69	0.8727	**0.1273**
81	**0.59**	42.65	0.9887	0.0086	10.94	0.8451	**0.1549**
82	**0.73**	34.70	0.9723	0.0207	8.98	0.8184	**0.1816**
83	**0.35**	44.45	0.9900	0.0075	14.15	0.8766	**0.1234**
84	**0.70**	41.01	0.9860	0.0103	12.93	0.8659	**0.1341**
85	**0.83**	47.26	0.9931	0.0054	21.82	0.9160	**0.0840**
86	**0.85**	49.56	0.9949	0.0038	18.29	0.9015	**0.0985**
87	**0.85**	52.51	0.9964	0.0026	20.21	0.9100	**0.0900**

88	**0.82**	46.35	0.9922	0.0058	15.76	0.8877	**0.1123**
89	**0.72**	47.92	0.9936	0.0049	15.98	0.8890	**0.1110**
90	**0.67**	40.81	0.9860	0.0103	14.87	0.8817	**0.1183**
91	**0.24**	45.48	0.9908	0.0066	13.60	0.8719	**0.1281**
92	**0.78**	41.28	0.9860	0.0103	10.60	0.8414	**0.1586**
93	**0.80**	43.64	0.9900	0.0075	10.25	0.8376	**0.1624**
94	**0.85**	40.47	0.9843	0.0119	8.30	0.8061	**0.1939**
95	**0.34**	43.00	0.9887	0.0086	9.68	0.8292	**0.1708**
96	**0.38**	44.64	0.9908	0.0066	10.24	0.8362	**0.1638**
97	**0.56**	42.79	0.9887	0.0086	15.94	0.8883	**0.1117**
98	**0.72**	38.97	0.9826	0.0134	10.76	0.8439	**0.1561**
99	**0.33**	36.93	0.9782	0.0164	4.46	0.6930	**0.3070**
100	**0.62**	44.25	0.9900	0.0075	11.35	0.8509	**0.1491**
101	**0.58**	34.43	0.9692	0.0231	10.10	0.8349	**0.1651**
102	**0.84**	36.37	0.9760	0.0186	9.25	0.8232	**0.1768**
103	**0.80**	43.85	0.9900	0.0075	15.86	0.8883	**0.1117**
104	**0.52**	36.37	0.9760	0.0186	8.92	0.8167	**0.1833**
105	**0.70**	40.82	0.9860	0.0103	8.42	0.8079	**0.1921**
106	**0.81**	38.87	0.9826	0.0134	9.67	0.8292	**0.1708**
107	**0.43**	39.26	0.9826	0.0134	6.49	0.7651	**0.2349**
108	**0.69**	39.27	0.9826	0.0134	9.74	0.8292	**0.1708**
109	**0.78**	43.10	0.9887	0.0086	12.06	0.8583	**0.1417**
110	**0.61**	36.15	0.9760	0.0186	9.81	0.8307	**0.1693**
111	**0.38**	35.81	0.9760	0.0186	5.36	0.7302	**0.2698**
112	**0.57**	39.63	0.9843	0.0119	6.30	0.7594	**0.2406**
113	**0.40**	40.40	0.9843	0.0119	7.34	0.7852	**0.2148**
114	**0.42**	43.44	0.9887	0.0086	12.30	0.8603	**0.1397**
115	**0.72**	40.95	0.9860	0.0103	11.87	0.8562	**0.1438**
116	**0.82**	39.90	0.9843	0.0119	13.63	0.8719	**0.1281**
117	**0.77**	35.60	0.9760	0.0186	6.34	0.7594	**0.2406**
118	**0.65**	36.66	0.9782	0.0164	9.79	0.8307	**0.1693**
119	**0.39**	41.77	0.9872	0.0094	11.68	0.8541	**0.1459**
120	**0.71**	46.31	0.9922	0.0058	13.68	0.8727	**0.1273**
121	**0.61**	41.86	0.9872	0.0094	10.92	0.8451	**0.1549**
122	**0.30**	37.23	0.9782	0.0164	6.87	0.7756	**0.2244**
124	**0.75**	45.43	0.9908	0.0066	20.77	0.9123	**0.0877**
125	**0.39**	43.60	0.9900	0.0075	10.06	0.8349	**0.1651**
126	**0.61**	37.07	0.9782	0.0164	7.94	0.7982	**0.2018**
127	**0.68**	45.94	0.9922	0.0058	14.89	0.8817	**0.1183**
128	**0.25**	41.93	0.9872	0.0094	11.21	0.8486	**0.1514**
129	**0.66**	46.43	0.9922	0.0058	16.14	0.8896	**0.1104**
130	**0.46**	48.96	0.9944	0.0040	16.22	0.8902	**0.1098**
131	**0.83**	48.33	0.9936	0.0049	15.56	0.8864	**0.1136**
132	**0.62**	47.47	0.9931	0.0054	15.69	0.8871	**0.1129**
133	**0.63**	38.40	0.9806	0.0147	6.11	0.7535	**0.2465**
134	**0.42**	40.11	0.9843	0.0119	9.93	0.8321	**0.1679**
135	**0.44**	39.77	0.9843	0.0119	10.44	0.8389	**0.1611**
136	**0.86**	37.26	0.9782	0.0164	10.84	0.8439	**0.1561**
137	**0.83**	41.16	0.9860	0.0103	11.31	0.8498	**0.1502**
138	**0.64**	39.89	0.9843	0.0119	10.07	0.8349	**0.1651**
139	**0.62**	40.64	0.9860	0.0103	8.87	0.8167	**0.1833**
140	**0.64**	38.33	0.9806	0.0147	11.52	0.8520	**0.1480**

141	**0.67**	48.56	0.9944	0.0040	16.59	0.8925	**0.1075**
142	**0.40**	42.84	0.9887	0.0086	8.42	0.8079	**0.1921**
143	**0.33**	42.29	0.9872	0.0094	9.52	0.8263	**0.1737**
144	**0.75**	44.60	0.9908	0.0066	11.64	0.8531	**0.1469**
145	**0.60**	41.67	0.9872	0.0094	13.74	0.8727	**0.1273**
146	**0.61**	43.78	0.9900	0.0075	12.53	0.8622	**0.1378**
148	**0.34**	43.61	0.9900	0.0075	16.14	0.8896	**0.1104**
149	**0.30**	40.42	0.9843	0.0119	9.42	0.8247	**0.1753**
150	**0.55**	38.91	0.9826	0.0134	10.90	0.8451	**0.1549**
151	**0.74**	38.42	0.9806	0.0147	8.76	0.8150	**0.1850**
152	**0.36**	39.02	0.9826	0.0134	7.38	0.7875	**0.2125**
153	**0.81**	43.82	0.9900	0.0075	12.26	0.8603	**0.1397**

Table 3 The SNR, SCR and Uncertainty of the ETO Parameter for Tyndall Targets.

Target #	**True Orient(deg.)**	**ETO (deg.)**	SNR (dB)	SNR Biased ETO (deg.)	STD (degree)	SCR (dB)	SCR Biased ETO (deg.)	**Uncertainty (degree)**
1	**0**	**48**	41.74	0.03	0.32	12.22	0.47	**0.47**
2	**45**	**70**	45.56	0.01	0.20	13.93	0.41	**0.41**
3	**90**	**90**	36.13	0.02	0.61	8.72	0.66	**0.66**
4	**0**	**31**	43.70	0.00	0.25	9.52	0.60	**0.60**
5	**30**	**35**	45.31	0.01	0.24	16.39	0.35	**0.35**
6	**0**	**-61**	41.30	0.01	0.34	9.76	0.58	**0.58**
7	**60**	**-19**	40.20	0.00	0.42	10.07	0.57	**0.57**
8	**0**	**-20**	41.21	0.01	0.34	11.60	0.49	**0.49**
9	**30**	**37**	38.56	0.01	0.46	10.07	0.57	**0.57**
10	**30**	**42**	37.42	0.03	0.56	15.07	0.38	**0.56**
11	**30**	**11**	37.59	0.02	0.49	7.38	0.77	**0.77**
12	**30**	**20**	41.56	0.03	0.32	7.75	0.73	**0.73**
13	**30**	**26**	33.24	0.03	0.91	8.45	0.67	**0.91**
14	**30**	**56**	44.11	0.00	0.25	12.71	0.45	**0.45**
15	**60**	**100**	40.24	0.00	0.42	10.95	0.52	**0.52**
16	**45**	**45**	43.06	0.01	0.28	14.43	0.40	**0.40**
17	**0**	**-1**	43.06	0.01	0.28	9.82	0.58	**0.58**
18	**0**	**95**	37.20	0.03	0.56	6.78	0.84	**0.84**
19	**90**	**96**	39.70	0.00	0.42	6.86	0.83	**0.83**
20	**0**	**-10**	39.93	0.00	0.42	8.00	0.72	**0.72**
21	**45**	**95**	38.69	0.01	0.46	8.90	0.64	**0.64**
22	**0**	**27**	39.59	0.00	0.42	8.98	0.64	**0.64**
23	**45**	**113**	47.83	0.00	0.16	17.11	0.34	**0.34**
24	**90**	**-30**	41.87	0.03	0.32	11.00	0.52	**0.52**
25	**0**	**-7**	41.45	0.01	0.34	9.17	0.62	**0.62**
26	**45**	**32**	42.59	0.01	0.28	9.91	0.58	**0.58**
27	**0**	**54**	37.68	0.02	0.49	11.02	0.52	**0.52**
28	**90**	**92**	38.79	0.01	0.46	8.20	0.70	**0.70**
29	**0**	**9**	37.26	0.03	0.56	4.40	1.30	**1.30**
30	**0**	**-50**	40.29	0.00	0.42	12.99	0.44	**0.44**
31	**0**	**-15**	42.45	0.03	0.32	16.72	0.34	**0.34**
32	**45**	**31**	41.66	0.03	0.32	10.46	0.55	**0.55**
33	**0**	**-6**	45.73	0.01	0.20	13.53	0.42	**0.42**

34	**0**	**17**	43.22	0.01	0.28	12.21	0.47	**0.47**
35	**0**	**6**	40.54	0.01	0.34	10.93	0.53	**0.53**
36	**0**	**31**	44.77	0.01	0.24	11.33	0.51	**0.51**
37	**0**	**-36**	40.23	0.00	0.42	16.46	0.35	**0.42**
38	**45**	**88**	41.45	0.01	0.34	9.02	0.64	**0.64**
39	**60**	**4**	38.51	0.01	0.46	8.95	0.64	**0.64**
40	**0**	**21**	45.50	0.01	0.20	12.68	0.45	**0.45**
41	**30**	**14**	38.59	0.01	0.46	8.54	0.67	**0.67**
42	**0**	**84**	38.39	0.02	0.49	11.97	0.48	**0.49**
43	**30**	**128**	39.33	0.01	0.46	7.89	0.73	**0.73**
44	**45**	**23**	41.77	0.03	0.32	9.81	0.58	**0.58**
45	**0**	**23**	39.26	0.01	0.46	6.87	0.83	**0.83**
46	**45**	**5**	40.28	0.00	0.42	9.05	0.63	**0.63**
47	**30**	**67**	44.93	0.01	0.24	12.89	0.44	**0.44**
48	**15**	**30**	38.04	0.02	0.49	8.67	0.66	**0.66**
49	**30**	**99**	40.13	0.00	0.42	10.92	0.53	**0.53**
50	**30**	**70**	41.92	0.03	0.32	11.32	0.51	**0.51**
51	**0**	**-9**	42.05	0.03	0.32	8.28	0.69	**0.69**
52	**30**	**-38**	37.23	0.03	0.56	5.62	1.02	**1.02**
53	**0**	**50**	34.03	0.04	0.76	11.01	0.52	**0.76**
54	**0**	**13**	43.04	0.01	0.28	12.81	0.45	**0.45**
55	**0**	**74**	40.68	0.01	0.34	9.70	0.59	**0.59**
56	**0**	**-6**	39.99	0.00	0.42	9.95	0.57	**0.57**
57	**0**	**76**	39.71	0.00	0.42	9.26	0.62	**0.62**
58	**0**	**-69**	37.22	0.03	0.56	10.06	0.57	**0.57**
59	**0**	**60**	41.96	0.03	0.32	8.55	0.67	**0.67**
60	**0**	**59**	40.13	0.00	0.42	11.64	0.49	**0.49**
61	**0**	**-18**	42.20	0.03	0.32	12.13	0.47	**0.47**
62	**0**	**-6**	44.12	0.00	0.25	15.13	0.38	**0.38**
63	**0**	**35**	43.47	0.01	0.28	11.33	0.51	**0.51**
64	**0**	**-68**	44.15	0.00	0.25	10.41	0.55	**0.55**
65	**0**	**24**	43.93	0.00	0.25	11.89	0.48	**0.48**
66	**0**	**37**	42.67	0.01	0.28	12.59	0.45	**0.45**
67	**0**	**8**	43.07	0.01	0.28	9.90	0.58	**0.58**
68	**0**	**-2**	48.31	0.00	0.16	15.42	0.37	**0.37**
69	**0**	**90**	42.79	0.01	0.28	12.57	0.45	**0.45**
70	**0**	**-1**	43.63	0.00	0.25	14.45	0.40	**0.40**
71	**0**	**-83**	40.32	0.00	0.42	12.68	0.45	**0.45**
72	**0**	**-1**	44.70	0.01	0.24	12.94	0.44	**0.44**
73	**0**	**-78**	45.26	0.01	0.24	13.63	0.42	**0.42**
74	**0**	**17**	46.28	0.01	0.20	6.76	0.84	**0.84**
75	**0**	**-20**	31.93	0.06	1.01	7.96	0.72	**1.01**
76	**0**	**13**	36.74	0.03	0.56	7.32	0.78	**0.78**
77	**0**	**5**	23.19	0.05	2.92	13.53	0.42	**2.92**
78	**0**	**-11**	42.55	0.01	0.28	12.09	0.47	**0.47**
79	**0**	**8**	25.79	0.03	1.99	12.68	0.45	**1.99**
80	**0**	**-6**	47.68	0.00	0.16	13.69	0.42	**0.42**
81	**0**	**-21**	42.65	0.01	0.28	10.94	0.53	**0.53**
82	**0**	**94**	34.70	0.04	0.72	8.98	0.64	**0.72**
83	**0**	**43**	44.45	0.00	0.25	14.15	0.40	**0.40**
84	**0**	**-81**	41.01	0.01	0.34	12.93	0.44	**0.44**
85	**0**	**8**	47.26	0.00	0.18	21.82	0.26	**0.26**

86	**0**	**6**	49.56	0.00	0.13	18.29	0.31	**0.31**
87	**0**	**21**	52.51	0.00	0.09	20.21	0.28	**0.28**
88	**0**	**-4**	46.35	0.01	0.20	15.76	0.36	**0.36**
89	**0**	**71**	47.92	0.00	0.16	15.98	0.36	**0.36**
90	**0**	**0**	40.81	0.01	0.34	14.87	0.38	**0.38**
91	**0**	**-70**	45.48	0.01	0.24	13.60	0.42	**0.42**
92	**0**	**15**	41.28	0.01	0.34	10.60	0.54	**0.54**
93	**0**	**6**	43.64	0.00	0.25	10.25	0.56	**0.56**
94	**0**	**33**	40.47	0.00	0.42	8.30	0.69	**0.69**
95	**45**	**23**	43.00	0.01	0.28	9.68	0.59	**0.59**
96	**0**	**19**	44.64	0.01	0.24	10.24	0.56	**0.56**
97	**0**	**0**	42.79	0.01	0.28	15.94	0.36	**0.36**
98	**0**	**-32**	38.97	0.01	0.46	10.76	0.53	**0.53**
99	**0**	**66**	36.93	0.03	0.56	4.46	1.27	**1.27**
100	**0**	**-84**	44.25	0.00	0.25	11.35	0.50	**0.50**
101	**290**	**142**	34.43	0.04	0.76	10.10	0.57	**0.76**
102	**270**	**66**	36.37	0.02	0.61	9.25	0.62	**0.62**
103	**260**	**76**	43.85	0.00	0.25	15.86	0.36	**0.36**
104	**0**	**-55**	36.37	0.02	0.61	8.92	0.64	**0.64**
105	**90**	**173**	40.82	0.01	0.34	8.42	0.68	**0.68**
106	**0**	**-57**	38.87	0.01	0.46	9.67	0.59	**0.59**
107	**0**	**163**	39.26	0.01	0.46	6.49	0.88	**0.88**
108	**0**	**90**	39.27	0.01	0.46	9.74	0.59	**0.59**
109	**0**	**45**	43.10	0.01	0.28	12.06	0.47	**0.47**
110	**90**	**69**	36.15	0.02	0.61	9.81	0.58	**0.61**
111	**0**	**44**	35.81	0.02	0.61	5.36	1.06	**1.06**
112	**90**	**141**	39.63	0.00	0.42	6.30	0.91	**0.91**
113	**0**	**-17**	40.40	0.00	0.42	7.34	0.78	**0.78**
114	**90**	**10**	43.44	0.01	0.28	12.30	0.47	**0.47**
115	**30**	**-71**	40.95	0.01	0.34	11.87	0.48	**0.48**
116	**150**	**144**	39.90	0.00	0.42	13.63	0.42	**0.42**
117	**60**	**42**	35.60	0.02	0.61	6.34	0.91	**0.91**
118	**0**	**10**	36.66	0.03	0.56	9.79	0.58	**0.58**
119	**0**	**-31**	41.77	0.03	0.32	11.68	0.49	**0.49**
120	**0**	**-91**	46.31	0.01	0.20	13.68	0.42	**0.42**
121	**45**	**132**	41.86	0.03	0.32	10.92	0.53	**0.53**
122	**60**	**42**	37.23	0.03	0.56	6.87	0.83	**0.83**
124	**90**	**79**	45.43	0.01	0.24	20.77	0.28	**0.28**
125	**45**	**22**	43.60	0.00	0.25	10.06	0.57	**0.57**
126	**60**	**66**	37.07	0.03	0.56	7.94	0.73	**0.73**
127	**0**	**79**	45.94	0.01	0.20	14.89	0.38	**0.38**
128	**0**	**34**	41.93	0.03	0.32	11.21	0.51	**0.51**
129	**0**	**7**	46.43	0.01	0.20	16.14	0.36	**0.36**
130	**0**	**9**	48.96	0.01	0.14	16.22	0.35	**0.35**
131	**0**	**65**	48.33	0.00	0.16	15.56	0.37	**0.37**
132	**0**	**62**	47.47	0.00	0.18	15.69	0.36	**0.36**
133	**0**	**-86**	38.40	0.02	0.49	6.11	0.94	**0.94**
134	**0**	**87**	40.11	0.00	0.42	9.93	0.58	**0.58**
135	**0**	**-79**	39.77	0.00	0.42	10.44	0.55	**0.55**
136	**0**	**60**	37.26	0.03	0.56	10.84	0.53	**0.56**
137	**90**	**146**	41.16	0.01	0.34	11.31	0.51	**0.51**
138	**45**	**51**	39.89	0.00	0.42	10.07	0.57	**0.57**

139	**100**	**123**	40.64	0.01	0.34	8.87	0.64	**0.64**
140	**0**	**3**	38.33	0.02	0.49	11.52	0.50	**0.50**
141	**0**	**5**	48.56	0.01	0.14	16.59	0.35	**0.35**
142	**45**	**9**	42.84	0.01	0.28	8.42	0.68	**0.68**
143	**45**	**35**	42.29	0.03	0.32	9.52	0.60	**0.60**
144	**0**	**-5**	44.60	0.01	0.24	11.64	0.49	**0.49**
145	**45**	**39**	41.67	0.03	0.32	13.74	0.42	**0.42**
146	**10**	**16**	43.78	0.00	0.25	12.53	0.46	**0.46**
148	**0**	**-47**	43.61	0.00	0.25	16.14	0.36	**0.36**
149	**0**	**39**	40.42	0.00	0.42	9.42	0.61	**0.61**
150	**0**	**28**	38.91	0.01	0.46	10.90	0.53	**0.53**
151	**0**	**24**	38.42	0.02	0.49	8.76	0.65	**0.65**
152	**0**	**3**	39.02	0.01	0.46	7.38	0.77	**0.77**
153	**150**	**154**	43.82	0.00	0.25	12.26	0.47	**0.47**

Table 4 The SNR and Uncertainty the ETL Parameter for Tyndall Targets.

Target #	**True Length (m)**	**ETL (m)**	SNR (dB)	STD	Uncertainty* (m)
1	**0.35**	**0.35**	41.74	0.000212	0.0003
2	**0.35**	**0.53**	45.56	0.000115	0.0004
3	**0.35**	**0.52**	36.13	0.000335	0.0012
4	**0.35**	**0.78**	43.70	0.000179	0.0015
5	**0.35**	**0.60**	45.31	0.000115	0.0006
6	**0.35**	**0.28**	41.30	0.000212	0.0002
7	**0.35**	**0.37**	40.20	0.000205	0.0004
8	**0.35**	**0.25**	41.21	0.000212	0.0002
9	**0.64**	**1.68**	38.56	0.000205	0.0077
10	**0.64**	**1.01**	37.42	0.000263	0.0036
11	**0.35**	**0.39**	37.59	0.000263	0.0005
12	**0.35**	**0.47**	41.56	0.000212	0.0006
13	**0.35**	**0.56**	33.24	0.000408	0.0017
14	**0.35**	**0.59**	44.11	0.000179	0.0008
15	**0.35**	**0.46**	40.24	0.000205	0.0006
16	**0.35**	**0.39**	43.06	0.000179	0.0004
17	**0.35**	**0.37**	43.06	0.000179	0.0003
18	**0.35**	**0.37**	37.20	0.000263	0.0005
19	**0.35**	**0.32**	39.70	0.000205	0.0003
20	**0.64**	**0.70**	39.93	0.000205	0.0013
21	**0.64**	**0.85**	38.69	0.000205	0.0020
22	**0.23**	**0.26**	39.59	0.000205	0.0002
23	**0.23**	**0.41**	47.83	0.000090	0.0002
24	**0.23**	**0.25**	41.87	0.000212	0.0002
25	**0.23**	**0.24**	41.45	0.000212	0.0002
26	**0.23**	**0.36**	42.59	0.000179	0.0003
27	**0.15**	**1.44**	37.68	0.000263	0.0072
28	**1.20**	**0.62**	38.79	0.000205	0.0010
29	**1.20**	**0.83**	37.26	0.000263	0.0024

* This uncertainty considers only the effect of random noise. The major uncertainty is caused by the presence of clutter and the error in estimating soil permittivity.

30	**0.30**	**0.75**	40.29	0.000205	0.0015
31	**0.30**	**0.58**	42.45	0.000212	0.0009
32	**0.11**	**0.53**	41.66	0.000212	0.0008
33	**0.27**	**0.38**	45.73	0.000115	0.0002
34	**0.30**	**0.28**	43.22	0.000179	0.0002
35	**0.40**	**1.18**	40.54	0.000212	0.0039
36	**0.60**	**0.72**	44.77	0.000115	0.0008
37	**0.60**	**0.43**	40.23	0.000205	0.0005
38	**0.25**	**0.18**	41.45	0.000212	0.0001
39	**0.60**	**0.67**	38.51	0.000205	0.0012
40	**0.60**	**0.55**	45.50	0.000115	0.0005
41	**0.60**	**0.78**	38.59	0.000205	0.0017
42	**0.60**	**0.51**	38.39	0.000263	0.0009
43	**0.86**	**0.38**	39.33	0.000205	0.0004
44	**0.86**	**1.05**	41.77	0.000212	0.0031
45	**0.91**	**1.40**	39.26	0.000205	0.0053
46	**0.91**	**0.15**	40.28	0.000205	0.0001
47	**2.70**	**2.23**	44.93	0.000115	0.0076
48	**1.00**	**1.19**	38.04	0.000263	0.0049
49	**1.00**	**0.32**	40.13	0.000205	0.0003
50	**1.00**	**0.95**	41.92	0.000212	0.0025
51	**0.50**	**0.65**	42.05	0.000212	0.0012
52	**0.50**	**0.56**	37.23	0.000263	0.0011
53	**0.05**	**0.30**	34.03	0.000408	0.0005
54	**0.05**	**0.45**	43.04	0.000179	0.0005
55	**0.05**	**0.19**	40.68	0.000212	0.0001
56	**0.05**	**0.16**	39.99	0.000205	0.0001
57	**0.05**	**1.11**	39.71	0.000205	0.0034
58	**0.05**	**2.45**	37.22	0.000263	0.0209
59	**0.05**	**1.22**	41.96	0.000212	0.0042
60	**0.05**	**1.52**	40.13	0.000205	0.0063
61	**0.05**	**0.71**	42.20	0.000212	0.0014
62	**0.05**	**0.21**	44.12	0.000179	0.0001
63	**0.40**	**0.46**	43.47	0.000179	0.0005
64	**0.40**	**0.71**	44.15	0.000179	0.0012
65	**0.40**	**0.60**	43.93	0.000179	0.0009
66	**0.40**	**0.32**	42.67	0.000179	0.0002
67	**0.40**	**0.82**	43.07	0.000179	0.0016
68	**0.30**	**0.38**	48.31	0.000090	0.0002
69	**0.30**	**0.62**	42.79	0.000179	0.0009
70	**0.30**	**0.51**	43.63	0.000179	0.0006
71	**0.30**	**0.30**	40.32	0.000205	0.0002
72	**0.30**	**0.90**	44.70	0.000115	0.0012
73	**0.30**	**0.29**	45.26	0.000115	0.0001
74	**0.30**	**0.39**	46.28	0.000115	0.0002
75	**0.60**	**0.69**	31.93	0.000499	0.0032
76	**0.90**	**1.06**	36.74	0.000263	0.0039
77	**0.30**	**0.40**	23.19	0.001236	0.0026
78	**0.60**	**0.85**	42.55	0.000179	0.0017
79	**0.90**	**1.53**	25.79	0.000954	0.0292
80	**0.08**	**0.28**	47.68	0.000090	0.0001
81	**0.08**	**0.29**	42.65	0.000179	0.0002

82	**NA**	**0.52**	34.70	0.000335	0.0012
83	**NA**	**0.60**	44.45	0.000179	0.0009
84	**NA**	**1.05**	41.01	0.000212	0.0031
85	**0.91**	**1.02**	47.26	0.000090	0.0013
86	**0.50**	**0.56**	49.56	0.000073	0.0003
87	**0.64**	**0.99**	52.51	0.000048	0.0006
88	**0.64**	**0.95**	46.35	0.000115	0.0014
89	**1.82**	**0.39**	47.92	0.000090	0.0002
90	**NA**	**1.38**	40.81	0.000212	0.0054
91	**0.30**	**0.71**	45.48	0.000115	0.0008
92	**1.22**	**2.22**	41.28	0.000212	0.0138
93	**NA**	**0.80**	43.64	0.000179	0.0015
94	**NA**	**1.54**	40.47	0.000205	0.0064
95	**NA**	**0.59**	43.00	0.000179	0.0008
96	**NA**	**1.30**	44.64	0.000115	0.0026
97	**0.43**	**1.45**	42.79	0.000179	0.0050
98	**0.43**	**0.55**	38.97	0.000205	0.0008
99	**0.30**	**0.39**	36.93	0.000263	0.0005
100	**0.30**	**0.32**	44.25	0.000179	0.0002
101	**1.00**	**0.39**	34.43	0.000408	0.0008
102	**1.09**	**0.60**	36.37	0.000335	0.0016
103	**0.91**	**1.10**	43.85	0.000179	0.0029
104	**NA**	**0.70**	36.37	0.000335	0.0022
105	**NA**	**0.77**	40.82	0.000212	0.0017
106	**0.48**	**0.53**	38.87	0.000205	0.0008
107	**0.91**	**0.17**	39.26	0.000205	0.0001
108	**NA**	**0.70**	39.27	0.000205	0.0013
109	**0.30**	**0.30**	43.10	0.000179	0.0002
110	**0.30**	**0.35**	36.15	0.000335	0.0005
111	**0.13**	**0.51**	35.81	0.000335	0.0012
112	**0.13**	**0.72**	39.63	0.000205	0.0014
113	**NA**	**0.70**	40.40	0.000205	0.0013
114	**0.13**	**0.21**	43.44	0.000179	0.0001
115	**0.46**	**0.98**	40.95	0.000212	0.0027
116	**0.46**	**0.95**	39.90	0.000205	0.0025
117	**0.46**	**0.68**	35.60	0.000335	0.0021
118	**0.40**	**0.66**	36.66	0.000263	0.0015
119	**0.25**	**1.08**	41.77	0.000212	0.0033
120	**0.46**	**0.49**	46.31	0.000115	0.0004
121	**0.60**	**0.53**	41.86	0.000212	0.0008
122	**1.00**	**0.22**	37.23	0.000263	0.0002
124	**0.46**	**0.49**	45.43	0.000115	0.0004
125	**0.41**	**0.46**	43.60	0.000179	0.0005
126	**0.51**	**0.58**	37.07	0.000263	0.0012
127	**0.30**	**0.63**	45.94	0.000115	0.0006
128	**0.30**	**0.76**	41.93	0.000212	0.0016
129	**0.23**	**0.26**	46.43	0.000115	0.0001
130	**0.30**	**0.38**	48.96	0.000073	0.0001
131	**0.48**	**0.44**	48.33	0.000090	0.0002
132	**NA**	**0.32**	47.47	0.000090	0.0001
133	**0.35**	**0.49**	38.40	0.000263	0.0008
134	**0.30**	**0.78**	40.11	0.000205	0.0017

135	**0.91**	**0.17**	39.77	0.000205	0.0001
136	**NA**	**0.60**	37.26	0.000263	0.0013
137	**0.30**	**1.03**	41.16	0.000212	0.0030
138	**3.60**	**0.22**	39.89	0.000205	0.0001
139	**0.46**	**0.44**	40.64	0.000212	0.0005
140	**0.30**	**0.59**	38.33	0.000263	0.0012
141		**0.53**	48.56	0.000073	0.0003
142	**0.23**	**0.87**	42.84	0.000179	0.0018
143	**0.13**	**0.27**	42.29	0.000212	0.0002
144	**0.23**	**0.33**	44.60	0.000115	0.0002
145	**0.23**	**0.57**	41.67	0.000212	0.0009
146	**0.23**	**0.33**	43.78	0.000179	0.0003
148	**0.15**	**0.81**	43.61	0.000179	0.0016
149	**0.15**	**0.68**	40.42	0.000205	0.0013
150	**0.60**	**0.45**	38.91	0.000205	0.0006
151	**0.60**	**0.62**	38.42	0.000263	0.0013
152	**0.50**	**0.24**	39.02	0.000205	0.0002
153	**1.02**	**1.16**	43.82	0.000179	0.0032

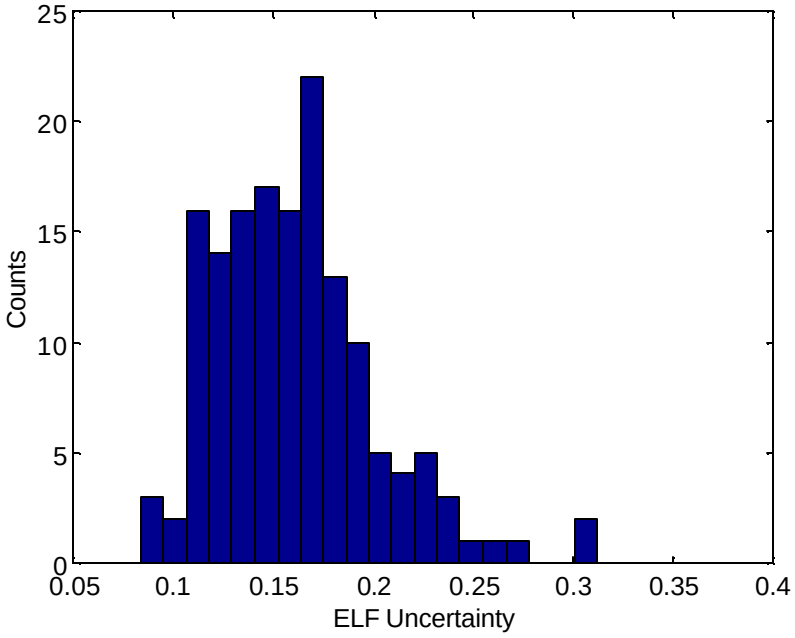

Figure 34 Histogram of the uncertainty of the estimated ELF values.

5.3 Feature Extraction Results for All Tyndall Targets

Table 5 summarizes the estimated depths, orientations and lengths of all Tyndall target in comparison with their true values. It should be noted that for non-linear object the length and orientation estimations are really meaningless. A more meaningful comparison is to compare the estimated length

and orientation with their true values for UXO-like (defined in Table 8, Appendix B:) targets. The histograms of estimation errors for length and orientation are shown in Figure 35 and Figure 36, respectively. As one can see, the length and orientation estimation for more than 50% of the UXO-like targets have length error less than 15 cm and orientation error less than 15 degrees.

Since the depth estimation is based upon the earliest detectable response from a target, it depends on the target geometry and orientations. For instance, a thin, vertical metal bar may have a stronger response coming from the bottom tip. It should be noted that the true depth was measured from the shallowest point of the target. The histograms of the depth estimation error for UXO-like targets only and for all the targets are also provided in Figure 37 and Figure 38, respectively. Both histograms show similar distributions. Over 50% of the targets have estimation error for depth less than 0.2 meters. This result is remarkable considering the wide range of variations of target orientation.

Although these tables and histograms provide useful information general performance of the current system and processing configuration, they are not useful in providing direction of improvements. Section 6.3, we will take a closer look at the features discrepancies for each individual target to gain more insights about the error source and to provide more useful information for future improvements.

Table 5 Comparison of Estimated and True Properties of Targets Buried at Tyndall Site.

No.	Type	True Depth (m)	Est. Depth (m)	True Orient. (deg)	Est. Orient. (deg)	True Length (m)	Est. Length (m)
1	105mm Inert	0.20	0.11	0	48	0.35	0.35
2	105mm Inert	0.20	0.22	45	70	0.35	0.53
3	105mm Inert	0.20	0.53	90	90	0.35	0.52
4	105mm Inert	0.40	0.67	0	31	0.35	0.78
5	105mm Inert	0.24	0.55	30	35	0.35	0.60
6	105mm Inert	0.40	0.31	0	-61	0.35	0.28
7	105mm Inert Heat	0.34	0.38	60	-19	0.35	0.37
8	105mm Inert Heat	0.43	0.50	0	-20	0.35	0.25
9	105mm Inert Sabot	0.60	0.49	30	37	0.64	1.68
10	105mm Inert Sabot	0.86	0.87	30	42	0.64	1.01
11	105mm Inert	0.62	0.86	30	11	0.35	0.39
12	105mm Inert	0.60	0.51	30	20	0.35	0.47
13	105mm Inert	0.50	0.66	30	26	0.35	0.56
14	105mm Inert	0.55	0.70	30	56	0.35	0.59
15	105mm Inert	0.73	0.97	60	100	0.35	0.46
16	105mm Inert	0.62	0.43	45	45	0.35	0.39
17	105mm Inert	0.68	0.59	0	-1	0.35	0.37
18	105mm Inert Heat	0.57	0.52	0	95	0.35	0.37
19	105mm Inert Heat	0.80	0.79	90	96	0.35	0.32
20	105mm Inert Sabot	0.81	1.36	0	-10	0.64	0.70
21	105mm Inert Sabot	0.68	0.62	45	95	0.64	0.85
22	60mm Mortar	0.70	0.66	0	27	0.23	0.26
23	60mm Mortar	0.75	0.30	45	113	0.23	0.41
24	60mm Mortar	0.54	0.78	90	-30	0.23	0.25
25	60mm Mortar	0.40	0.45	0	-7	0.23	0.24
26	60mm Mortar	0.33	0.58	45	32	0.23	0.36
27	20mm Projectile	0.63	0.40	0	54	0.15	1.44
28	MK82 500lb	1.00	1.36	90	92	1.20	0.62
29	MK82 500lb	1.40	1.69	0	9	1.20	0.83
30	75mm hep Projectile	0.50	0.47	0	-50	0.30	0.75
31	90mm Projectile	0.11	0.36	0	-15	0.30	0.58
32	4.2” Mortar	0.30	0.71	45	31	0.11	0.53

33	50 mm Russian Mortar	**0.23**	**0.54**	**0**	**-6**	**0.27**	**0.38**
34	3 " AA Projectile	**0.21**	**0.39**	**0**	**17**	**0.30**	**0.28**
35	BDU33 (Tail only)	**0.50**	**0.71**	**0**	**6**	**0.40**	**1.18**
36	BDU33 (Bent Tail)	**0.36**	**0.71**	**0**	**31**	**0.60**	**0.72**
37	BDU33 (Bent Tail)	**0.40**	**0.07**	**0**	**-36**	**0.60**	**0.43**
38	BDU33 (No Tail)	**0.40**	**0.09**	**45**	**88**	**0.25**	**0.18**
39	BDU33	**0.80**	**0.65**	**60**	**4**	**0.60**	**0.67**
40	BDU33	**0.58**	**0.56**	**0**	**21**	**0.60**	**0.55**
41	BDU33	**0.42**	**0.89**	**30**	**14**	**0.60**	**0.78**
42	BDU33	**0.70**	**1.06**	**0**	**84**	**0.60**	**0.51**
43	155mm	**1.40**	**1.66**	**30**	**128**	**0.86**	**0.38**
44	RR Tie	**0.92**	**1.13**	**45**	**23**	**0.86**	**1.05**
45	55gal Drum	**1.85**	**1.11**	**0**	**23**	**0.91**	**1.40**
46	55gal Drum	**1.46**	**0.31**	**45**	**5**	**0.91**	**0.15**
47	2000lb	**1.40**	**0.96**	**30**	**67**	**2.70**	**2.23**
48	8" Shell	**0.90**	**0.71**	**15**	**30**	**1.00**	**1.19**
49	8" Shell	**0.80**	**0.29**	**30**	**99**	**1.00**	**0.32**
50	8" Shell	**1.43**	**1.23**	**30**	**70**	**1.00**	**0.95**
51	81mm Mortar	**0.80**	**0.70**	**0**	**-9**	**0.50**	**0.65**
52	81mm Mortar	**1.00**	**0.54**	**30**	**-38**	**0.50**	**0.56**
53	Fragment	**0.06**	**0.07**	**0**	**50**	**0.05**	**0.30**
54	Fragment	**0.11**	**0.17**	**0**	**13**	**0.05**	**0.45**
55	Fragment	**0.06**	**0.22**	**0**	**74**	**0.05**	**0.19**
56	Fragment	**0.10**	**0.31**	**0**	**-6**	**0.05**	**0.16**
57	Fragment	**0.33**	**0.43**	**0**	**76**	**0.05**	**1.11**
58	Fragment	**0.30**	**0.57**	**0**	**-69**	**0.05**	**2.45**
59	Fragment	**0.33**	**0.32**	**0**	**60**	**0.05**	**1.22**
60	Fragment	**0.17**	**0.25**	**0**	**59**	**0.05**	**1.52**
61	Fragment	**0.30**	**0.41**	**0**	**-18**	**0.05**	**0.71**
62	Fragment	**0.30**	**0.02**	**0**	**-6**	**0.05**	**0.21**
63	Alum. Barb Wire	**0.10**	**0.07**	**0**	**35**	**0.40**	**0.46**
64	Alum. Barb Wire	**0.12**	**0.11**	**0**	**-68**	**0.40**	**0.71**
65	Alum. Barb Wire	**0.43**	**0.31**	**0**	**24**	**0.40**	**0.60**
66	Alum. Barb Wire	**0.40**	**0.55**	**0**	**37**	**0.40**	**0.32**
67	Alum. Barb Wire	**0.50**	**0.03**	**0**	**8**	**0.40**	**0.82**
68	Steel Plate	**0.17**	**0.47**	**0**	**-2**	**0.30**	**0.38**
69	Steel Plate	**0.30**	**0.69**	**0**	**90**	**0.30**	**0.62**
70	Steel Plate	**0.32**	**0.45**	**0**	**-1**	**0.30**	**0.51**
71	Steel Plate	**0.58**	**0.20**	**0**	**-83**	**0.30**	**0.30**
72	Steel Plate	**0.51**	**0.10**	**0**	**-1**	**0.30**	**0.90**
73	Steel Plate	**0.23**	**0.46**	**0**	**-78**	**0.30**	**0.29**
74	Cal. Metal Pipe*	**0.30**	**0.31**	**0**	**17**	**0.30**	**0.39**
75	Cal. Metal Pipe*	**1.10**	**1.12**	**0**	**-20**	**0.60**	**0.69**
76	Cal. Metal Pipe*	**1.50**	**1.63**	**0**	**13**	**0.90**	**1.06**
77	Cal. Metal Pipe*	**0.12**	**0.34**	**0**	**5**	**0.30**	**0.40**
78	Cal. Metal Pipe*	**0.26**	**0.60**	**0**	**-11**	**0.60**	**0.85**
79	Cal. Metal Pipe*	**0.43**	**0.65**	**0**	**8**	**0.90**	**1.53**
80	Clusters of nails	**0.10**	**0.33**	**0**	**-6**	**0.08**	**0.28**
81	Clusters of nails	**0.57**	**0.41**	**0**	**-21**	**0.08**	**0.29**
82	55 Gal Lid	**0.20**	**0.68**	**0**	**94**	**0.00**	**0.52**
83	55 Gal Lid	**0.40**	**0.55**	**0**	**43**	**0.00**	**0.60**
84	55 Gal Lid	**0.70**	**1.00**	**0**	**-81**	**0.00**	**1.05**
85	Pipes Diverge	**0.20**	**0.17**	**0**	**8**	**0.91**	**1.02**
86	Pipes Diverge	**0.34**	**0.20**	**0**	**6**	**0.50**	**0.56**
87	Pipes Diverge	**0.45**	**0.38**	**0**	**21**	**0.64**	**0.99**
88	Pipes Diverge	**0.55**	**0.49**	**0**	**-4**	**0.64**	**0.95**
89	Pipes Ortho	**0.44**	**0.50**	**0**	**71**	**1.82**	**0.39**
90	Pipes Ortho	**0.46**	**0.68**	**0**	**0**	**0.00**	**1.38**

91	Rebar 90° Arc Mid	**0.53**	**0.09**	**0**	**-70**	**0.30**	**0.71**
92	Rebar 90° Arc End	**0.40**	**0.16**	**0**	**15**	**1.22**	**2.22**
93	Pipes Ortho Attac	**0.65**	**0.87**	**0**	**6**	**0.00**	**0.80**
94	Pipes Ortho Attac	**1.00**	**1.17**	**0**	**33**	**0.00**	**1.54**
95	Paint Can (Open)	**0.12**	**0.41**	**45**	**23**	**0.00**	**0.59**
96	Paint Can (Top On)	**0.45**	**0.60**	**0**	**19**	**0.00**	**1.30**
97	Metal Box	**0.70**	**1.37**	**0**	**0**	**0.43**	**1.45**
98	Metal Box	**0.99**	**0.88**	**0**	**-32**	**0.43**	**0.55**
99	Rebar–strt + bent	**0.58**	**0.88**	**0**	**66**	**0.30**	**0.39**
100	Rebar 90° Mid Arc	**1.60**	**0.37**	**0**	**-84**	**0.30**	**0.32**
101	RR Tie	**1.66**	**1.52**	**290**	**142**	**1.00**	**0.39**
102	160mm Mortar	**1.20**	**1.47**	**270**	**66**	**1.09**	**0.60**
103	Frag (Exploded)	**0.21**	**0.96**	**260**	**76**	**0.91**	**1.10**
104	Tire Rim	**0.70**	**0.46**	**0**	**-55**	**0.00**	**0.70**
105	Base Plate (Fuse)	**0.48**	**0.55**	**90**	**173**	**0.00**	**0.77**
106	Tine (Steel Plate)	**0.79**	**0.49**	**0**	**-57**	**0.48**	**0.53**
107	5” Gun Round	**1.40**	**0.75**	**0**	**163**	**0.91**	**0.17**
108	Tire Rim	**0.66**	**0.47**	**0**	**90**	**0.00**	**0.70**
109	Angle Iron	**0.92**	**1.04**	**0**	**45**	**0.30**	**0.30**
110	Angle Iron	**0.38**	**0.45**	**90**	**69**	**0.30**	**0.35**
111	Soda Can	**0.40**	**1.26**	**0**	**44**	**0.13**	**0.51**
112	Soda Can	**0.41**	**0.33**	**90**	**141**	**0.13**	**0.72**
113	Soda Can Crushed	**0.50**	**0.71**	**0**	**-17**	**0.00**	**0.70**
114	Soda Can Stacked	**0.20**	**0.28**	**90**	**10**	**0.13**	**0.21**
115	Pipe Att End (90°)	**0.77**	**1.08**	**30**	**-71**	**0.46**	**0.98**
116	Pipe Att End (90°)	**0.74**	**0.65**	**150**	**144**	**0.46**	**0.95**
117	Metal Box Open	**0.65**	**0.95**	**60**	**42**	**0.46**	**0.68**
118	Metal Box Closed	**1.00**	**0.30**	**0**	**10**	**0.40**	**0.66**
119	Exploded Scrap (2)	**0.52**	**0.58**	**0**	**-31**	**0.25**	**1.08**
120	Bomb Parts	**0.20**	**0.75**	**0**	**-91**	**0.46**	**0.49**
121	Panel Large	**0.78**	**1.34**	**45**	**132**	**0.60**	**0.53**
122	Scrap & Wire	**0.99**	**0.22**	**60**	**42**	**1.00**	**0.22**
123	Exploded scrap	**0.40**		**30**		**0.00**	
124	Panel Medium	**0.30**	**0.38**	**90**	**79**	**0.46**	**0.49**
125	Looped Pipe	**0.50**	**0.42**	**45**	**22**	**0.41**	**0.46**
126	Exploded Tube	**0.50**	**1.48**	**60**	**66**	**0.51**	**0.58**
127	Mine AT	**0.06**	**0.58**	**0**	**79**		**0.63**
128	Steel Plate Stacked	**0.30**	**0.43**	**0**	**34**	**0.30**	**0.76**
129	60mm Mortar	**0.10**	**0.20**	**0**	**7**	**0.23**	**0.26**
130	Angle Iron (2)	**0.15**	**0.22**	**0**	**9**	**0.30**	**0.38**
131	Scrap Crushed	**0.21**	**0.61**	**0**	**65**	**0.48**	**0.44**
132	Rim	**0.30**	**0.61**	**0**	**62**	**0.00**	**0.32**
133	Plate & 105mm Sb	**0.20**	**0.52**	**0**	**-86**	**0.35**	**0.49**
134	Plate	**0.34**	**0.68**	**0**	**87**	**0.30**	**0.78**
135	Rebar	**1.00**	**0.19**	**0**	**-79**	**0.91**	**0.17**
136	Paint Can Open D	**0.33**	**0.18**	**0**	**60**	**0.00**	**0.60**
137	Rebar 90° Arc Mid	**0.16**	**0.75**	**90**	**146**	**0.30**	**1.03**
138	BDU Bar Fin	**0.12**	**0.28**	**45**	**51**	**3.60**	**0.22**
139	Crushed Box	**0.33**	**0.30**	**100**	**123**	**0.46**	**0.44**
140	Angle Iron (2)	**0.33**	**0.18**	**0**	**3**	**0.30**	**0.59**
141	Mine AT	**0.14**	**0.54**	**0**	**5**		**0.53**
142	60mm Mortar	**0.36**	**0.14**	**45**	**9**	**0.23**	**0.87**
143	Soda Can	**0.10**	**0.55**	**45**	**35**	**0.13**	**0.27**
144	60mm Mortar	**0.30**	**0.50**	**0**	**-5**	**0.23**	**0.33**
145	60mm Mortar	**0.30**	**0.37**	**45**	**39**	**0.23**	**0.57**
146	60mm Mortar	**0.33**	**0.16**	**10**	**16**	**0.23**	**0.33**
147	Scrap Tin Folded	**0.16**		**0**		**0.30**	
148	Sphere	**0.50**	**0.26**	**0**	**-47**	**0.15**	**0.81**

149	Sphere	**0.30**	**0.67**	**0**	**39**	**0.15**	**0.68**
150	UXO	**0.50**	**0.82**	**0**	**28**	**0.60**	**0.45**
151	Pipe	**0.50**	**0.44**	**0**	**24**	**0.60**	**0.62**
152	Rebar	**0.50**	**0.61**	**0**	**3**	**0.50**	**0.24**
153	Rebar	**0.50**	**1.00**	**150**	**154**	**1.02**	**1.16**

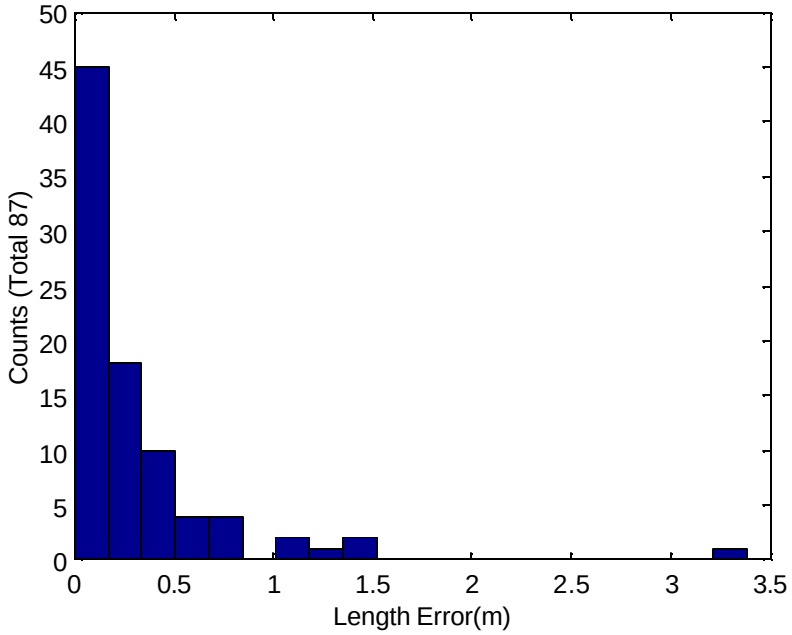

Figure 35 Histogram of the length estimation error for the total 87 UXO-like targets.

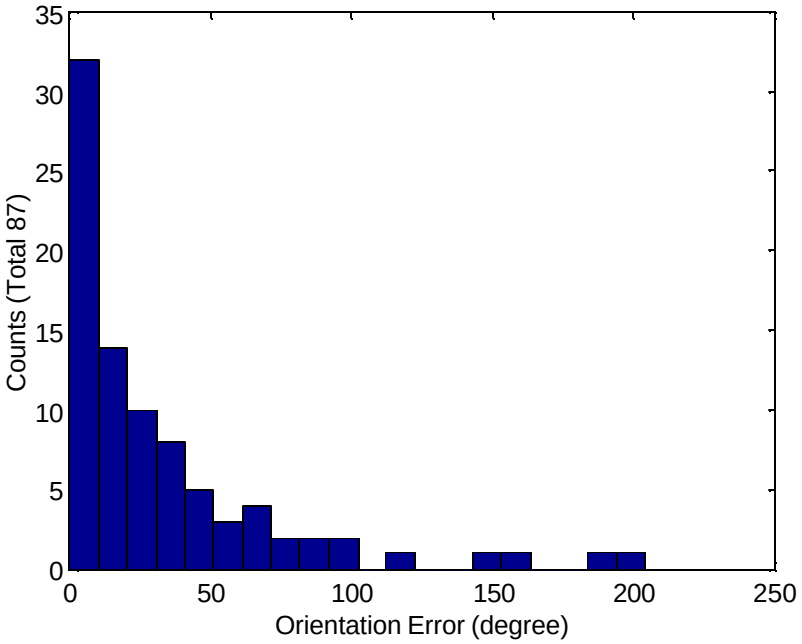

Figure 36 Histogram of the orientation estimation error for the total 87 UXO-like targets.

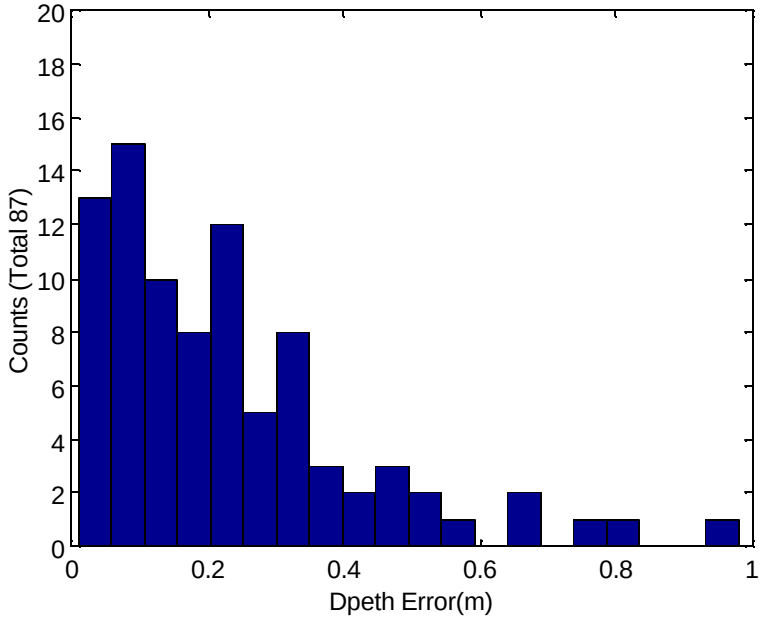

Figure 37 Histogram of the depth estimation error for the total 87 UXO-like targets.

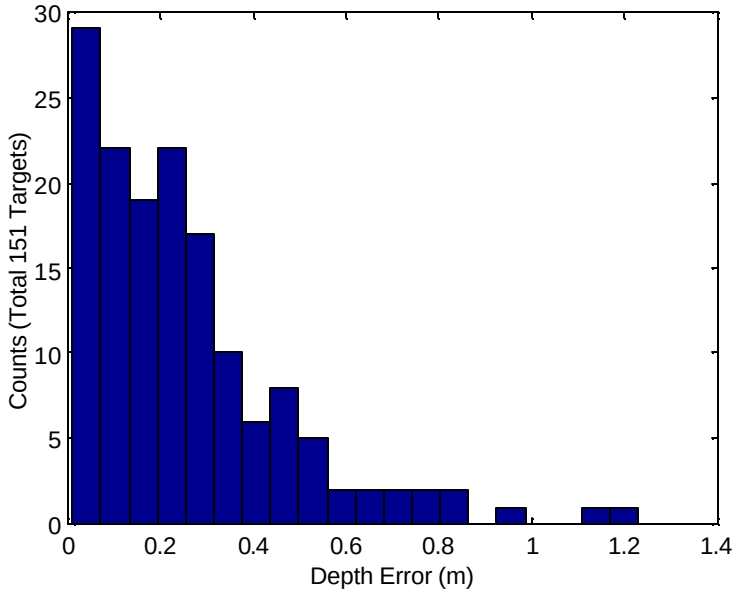

Figure 38 Histogram of the depth estimation error for all the targets.

6 UXO Classification Based On UWB, Fully-Polarimetric GPR Data

6.1 Introduction

The UXO classification performance using the UWB, fully-polarimetric features discussed previously is evaluated here. All Tyndall targets are classified as either UXO-like or non-UXO-like based on the geometry as listed in the last column of Table 8. This designation was done based on the dimensions and photos of each target provided by the Tyndall personnel. UXO-like targets includes elongated objects that have length-to-diameter ratios greater than three. The ground truth of the Tyndall targets can be found in Table 8, Figure 77 and Figure 78. It should be noted that none of the feature extraction process incorporates any of the ground truth information. A low-level UXO-like/Non-UXO classification criteria will be based on the value of ELF+DEN. Such a value is related to the linearity of the target geometry. Conventional ROC curves will be used in conjunction with the ground truth to evaluate the classification performance. In particular, the UXO Detection Rate (DR) and false alarm rate (FAR) will be examined. A second-level classification for UXO types will also be performed based on the UXO length. The specific UXO types to be classified include the 105mm projectile, the 60mm mortar, the 500lb bomb, and the 8in shell.

6.2 UXO-Like Classification Using (ELF+DEN) Criteria

Figure 39 shows the extracted ELF and DEN for Tyndall targets as small dots in a two-dimensional plot. The known targets (see Table 1) whose ground truths were known at the time of measurements are also marked with special symbols. Based on the distribution of the known targets, the (ELF+DEN) criterion was selected to discriminate UXO-like targets. Each different value of (ELF+DEN) corresponds to a 45-degree line in the ELF vs. DEN plot as illustrated by the dashed line for ELF+DEN=1.1. Increasing the (ELF+DEN) threshold will move the threshold line toward the upper-right corner. On the other hand, a lower (ELF+DEN) threshold will move the threshold line toward the lower-left corner. The total range of (ELF+DEN) is from 0 to 2. Recall that both ELF and DEN features are related to the linearity of the target geometry. It should be noted that the natural resonant feature has been implicitly included in both ELF and DEN features since both of them are extracted from the late-time region. A target that is resonant strongly will have a higher SNR in the late-time region and results in more accurate ELF and DEN estimation as discussed in Section 5.2.1. After choosing a threshold value of (ELF+DEN), all the targets having (ELF+DEN) values greater than the threshold are classified as UXO-like targets. These targets correspond to dots locating at the right side of the threshold line. Other targets are subsequently classified as non-UXO targets.

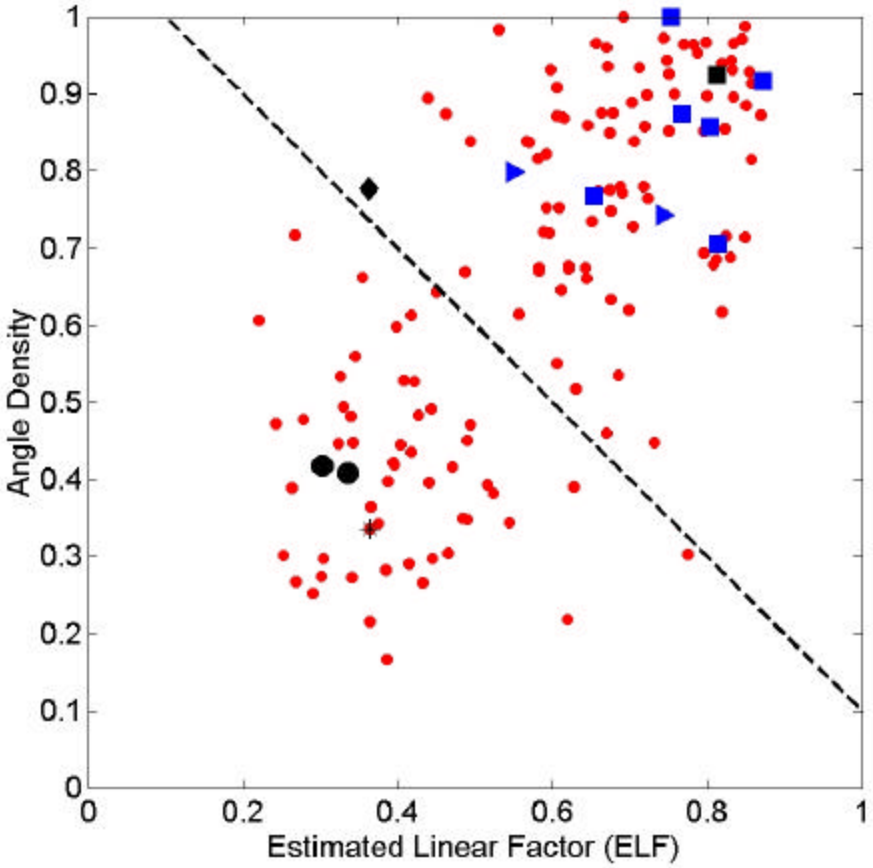

Figure 39 Processed ELF and DEN for each target (red dot). The results for known targets are also indicated by special marks:

Blue squares:	Calibration pipes and rebars.
Blue triangles:	New buried UXO and narrow pipe of similar length (60 cm) buried at 0.5m depth with 45-degree inclination angle.
Black square:	Horizontally buried rebar (depth=0.5 m, length=1.02m);
Black circles:	6" metallic spheres buried at 30cm and 50 cm depths.
Black "*" :	No target site.
Black diamond:	Vertically buried rebar.

Figure 40 plots the same ELF vs. DEN information as in Figure 39, except that all the UXO-like targets are marked with small triangle and all the non-UXO items are marked with small squares based on the designation shown in Table 8. It is noticed that although most UXO-like targets cluster toward the upper-right quadrant, there are significant amount of UXO-like targets located near the lower-left quadrant. These UXO-like targets are most likely to be dropped for a chosen threshold. It is also observed that many non-UXO objects appear in the upper-right quadrant. These objects will most likely be classified as UXO-like targets for a chosen threshold and thus resulting in false alarms. As will be discussed in Section 6.3 with much greater detail, some of these are due to the system limitation of the current configuration and measurement approaches. Here, we will examine the ROC curves anyway to evaluate how the current configuration performs in the classification of UXO.

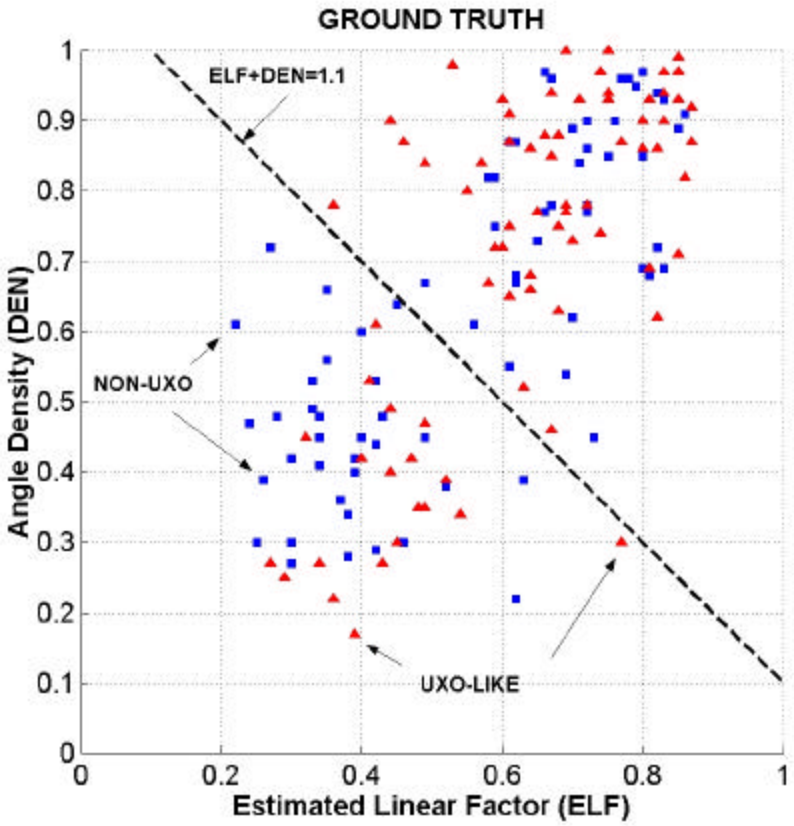

Figure 40 Plot of the ELF vs. DEN for each measurements taken over total target set. Squares indicate non-UXO targets. Triangles indicate UXO-like targets.

6.2.1 Stage 1: Classification for UXO-Like and Non-UXO Discrimination

Figure 41 plots the Detection Rate (DR) vs. the false alarm rate (FAR) using the described (ELF+DEN) classifier for UXO-like and non-UXO discrimination. As expected, when ELF+DEN=2 (maximum threshold), both DR and FAR fall to zero. Conversely, when ELF+DEN=0 (minimum threshold), the plot shows that DR=100% and FAR=100%. As the threshold decreases from 2 to 0, the line is traced out from left to right.

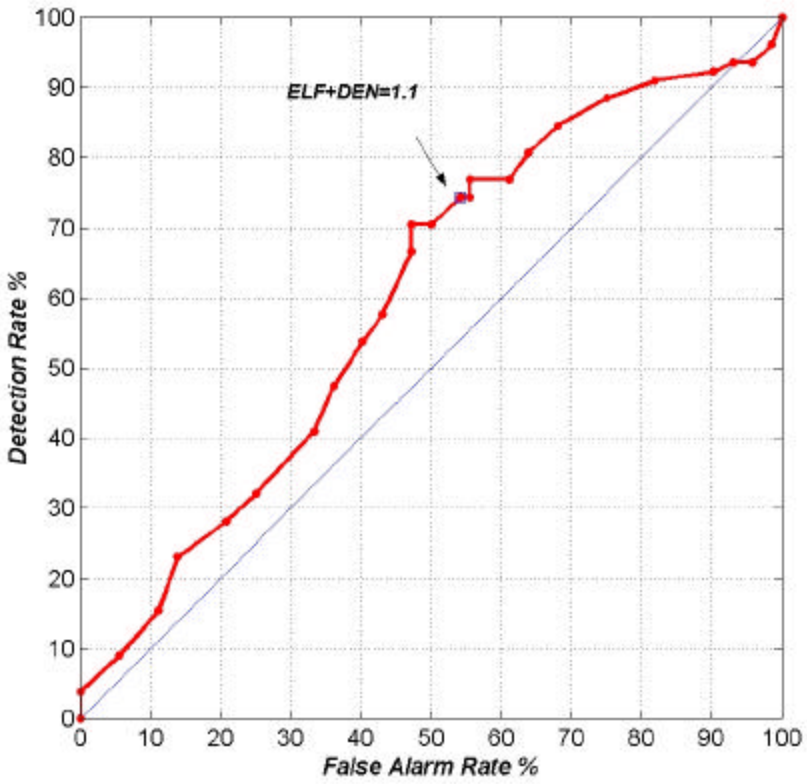

Figure 41 ROC Curve Using the ELF+DEN Threshold

If the line ELF+DEN=1.1 is used as a threshold, the DR and FAR are approximately 74% and 54%, respectively. It was found that many of the dropped UXO-like targets had an inclination angle greater than 45 degrees. These targets are expected to have a weaker scattered field. The main scattering sources in these cases were from the ends of the targets, which have low linearity features. This causes the ELF and DEN to be much lower than those obtained when the target was horizontal. Some possible solutions to this problem are being investigated, such as ellipticity [5], ramp response processing [6][7], and multi-position scanning. The ROC curve for UXO-like targets with inclination angle less than 45 degrees is shown in Figure 42. Note that in this case all the UXO-like targets that have inclination angle greater than 45 degrees are considered as non-UXO items. If an ELF+DEN=1.1 threshold is used the DR and FAR are approximately 88% and 50%, respectively.

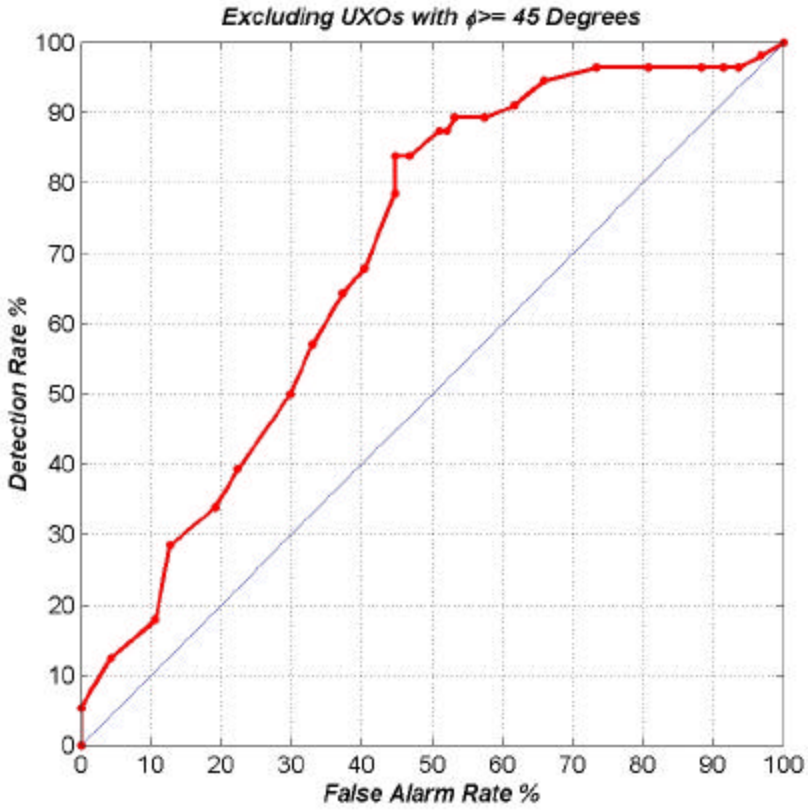

Figure 42 ROC Curve Excluding UXOs with Inclination Angle Greater than 45 Degrees

The average depth of targets buried in the Lower Pad (see Appendix A) was 0.315m, while the average depth of targets buried in the Upper Pad (see Appendix A) was 0.711m. The ROC curves for UXO-like targets in the Upper and Lower Pad with inclination angle less than 45 degrees are shown in Figure 43 and Figure 44, respectively.

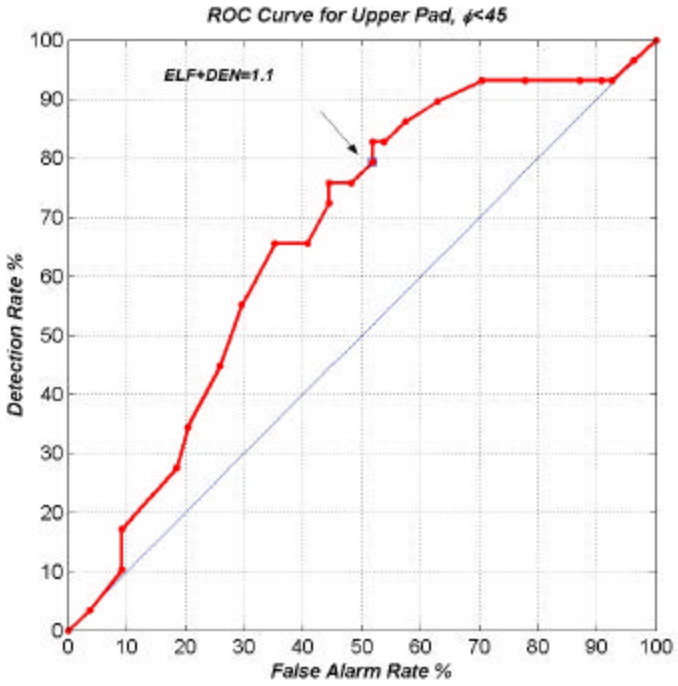

Figure 43 ROC Curve for Upper Pad Excluding UXOs with Inclination Angle Greater than 45 Degrees

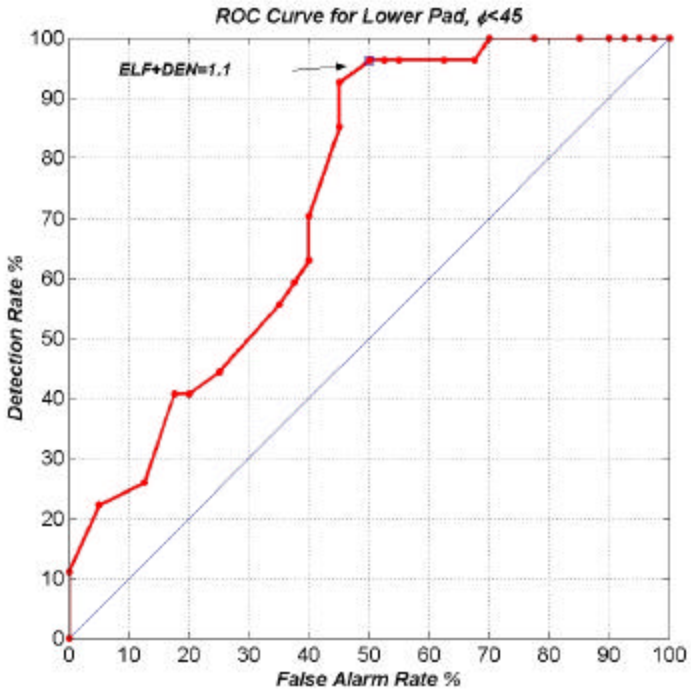

Figure 44 ROC Curve for Lower Pad Excluding UXOs with Inclination Angle Greater than 45 Degrees

Again, if the ELF+DEN=1.1 threshold is used the DR and FAR for the Upper Pad are approximately 79% and 51%. Using the same threshold the DR and FAR for the Lower Pad are approximately 96% and 50%. The detection rate in the Lower Pad is much better, but the false alarm rate is still not reduced.

6.2.2 Stage 2: Classification for Specific UXO Types

Another criteria is needed in order to better discern UXO-like targets from false alarms. Many UXO sites may have some background information about what types of UXO's are present, or one may be interested in testing for particular types. In this case, one can use the Estimated Target Length (ETL) feature as an additional classifier. For example, suppose one asks the question, 'Is this target a 105mm projectile?' In this framework, all targets that do not classify as 105mm projectiles are false alarms. A range of lengths, centered around the true length of the 105mm projectile, is used to filter all of the UXO-like targets selected in Stage 1. Figure 45 shows the ROC curves of the 105mm UXO classification results that were obtained by varying the ELF+DEN threshold from 0 to 2.

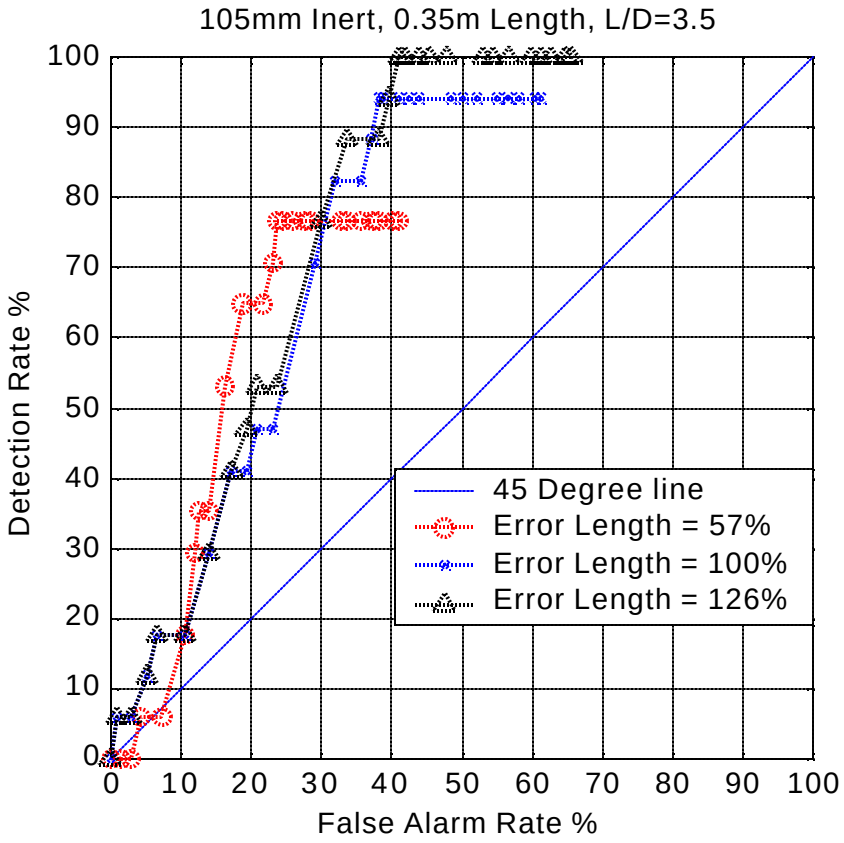

Figure 45 ROC Curve for 105mm Projectile Based on True and Estimated Lengths.

The three lines represent length-error-tolerance (LET). If the difference between the estimated length and the true is within the LET, the target is classified as the desired UXO. Notice that for LET=126% the detection rate reaches 100% while the FAR is only approximately 41%.

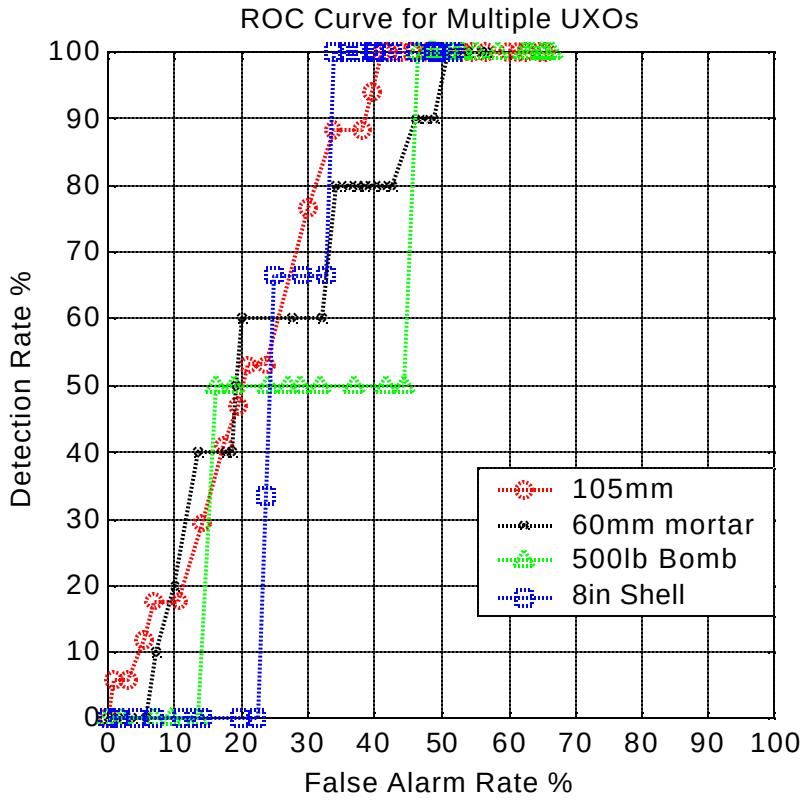

Figure 46 ROC Curve for Multiple UXO's Using True and Estimated Lengths.

Figure 46 shows the ROC curves of the classification of 105mm projectiles, 60mm mortars, 500lb bombs, and 8in shells. It shows that detection of all of these UXO's reaches 100% before the false alarm rate reaches 50%. We note that the LET for each UXO type was chosen such that 100% DR is obtained. The required tolerance error for the predicted lengths for 105mm, 60mm, 500lb bomb and 8-inch shell are 125%, 150%, 67% and 50%, respectively. The true lengths of these UXOs are 34cm, 23cm, 120cm and 100cm, respectively. This demonstrates the ability to look for given UXO types using the current classification algorithm. It should be noted that there were only two 500lb bombs and three 8" shells, therefore the ROC curve is not as smooth as the 105mm one. If there were more 500lb bombs, that the ROC curve would likely resemble the 105mm curve more closely.

6.3 Further Investigation on the Dropped UXO and False Alarms

With an ELF+DEN=1.1 threshold applied, as an example, all of the targets are separated into four groups: correctly identified UXO's, correctly identified non-UXO's, dropped UXO's, and false alarms. The dropped UXO's are the main concern and will be discussed in Section 7.3.1. Then the false alarms will be investigated in Section 7.3.2. New ROC curves will be presented reflecting the findings discussed in the non-detection and false alarms sections. Finally, a comparison between the estimated lengths and depths and the ground truth will be made for correctly identified UXO-like targets.

6.3.1 Dropped UXO's based on ELF+DEN=1.1 Threshold

The list of dropped UXO's based on the ELF+DEN=1.1 threshold (Table 6) shows that almost 90% of the dropped UXO-like targets only had initial scan data, i.e. no additional orthogonal scans, described in Chapter 3. Such a measurement procedure complied with what described in the Section 4.5, Items (d) and (e) of the submitted Demonstration Plan 1 prior to the trip. According to that plan, orthogonal data were only collected when the overnight processed results indicate a significant depolarization property (e.g. ELF greater than 0.5). Since the directions of the orthogonal passes were determined from the estimated target orientations. For targets that did not have detectable responses or had strong responses that clearly showed non-linear feature (i.e. low ELF), no orthogonal data were collected.

This suggests that the initial scan produced little in the way of UXO-like features, i.e. resonance, linearity, and good angle density during the on-site processing. Based on this, the decision was made not to collect additional scans for these targets, since no orientation estimation can be made to determine target orientation from the additional scans. This strongly suggests that, if additional scan data had been collected along two arbitrary lines, regardless of the on-site processing results during the initial scan, better responses might have been obtained with more accurate classifications.

The possible causes that might result in non-detection are included in the comment field and will be examined individually below.

Table 6 List of Dropped UXO-Like Targets

	Type	Depth (m)	ϕ	θ	L (m)	Max Dia. (m)	Location	Comments*
6	105mm Inert	0.40	45	0	0.35	0.105	Lower Pad	C
7	105mm Inert Heat	0.34	45	60	0.35	0.105	Lower Pad	B
8	105mm Inert Heat	0.43	0	0	0.35	0.105	Lower Pad	B
17	105mm Inert	0.68	0	0	0.35	0.105	Upper Pad	A
18	105mm Inert Heat	0.57	45	0	0.35	0.105	Upper Pad	C
19	105mm Inert Heat	0.80	45	90	0.35	0.105	Upper Pad	C
22	60mm Mortar	0.70	0	0	0.23	0.060	Upper Pad	
24	60mm Mortar	0.54	45	90	0.23	0.060	Upper Pad	C
25	60mm Mortar	0.40	30	0	0.23	0.060	Upper Pad	
29	MK82 500lb	1.40	35	0	1.20	0.350	Upper Pad	D
32	4.2" Mortar	0.30	45	45	0.50	0.110	Upper Pad	E
39	BDU33	0.80	0	60	0.60	0.106	Upper Pad	A
40	BDU33	0.58	45	0	0.60	0.106	Upper Pad	C

* A. high clutter level; B. insufficient background subtraction; C. large inclination angle; D. partially touching water table; E. multiple targets

42	BDU33	0.70	90	0	0.60	0.106	Upper Pad	C
43	155mm	1.40	60	30	0.86	0.155	Upper Pad	D
102	160mm Mortar	1.20	60	270	1.00		Upper Pad	D
107	5" Gun Round	1.40	80	0	0.91	0.127	Upper Pad	C
109	Angle Iron	0.92	0	0	0.30	0.00635	Upper Pad	
135	Rebar	1.00	90	0	0.91	0.019	Lower Pad	C
142	60mm Mortar	0.36	45	45	0.23	0.060	Lower Pad	

Investigation of targets 22, 25, 109, and 142 revealed that there were no simple explanations for these non-detections. It appears, for target 142, (see Figure 47 and Figure 48) there is a very low signal level, but no definitive explanation for non-detection could be found. Further study of these three targets is being pursued presently.

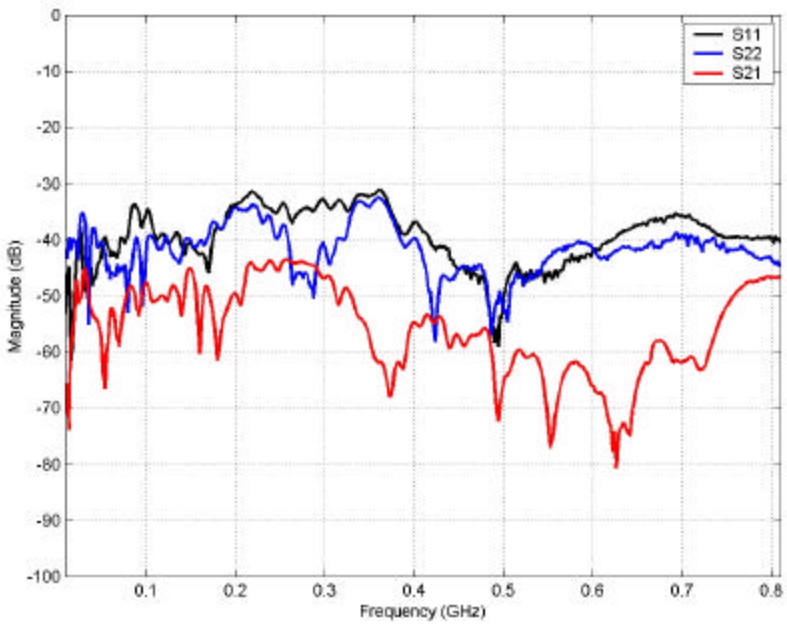

Figure 47 Target # 142: Frequency-Domain Response

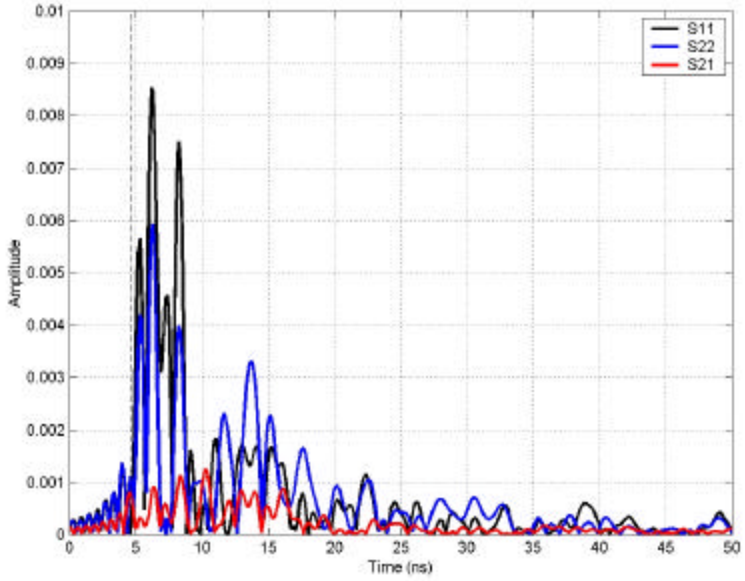

Figure 48 Target # 142: Time-Domain Response

- **High Clutter Level**

The data for targets 17 and 39 show that their response had unusually high clutter levels in the late-time region, shown in Figure 49 and Figure 51. These late-time responses have complex structures unlike damped resonances. This results in a low SCR that causes ELF to be biased as discussed in Chapter 4, Figure 8. There also seems to be no observable resonance region in the time-domain response from these targets, shown in Figure 50 and Figure 52.

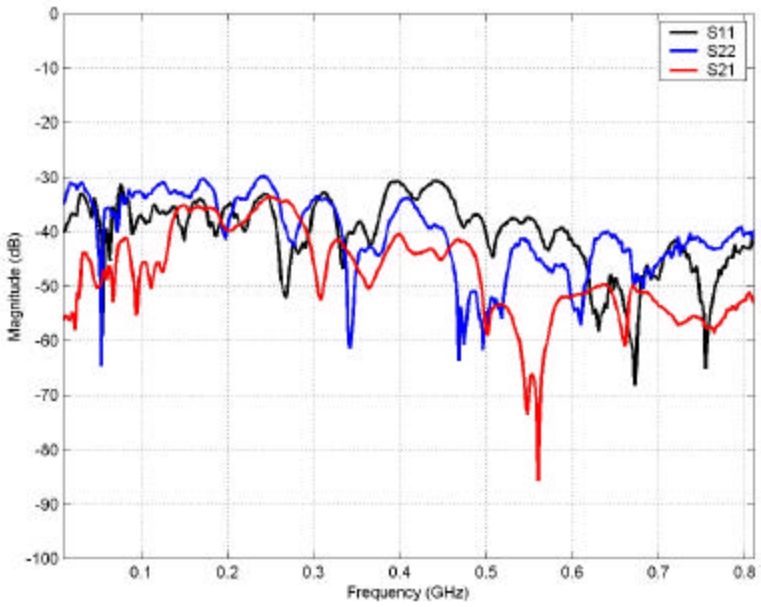

Figure 49 Target # 17: Frequency-Domain Response

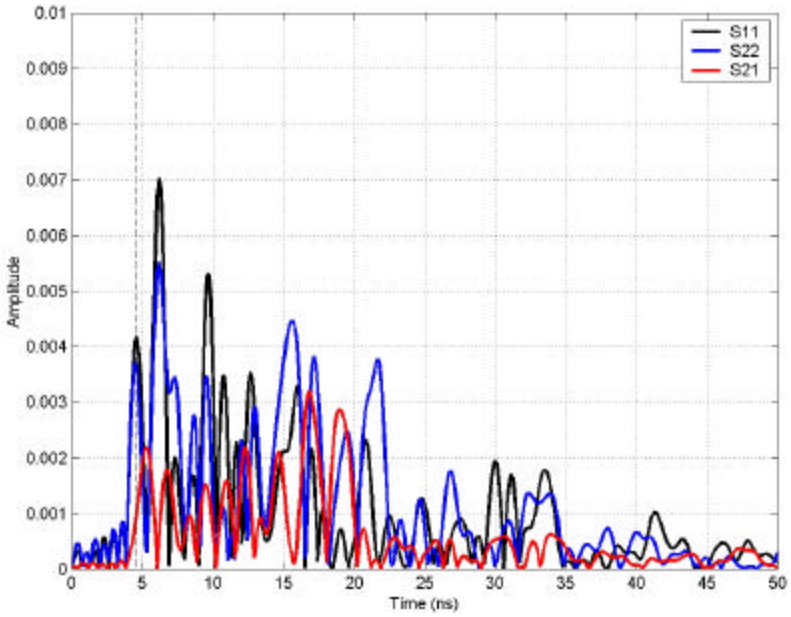

Figure 50 Target # 17: Time-Domain Response

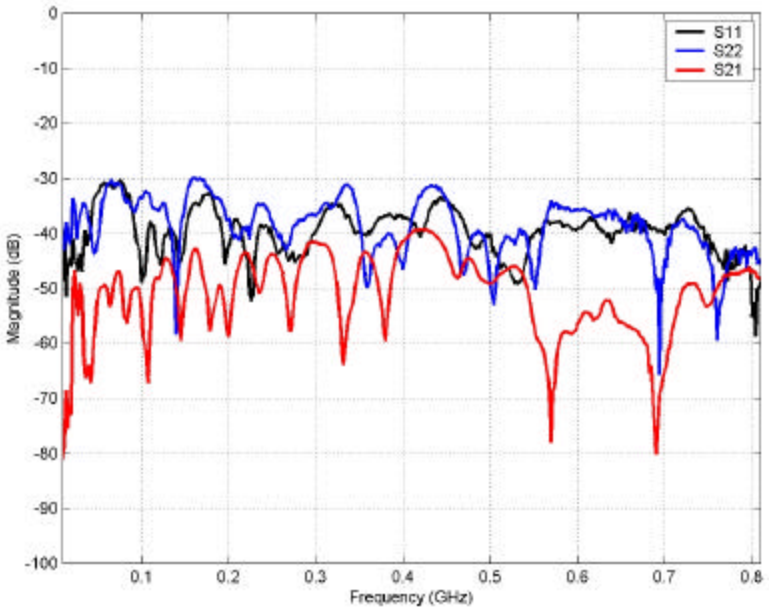

Figure 51 Target # 39: Frequency-Domain Response

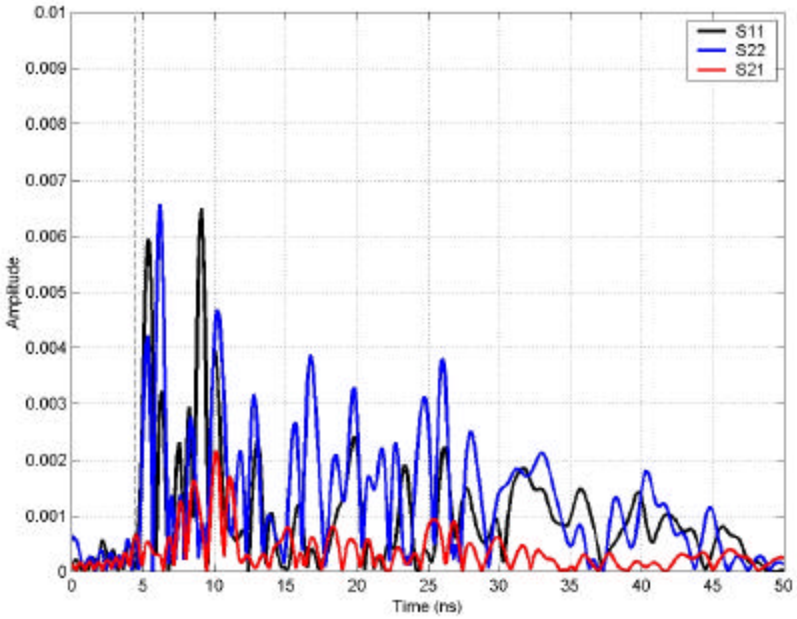

Figure 52 Target # 39: Time-Domain Response

- **Insufficient Background Subtraction**

The strong responses near 5ns and 11ns positions observed in Figure 53 and Figure 54 for target #7 and #8, respectively, clearly indicate that the background subtraction was not effective. When this occurs, the responses from a shallow target are severely contaminated, thus resulting in incorrect features. Figure 55 and Figure 56 show the same data sets as shown in Figure 53 and Figure 54 after choosing another background data for background subtraction. As one can see, the surface and arm junction reflections are now removed more effectively and the results show clear UXO-like features with DEN=0.76&0.83 and ELF=0.67&0.61 for targets 7 and 8, respectively.

The unusual larger early-time responses occurring in Figure 53 and Figure 54 can be used as an indicator of needing new background data during the feature extraction process to prevent this situation from happening in the future.

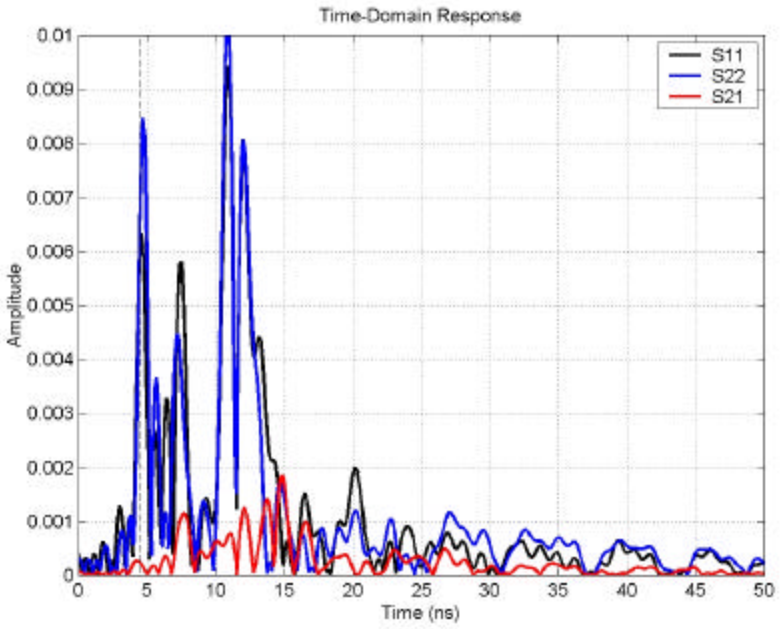

Figure 53 Target # 7 with poor background subtraction

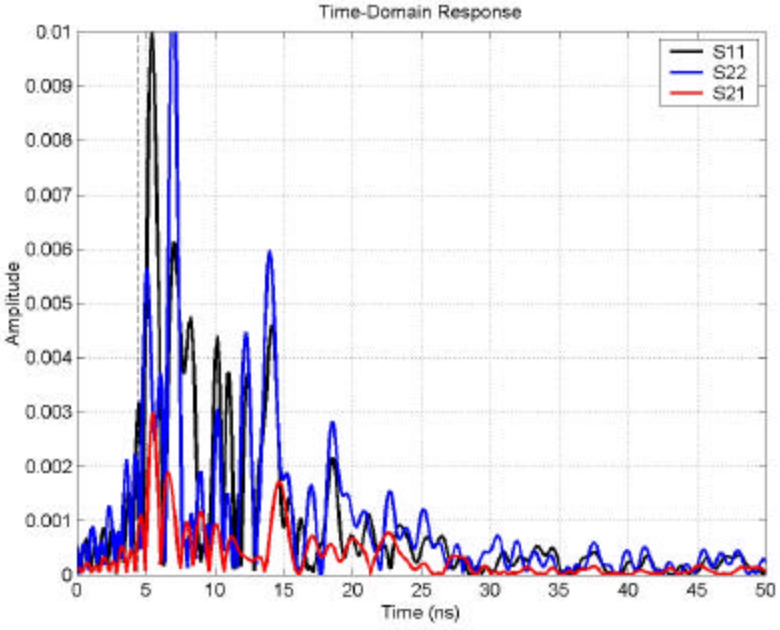

Figure 54 Target # 8 with poor background subtraction

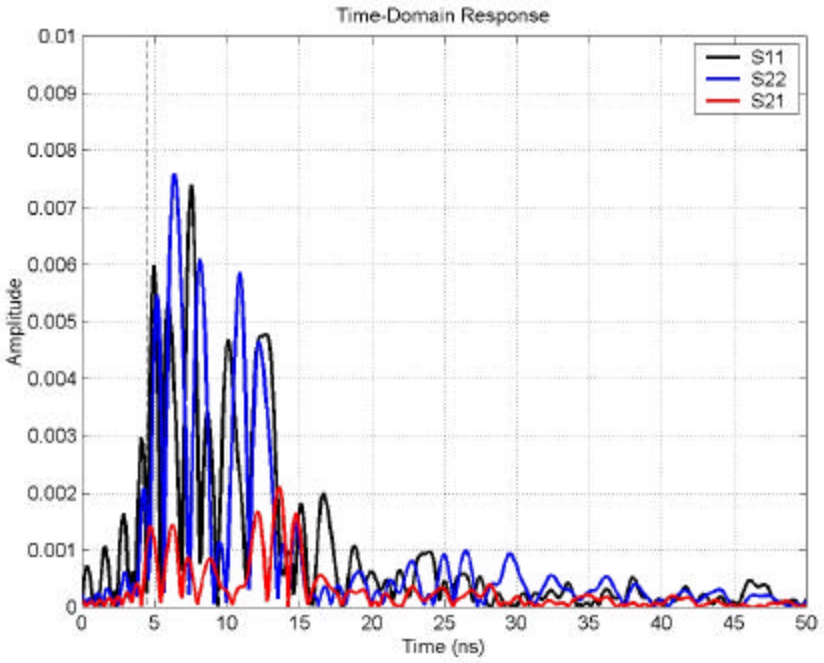

Figure 55 Target # 7 with better background subtraction

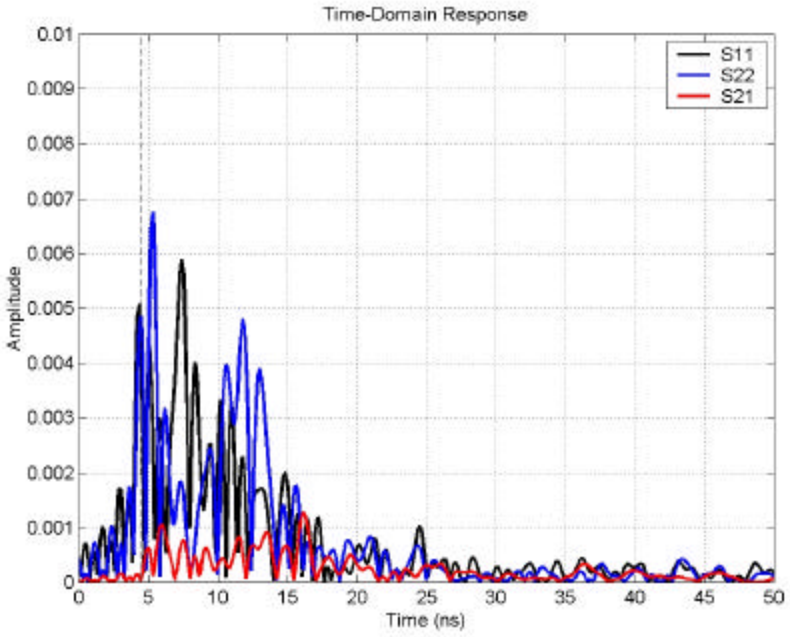

Figure 56 Target # 8 with better background subtraction

- **Large Inclination Angle**

A large portion of the dropped UXO's (see Table 6) had an inclination angle of 45° or greater. For such an orientation, the maximum response occurs when the antenna is offset from directly over the target. The crucially important fundamental resonant mode is more weakly excited when the incident waves hit a linear target from an off-normal direction. This is shown in Figure 50 from the signal magnitude. A possible approach to overcome the problem is to use an additional antenna with a 45 degree off-normal look angle.

Notice that targets 42, 107, and 135 were all approximately vertical in orientation. When seen from above these targets would have low ELF and DEN, because they appear symmetric. Solutions to this problem are being investigated, such as ramp response processing, ellipticity, and multi-position scanning, as discussed earlier.

- **Partially Touching Water Table**

The ground truth indicates that targets 29, 43, and 102 were all partially buried below the water table due to their tilt, illustrated in Figure 50. The effect that changes in the electrical properties of the soil caused by the water table on feature extraction is yet unknown. Further study would be to determine the reactions between the water table and electromagnetic scattering, via modeling techniques, which we are actively pursuing.

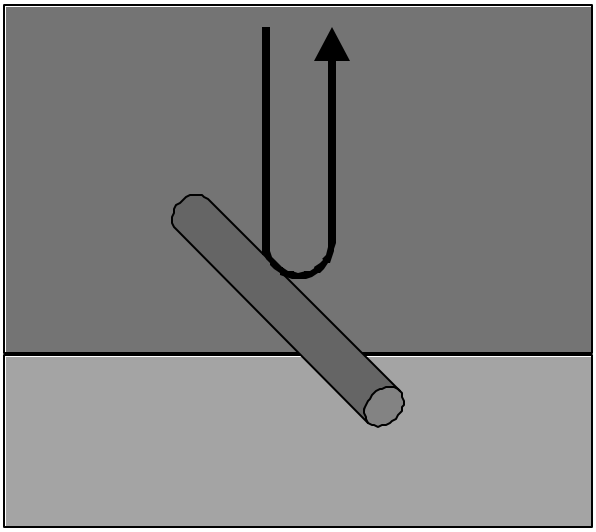

Figure 57 Example of a Target Partially Touching the Water Table.

- **Multiple Targets**

Target 32 actually should have a length of 0.495m and max. diameter of 0.11m according to the ground truth. However, it appears from Figure 58 and Figure 59 that there may be two sets of resonance. The first group beginning at approximately 11ns would produce the features matched to the ground truth target. The second set, which starts approximately at 29ns, may be another target, clutter in the sense that it was not emplaced as part of the test. The second set shows marginal ELF (0.44) and DEN (0.49). While the first set, upon further investigation has very good ELF (0.68) and DEN (0.91).

The resonance spectrum indicates two resonant frequencies located at approximately 100MHz and 150MHz. The latter has a weaker response and corresponds to the first resonance group. During the previous processing, the second group was chosen because it is later in time. The result was DEN=0.49 and ELF=0.44, which fell below the DEN+ELF=1.1 threshold. Figure 60 shows the time domain response with the correctly centered frequency-domain band-pass filter (at 150 MHz). Notice that there is obvious resonance in the time region from 14ns to 26ns, which produced an ELF=0.68 and a DEN=0.91. The features extracted from the time region match those of the ground truth target.

When there are multiple UXOs located near each other, depending on the distance, relative orientations or whether there is a physical contact, multiple resonant modes would occur. For weak interaction cases, each resonant mode is associated with individual UXO as if the UXO is present by itself. For strong interaction cases, not only individual resonance will be changed but also new "system resonance" will also occur due to the mutual interactions. Iterative procedures can be applied to tune the bandpass filter to each resonant peak in the late-time spectrum (Chapter 4) to extract the individual lengths. For instance, two UXOs that have similar lengths and are physically in contact to form a "+" geometry would have "|", "-" and "L" modes, all have similar but slightly different resonant frequencies and very different damping factors. The polarization features such as orientation (ETO) and linearity (ELF) would have a major impact from multiple UXOs located at the same site since a current algorithm could not differentiate a "+" target from a "o" shape target due to the rotational symmetry. Such a problem could be alleviated in the future by including the scattering pattern or magnetic signatures that might generate significantly different signatures.

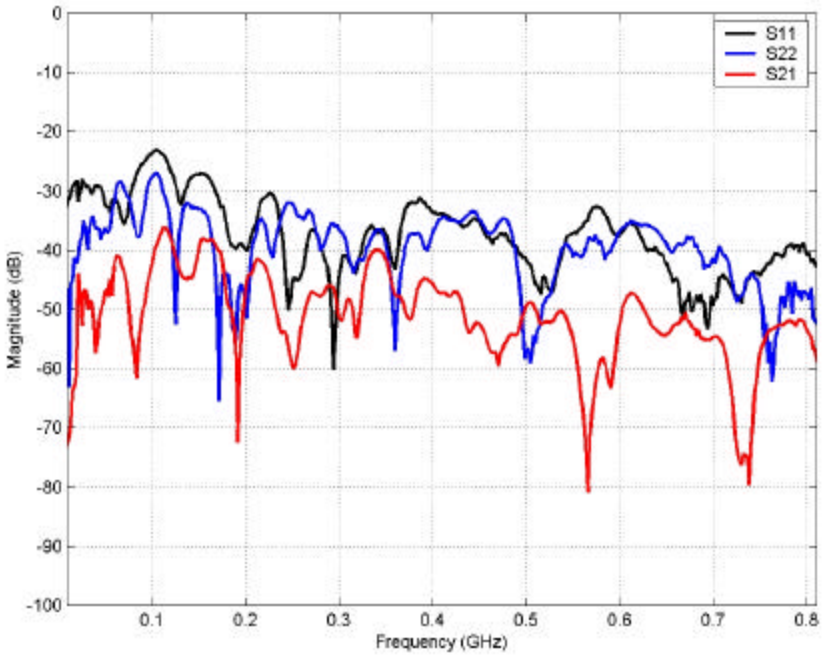

Figure 58 Target # 32: Frequency-Domain Response

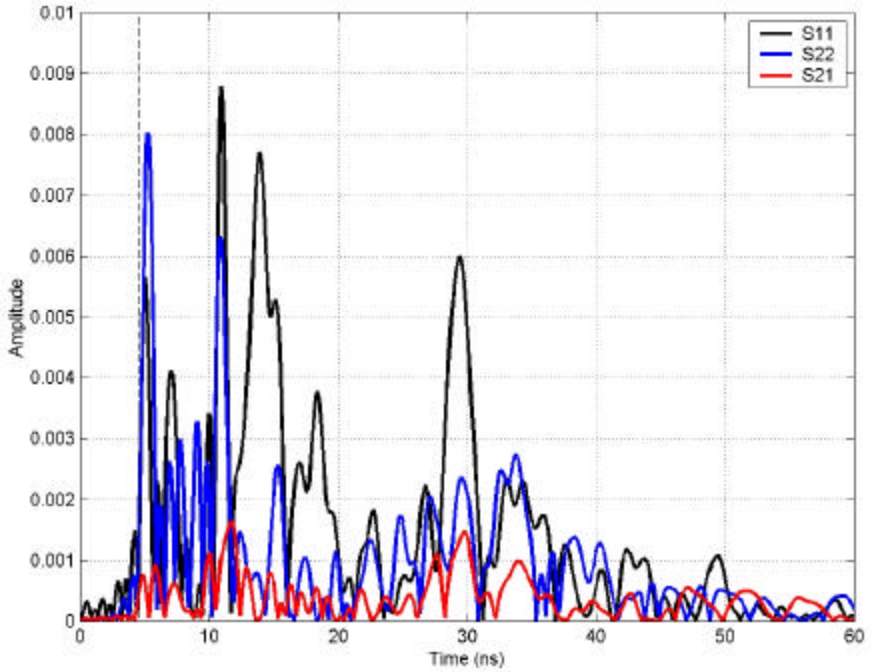

Figure 59 Target # 32: Time-Domain Response

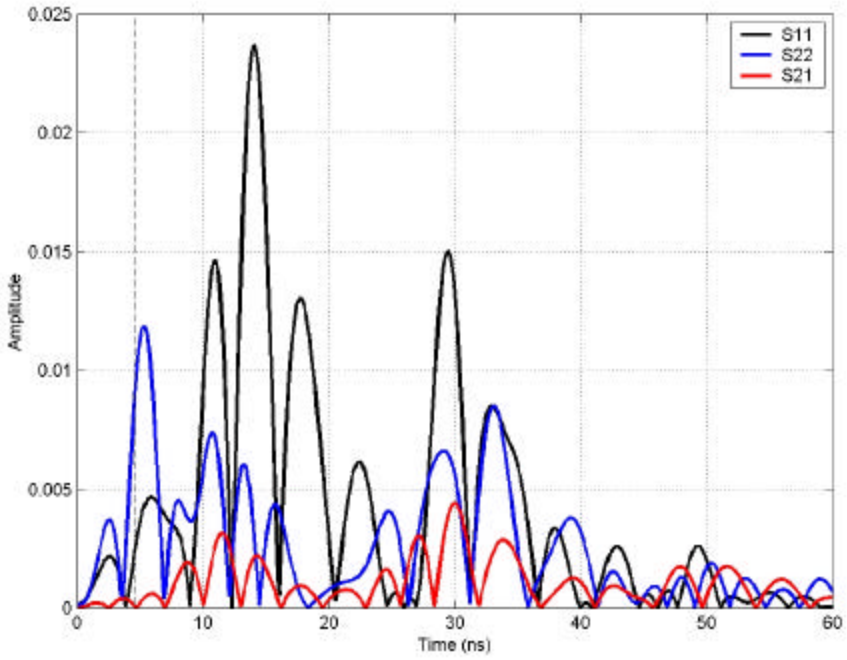

Figure 60 Target # 32: Time-Domain Response with Correct Frequency Band-Pass Filter Applied

6.3.2 False Alarms

Which targets produce false alarms depends on the criterion we use in the ELF+DEN value we choose in the classification scheme. For the purposes of this section, false alarms are defined as non-UXO-like targets which have an ELF+DEN greater than 1.1, listed in Table 7. Some of the possible reasons for some of the false alarms are presented below.

Table 7 List of False Alarms with an ELF+DEN=1.1 Threshold

False-Alarm Targets Above Threshold (ELF+DEN=1.1)									Reasons*
No.	Type	Depth (m)	ϕ	θ	L (m)	W (m)	Max Dia. (m)	Location	
53	Fragment	0.06	0		0.05	0.05	0.006	Lower Pad	A
63	Alum. Barb Wire	0.10			0.40			Lower Pad	A
64	Alum. Barb Wire	0.12			0.40			Lower Pad	A
68	Steel Plate	0.17	0	0	0.30	0.30	0.006	Lower Pad	A
80	Clusters of nails	0.10	0	0	0.08		0.152	Lower Pad	A
137	Rebar 90? Arc Mid	0.16	30	90	0.30	0.30	0.019	Lower Pad	A
141	Mine AT	0.14	0	0				Lower Pad	A
69	Steel Plate	0.30	45	0	0.30	0.30	0.013	Lower Pad	B
84	55 Gal Lid	0.70	90	0			0.640	Upper Pad	B
106	Tine (Steel Plate)	0.79	90	0	0.48	0.24	0.019	Upper Pad	B
108	Tire Rim	0.66	90	0		0.15	0.330	Upper Pad	B
115	Pipe Att End (90?)	0.77	100	30	0.46	0.46	0.019	Upper Pad	B
116	Pipe Att End (90?)	0.74	100	150	0.46	0.46	0.019	Upper Pad	B
35	BDU33 (Tail only)	0.50	0	0	0.40		0.106	Lower Pad	C
103	Frag (Exploded)	0.21	15	260	0.91			Upper Pad	C
126	Exploded Tube	0.50	30	60	0.51		0.076	Upper Pad	C
97	Metal Box	0.70	0	0	0.43	0.13		Lower Pad	C
98	Metal Box	0.99	0	0	0.43	0.13		Upper Pad	C
117	Metal Box Open	0.65	20	60	0.46	0.15	0.006	Upper Pad	C
139	Crushed Box	0.33	40	100	0.46	0.15		Lower Pad	C
65	Alum. Barb Wire	0.43			0.40			Lower Pad	
67	Alum. Barb Wire	0.50			0.40			Lower Pad	
70	Steel Plate	0.32	0	0	0.30	0.20	0.006	Lower Pad	
81	Clusters of nails	0.57	0	0	0.08		0.152	Upper Pad	
82	55 Gal Lid	0.20	0	0			0.640	Upper Pad	
92	Rebar 90? Arc End	0.40	0	0	1.22		0.019	Lower Pad	
93	Pipes Ortho Attac	0.65	0	0				Upper Pad	
94	Pipes Ortho Attac	1.00	0	0				Upper Pad	
105	Base Plate (Fuse)	0.48	30	90		0.10	0.300	Upper Pad	
112	Soda Can	0.41	0	90	0.13		0.076	Upper Pad	
118	Metal Box Closed	1.00	0	0	0.40	0.40		Upper Pad	
120	Bomb Parts	0.20	0	0	0.46	0.46	0.006	Upper Pad	
121	Panel Large	0.78	0	45	0.60	0.46	0.006	Upper Pad	

* A. Close Distance and Offset; B. Linear Edge; C. Linear Shape but Length to Diameter Ratio Greater than Three

124	Panel Medium	0.30	0	90	0.46	0.25	0.006	Upper Pad
131	Scrap Crushed	0.21	0	0	0.48	0.23	0.006	Lower Pad
132	Rim	0.30	45	0		0.15	0.330	Lower Pad
136	Paint Can Open ?	0.33	45	0				Lower Pad

- **Shallow Burial with Offset**

Small targets buried at shallow depths, offset from the center of the antenna, were a major cause of false alarms. With the very shallow depths, the far-field scattering matrix assumption, presented in Chapter 4, becomes invalid. This situation is illustrated in Figure 61; targets 53, 63, 64, 68, 80, 137, and 141 were probably misidentified for this reason. A strong response from one antenna arm and a weak response from the other would cause a high ELF and DEN, like the response of a longer linear object, thus causing the false alarm.

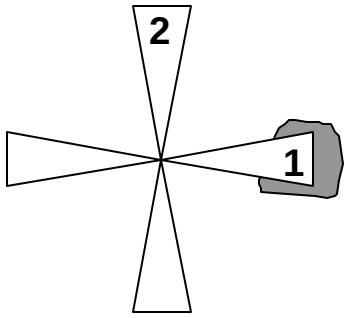

Figure 61 Problem associated with the polarization feature for small objects close to surface

One example of this situation was observed in the response of the AT Mines, shown in Figure 62. Targets 127 and 141 are AT Mines (see Figure 62) buried at a depth of 0.06m and 0.14m, respectively. These targets are rotationally symmetric, yet in the processing of their late-time region of their time-domain responses high ELF and DEN appear. In Figure 63 and Figure 64, a strong resonant peak appears at approximately 130 MHz in both frequency spectrums. A solution to this situation is to use a secondary antenna with a smaller footprint to detect objects closer to the surface. In addition, improving the position accuracy of the antenna could decrease the possibility of this situation occurring.

Figure 62 Target # 127 & 141 (AT Mine)

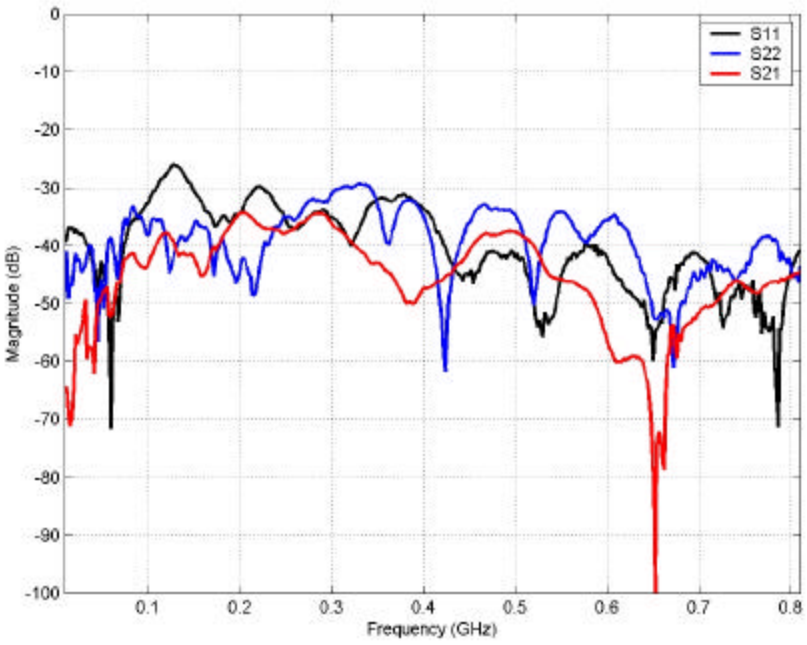

(a) frequency-domain data

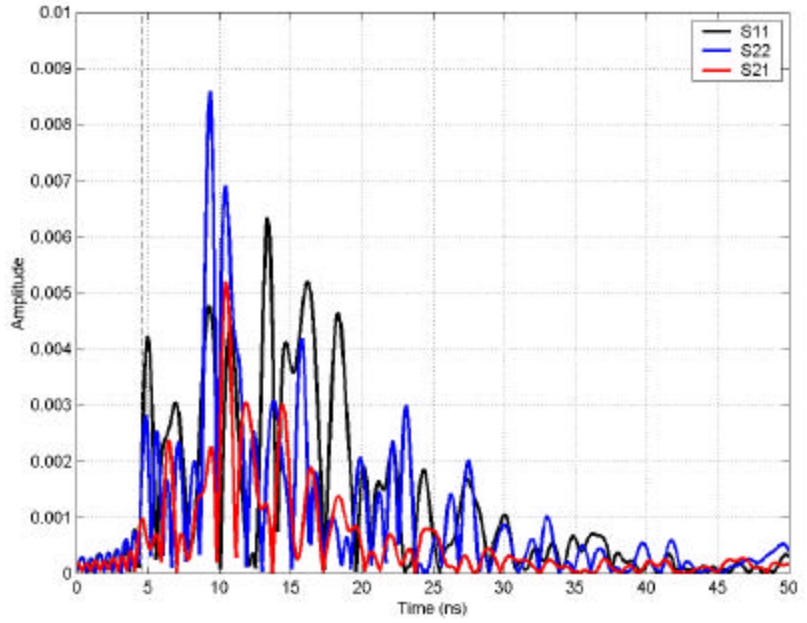

(b) time-domain data

Figure 63 Measured Responses of Target # 127 (AT Mine).

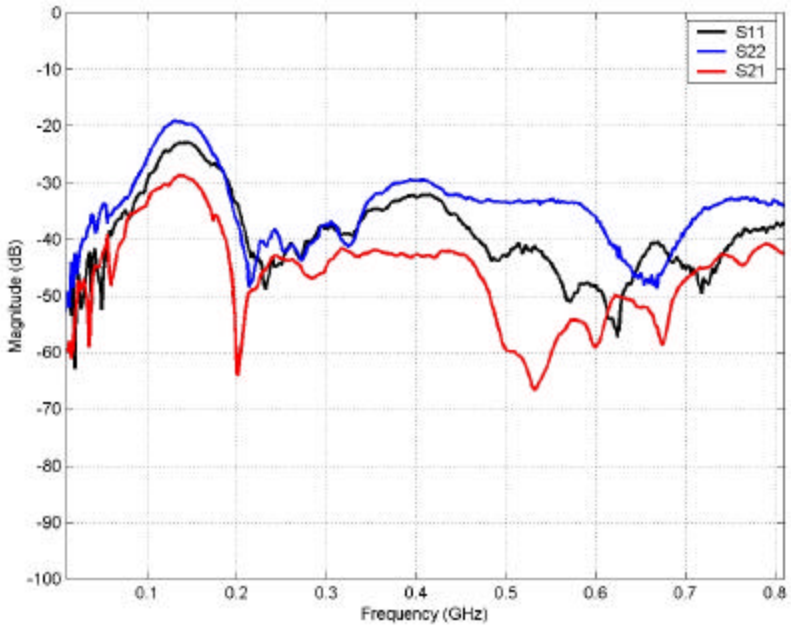

(a)

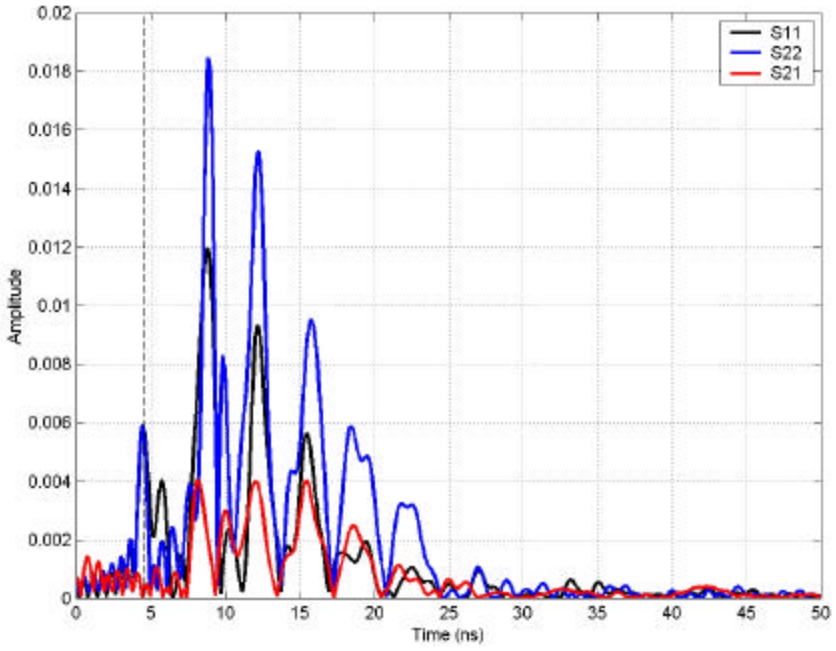

(b)

Figure 64 Measured Responses of Target # 141 (AT Mine).

- **Linear Edge**

Targets 69, 84, 106, 115, 116, and 108 are non-linear objects when the inclination angle is zero degrees, i.e. horizontal. When the inclination angle is 90° (as it is in this case) the objects are observed from one side and would appear linear, as shown in Figure 65. When seen from the side a plate appears long and narrow (very linear) and has a high ELF and DEN. Objects in this case would have a highly damped resonance compared with actual UXO's. It is believed that this high damping factor will help remove these targets from being chosen as UXO-like. Other features such as ramp response, depolarization, ellipticity, and specific scattering patterns may also be incorporated to classify this situation.

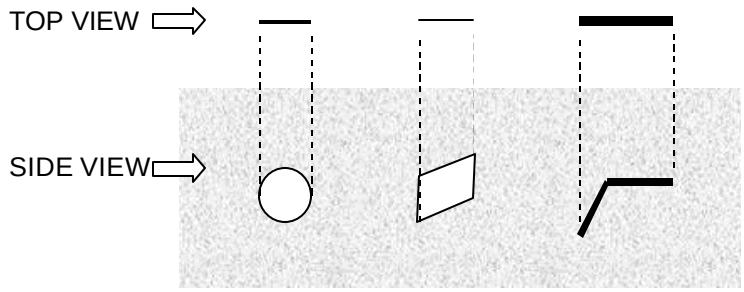

Figure 65 Vertically oriented non-UXO objects show linear scattering properties when observed directly above.

- **Non-UXO Targets with Large L/D Ratio**

For targets 35, 97, 98, 103, 117, 126, and 139, they all have a linear shape with L/D ratios greater than three. Figure 66 shows pictures of these targets. Since these targets have a linear shape, they will have a high ELF and DEN. These targets will be re-classified as UXO-like under the current classification criteria.

(a) Target # 35 BDU33 Tail Only (First 16" of target seen above)

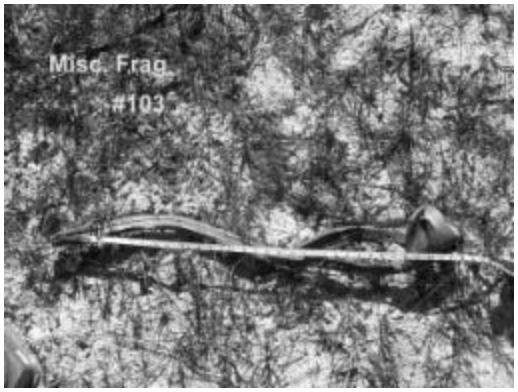

(b) Target # 103

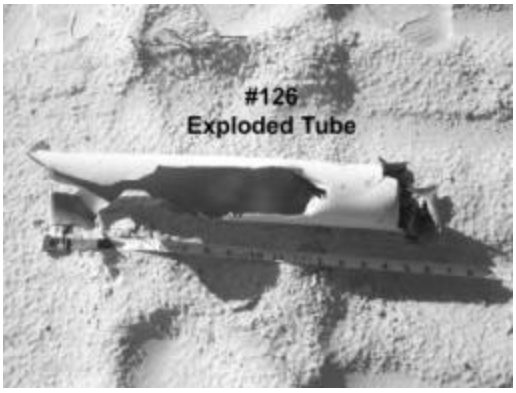

(c) Target # 126

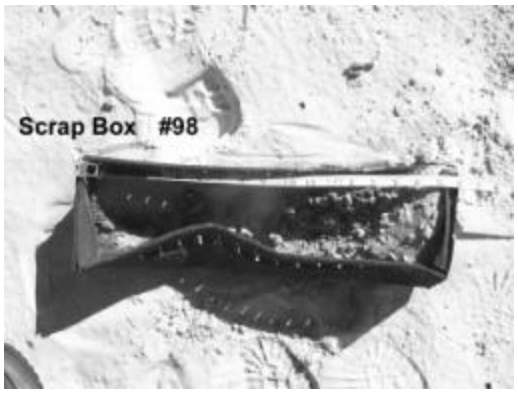

(d) Target # 98

Figure 66 False alarm targets with L/D ratio greater than three.

Note that the exact reasons for the other 18 false alarm targets are still yet to be determined. This is being pursued via experiments and numerical simulations.

- **Reassignment of UXO-Like Targets Based on L/D Ratio ^{3} 3 Criteria**

Some of the false alarm targets were reclassified as "UXO-like" after a study of their geometry, made possible by the ground truth. Targets 35, 97, 98, 103, 117, 126, and 139 from part C were all reclassified as UXO-like. This re-assignment increased the detection rate and decreased the false alarm rate slightly.

6.3.3 New ROC Curves after Re-processing

The ROC Curves presented in this sub-section include the re-assignment of all of the targets mentioned in the previous section and the corrections for dropped targets from categories A, B, and C in Section 7.3.1. Figure 67 shows the new ROC curve. The improvements are significant. When a threshold of ELF+DEN=1.1 is used, the DR is approximately 94% and the FAR is approximately 51%.

Figure 68 shows the new ROC curve obtained if UXO-like targets with an inclination angle greater than 45 degrees are excluded. A detection rate of 100% is achieved with much fewer false alarms. When a threshold of ELF+DEN=1.1 is used, the DR is 100% and the FAR is approximately 56%.

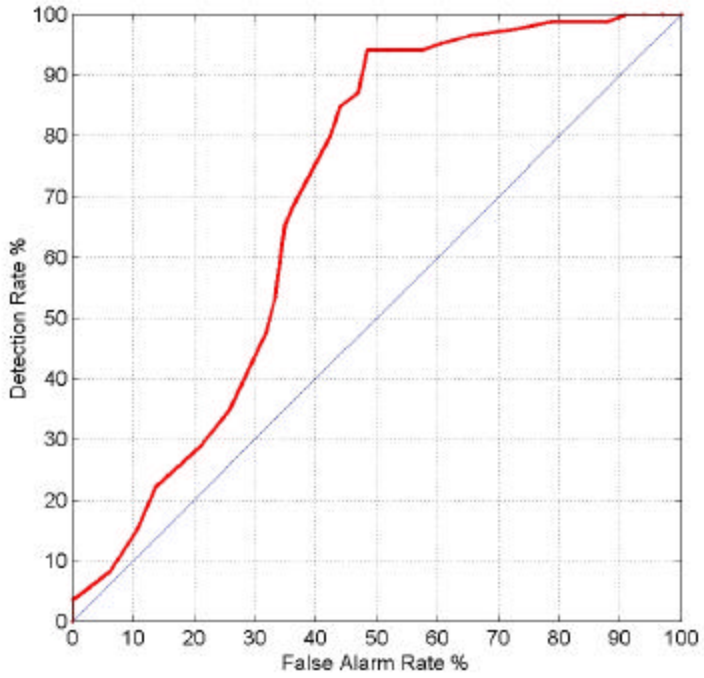

Figure 67 ROC Curve After Corrections

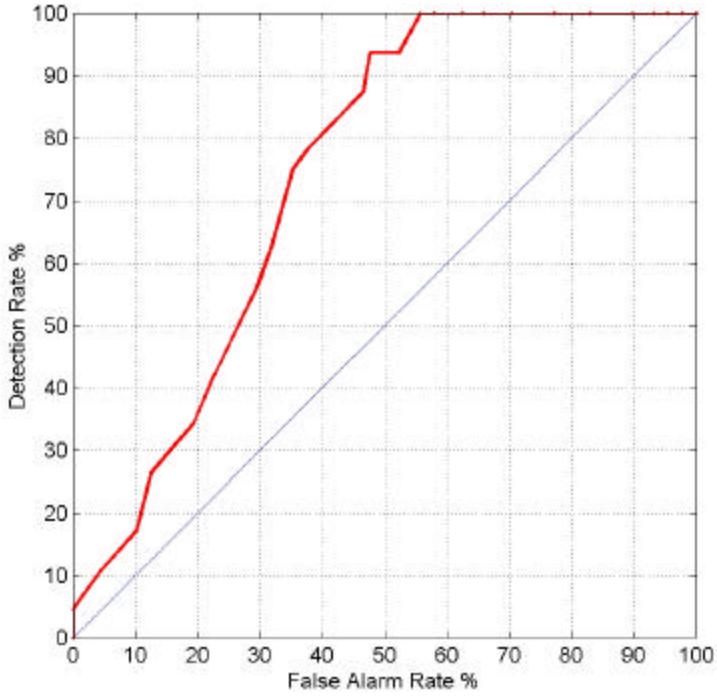

Figure 68 ROC Curve Excluding UXOs with Inclination Angle Greater than 45 Degrees, After Correction.

6.4 Further Investigation of Errors of Extracted Features

Out of the correctly chosen UXO-like targets, with an ELF+DEN threshold of 1.1, the orientations, depths and lengths estimated from feature extraction are compared with the ground truth , respectively.

Some discrepancies in the estimation of target orientation are identified with the possible reasons below and shown in Figure 69.

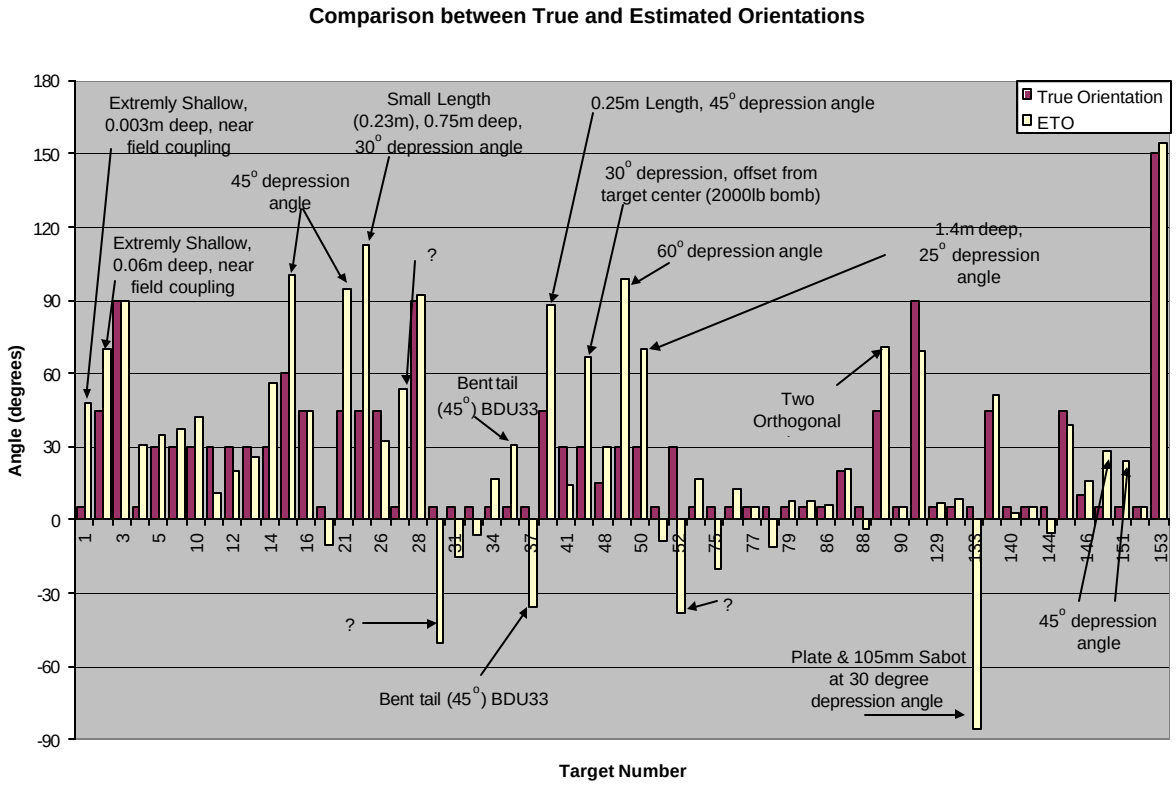

Figure 69 Comparison between the True and Estimated Orientations of Correctly Identified UXO-Like Targets.

Targets 1 and 2 are identified on the graph as being at extremely shallow depths that caused near field coupling with the arms of the antenna. The exact effect this situation will have on the estimation of features is not completely known.

Targets 15, 21, 23, 38, 47, 49, 50, 150, and 151 are identified as having an inclination angle of 25 degrees or greater. It was observed that this inclination angle causes some variations in the estimation of orientation.

Targets 36 and 37 are both BDU33 projectiles with their tails bent at a 45 degree angle. This geometry caused an orientation ambiguity of approximately 45 degrees, which both targets demonstrate.

Targets 89 and 133 both have multiple objects buried which caused ambiguities in the estimated orientation.

A comparison between the true and estimated target depth of correctly chosen targets is shown in Figure 70. The dark lines show the range of depths for a given target. This range was determined from the target length and the inclination angle of the target, since a stronger radar response may be from either end of an UXO with a nonzero inclination angle. The white bars show the estimated depth of the target. It should be noted that targets with a zero degree inclination angle have only a horizontal dark line to denote their true depth. One reason for errors in estimation is that the dielectric constant of the soil changes slightly with depth. Another reason is that if the antenna is offset from the target, the round trip from antenna to target is longer than if the antenna is directly over the target, which results in larger estimation depths. The estimated depth is also affected by the operator's ability to identify the first back-scattered response (not necessarily the strongest) peak from a target, in order to locate the shallowest point of an UXO. The depth estimation accuracy can be improved in the future by utilizing multiple-position data using the migration information of the responses.

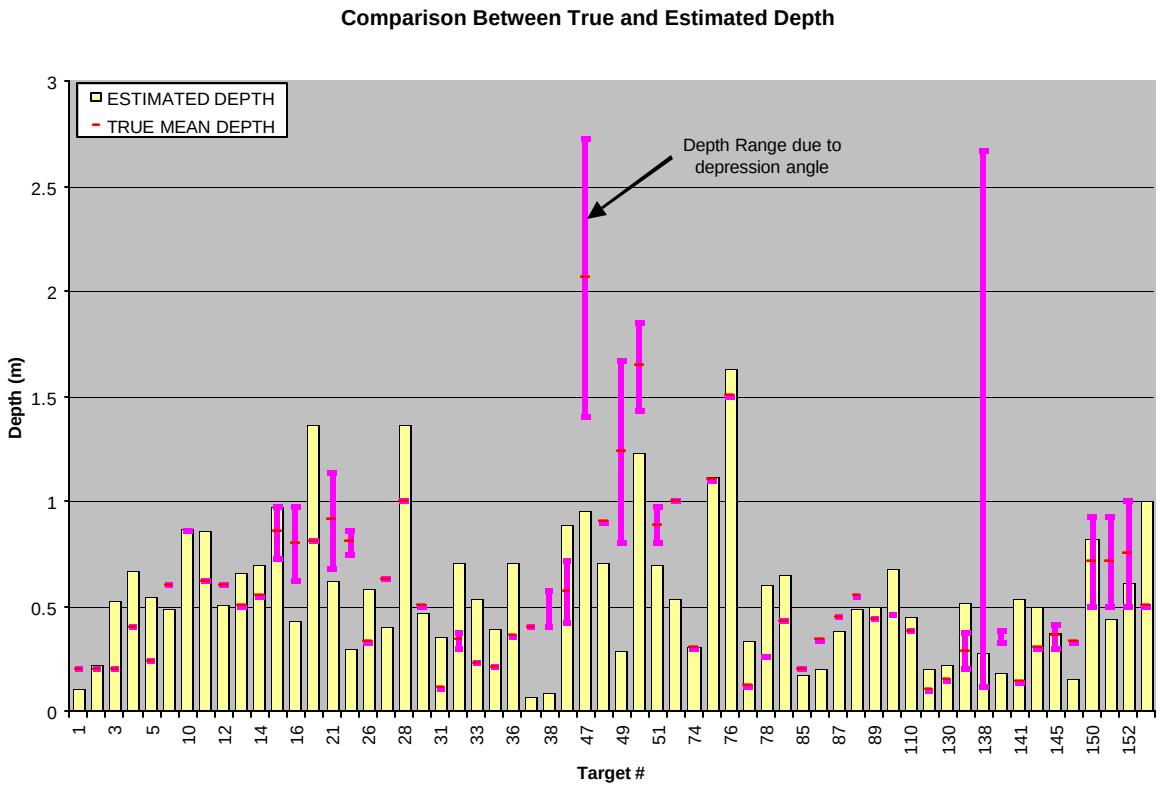

Figure 70 Comparison Between True and Estimated Depth of Correctly Identified UXO-Like Targets.

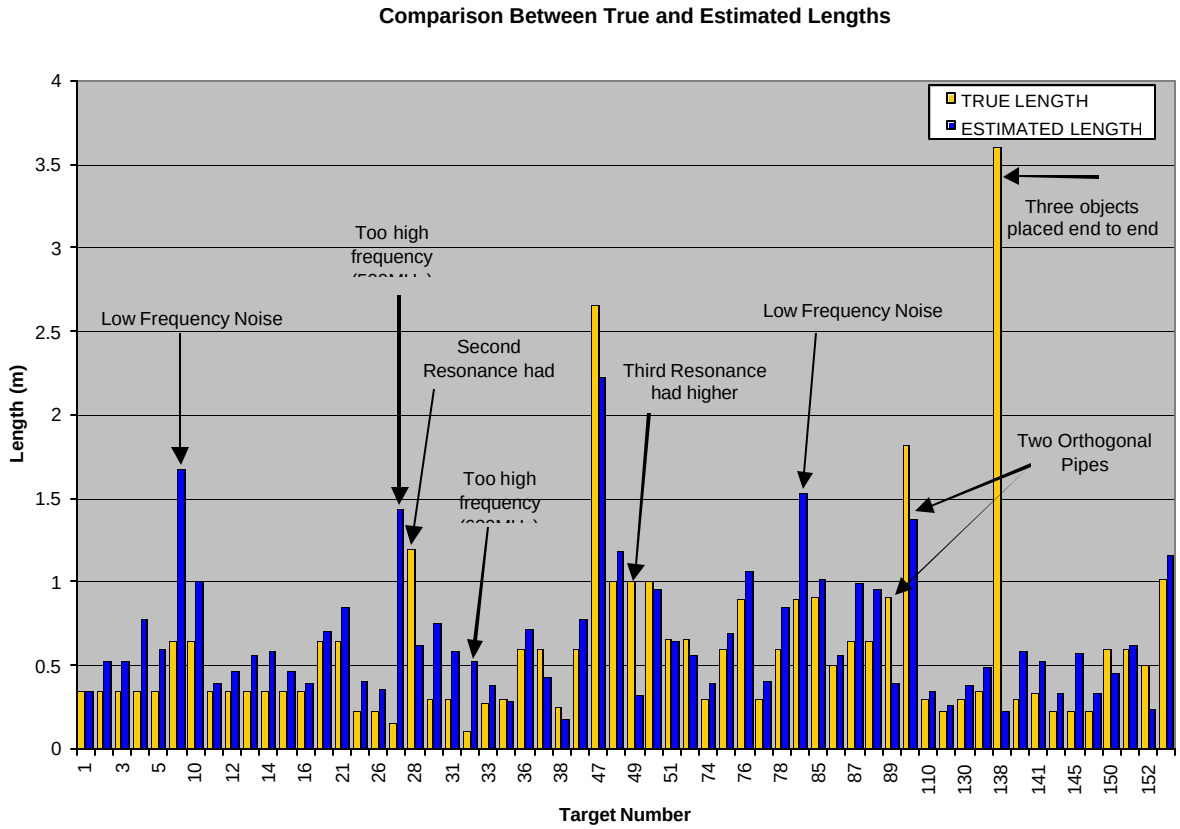

Figure 71 Comparison between the True and Estimated Lengths of Correctly Identified UXO-Like Targets.

A comparison of the true and estimated target length is also shown in Figure 71. Possible explanations for discrepancies in length estimation are also given. Small errors in length estimation can be attributed to the changing dielectric constant of the soil at larger depths. In addition, the contour length along the body of a target is longer than the actual nose-to-tail length. Since, the induced current travels along the surface of the object, the resonance of the back-scattered response is dependent upon the contour length. This usually causes an over estimation in length in some targets. Target 138 has a very long true length according to the ground truth. When the photo of the target was examined it was found that there are three objects buried end-to-end as shown in Figure 72. One of the objects (the BDU) has a length of 10" or 0.25m, which is very close to the estimated length for target #138 and, of course, the BDU is a desired target.

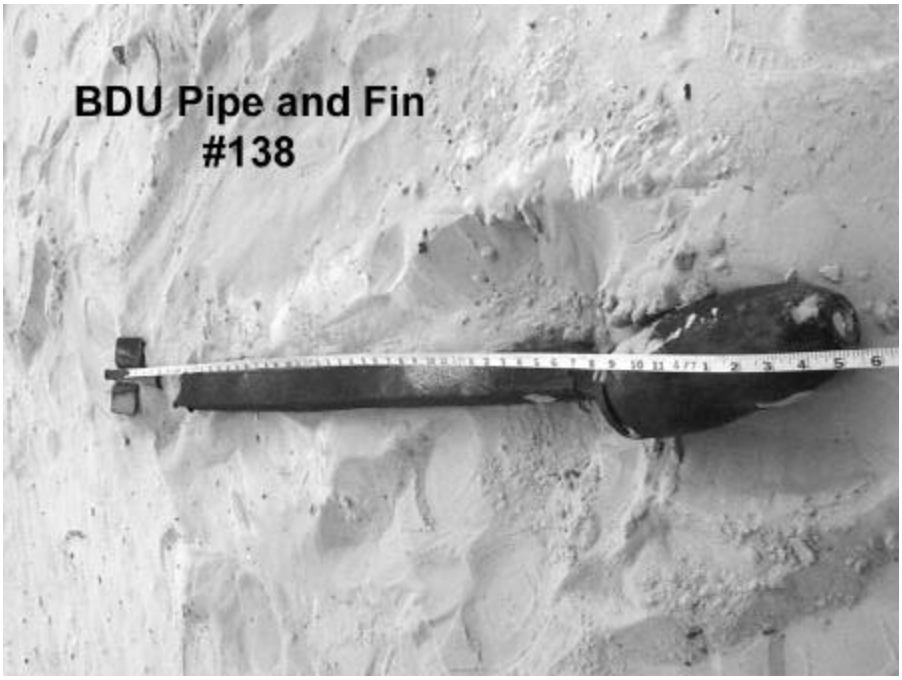

Figure 72 Target # 138 BDU, Pipe, and Fin

7 Conclusions and Current Tasks

The results here are exciting because this is the first time that a GPR team has been able to identify a large percentage of false alarm sources as well as the sources of non-detection by examining the measured data and the ground truth in depth. There has been a missing aspect in the previous demonstrations, which did not allow a closed-loop evaluation for improving the processing techniques and system design. Great effort was made at the Tyndall site to achieve a comprehensive set of targets to provide a large variety of target conditions, including many diverse non-UXO-like objects. While this tended to produce many false alarms, these conditions allowed many false alarm sources to be discovered. The main sources were targets much smaller than the antenna footprint offset from the center of the antenna and non-linear objects that have a linear edge, e.g. a flat plate on its edge. Substantial insight was gained from the study of the false alarms and non-detections. New techniques for discriminating between UXO-like and non-UXO-like targets are being developed and will be incorporated into the next field measurements. Notice that the causes of false alarms and non-detection found here are likely to apply to other sites. Therefore, the improvements made at Tyndall will improve the results at other sites.

The results from the measurements taken at Tyndall AFB are quite encouraging. For example, at a moderate ELF+DEN threshold a detection rate of approximately 94% and a false alarm rate of approximately 51% was achieved. As far as the classification of a specific ordnance type is concerned, the results based on the 105mm, 60mm mortar, 8-inch shell and 500lb bomb showed very encouraging classification capability. Overall, there were good agreements between the true length, depth, and orientation of the targets and the features extracted from the measured data.

The current system is not able to differentiate between UXO's and non-UXO targets with Length-to-Diameter (L/D) ratio greater than 3, since the current features extracted only provide information about a target's length, depth, orientation, and linearity. These features are not able to distinguish between a bomb and a piece of rebar. The Tyndall site had many linear non-UXO targets, in order for the site to be difficult. In order to further separate the UXO's from the elongated non-UXO items other signal processing techniques are being investigated. These techniques include ramp response, induced ellipticity, and back-scattering patterns due to different geometry.

The current system and processing algorithm had difficulty in identifying UXO-like targets with inclination angles greater than 45 degrees and UXO's that were buried partially in the water table. This is likely due to a much weaker backscattered field and complex scattering mechanisms associated with these orientations. The large inclination angle problem could be improved by using an additional side-looking antenna whose main radiation direction beam is off normal from the downward direction. Figure 74 and Figure 75 show two possible new antenna configurations that could provide better tilted illumination on a steeply inclined UXO that give poor polarization and resonance signatures under the current configuration shown in Figure 73. Figure 74 shows a dielectric loaded horn antenna with a tilt design that generates a tilted radiation beam. Figure 75 shows the configuration that places the existing antenna on top of a dielectric wedge to tilt the radiation beam. Measured data (see Blossom Point Demonstration Plan 2) has indicated that one can begin to obtain significant resonant and linearity signature when the incident angle is tilted more than 15 degrees away from the UXO axis.

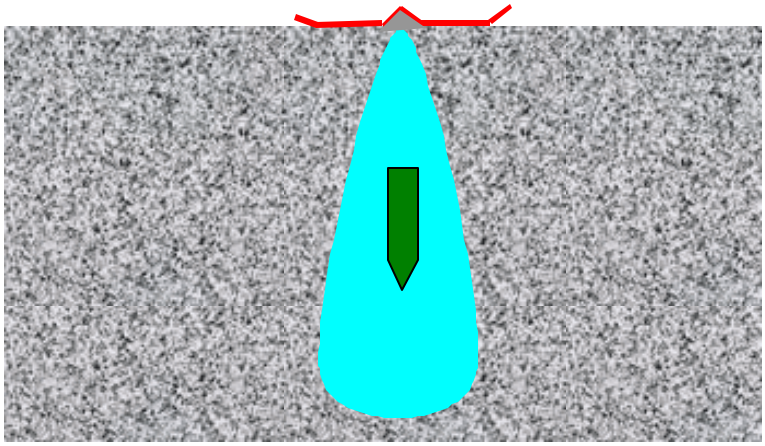

Figure 73 Current antenna configuration with downward radiation beam.

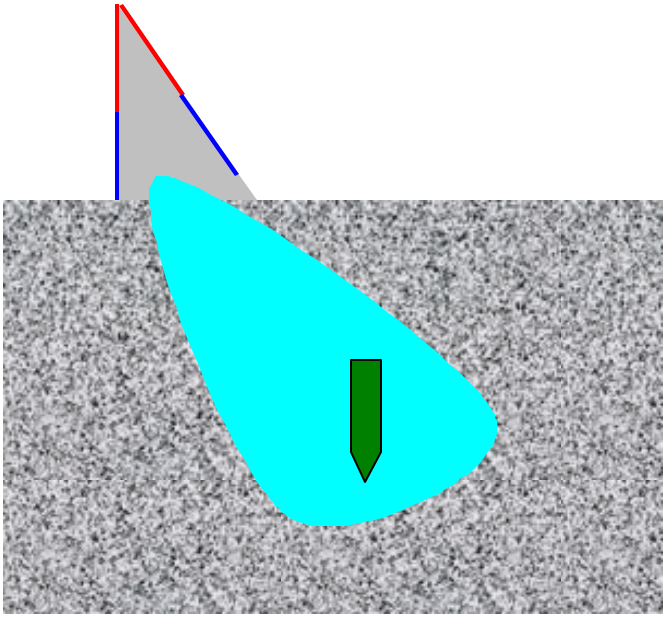

Figure 74 Possible new antenna configuration with tilted radiation beam by using tilted a new dielectric loaded horn antenna.

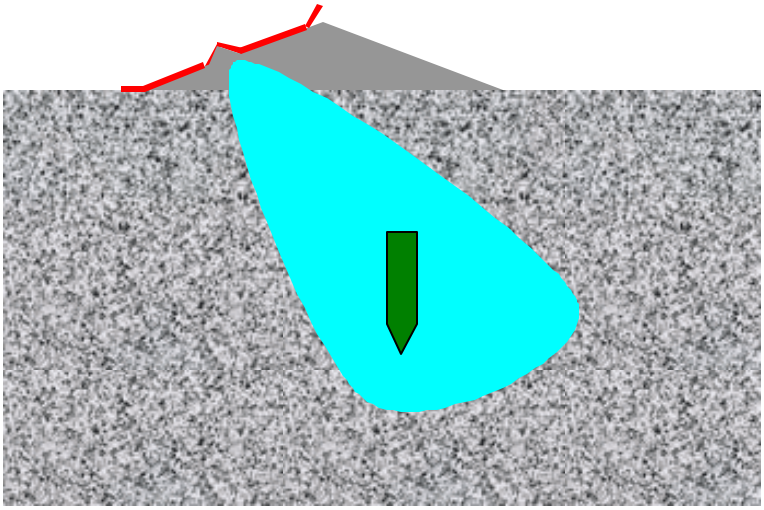

Figure 75 Existing antenna sitting on top of a dielectric wedge to provide a tilted radiation beam in the ground.

Another improvement could be made by utilizing multi-position data of the back-scattered response of a target. Also new processing techniques such as ramp response could help identify targets with a near vertical orientation.

The two major false alarm sources that limited the performance of the radar system include: (a) non-UXO objects that appear as linear shapes when observed directly above, e.g., vertically oriented square plate; (b) shallowly buried small objects that were offset from the antenna during the measurement due to position uncertainty. The first false alarm source could be reduced by using the additional side-looking antenna, i.e. an antenna with tilted beam, which will allow the incident wave to hit the target closer to broadside such that a larger back-scattered field is created. Recent study conducted at OSU/ESL has shown that the false alarms caused by the second source could be greatly reduced by examining the spatial variation behavior of the extracted features. This requires multiple position data with a finer sampling spacing. More details about this approach will be discussed in the Phase II Demonstration Plan. Another approach to reduce the false alarms caused by the offset is to increase the positioning accuracy as well as an additional antenna with a small footprint. A new dielectric-loaded horn antenna that has a smaller footprint (14" by 14") than the current HFB antenna (6' by 6') has been developed and shown in Figure 76. The additional antenna has a larger frequency bandwidth with a range of approximately 0.1-3.0 GHz. The smaller footprint will allow for more accurate positioning of the center of the antenna over the target, which will avoid the problem of a target lying under only one arm of the antenna. It will also has an improved detection capability for smaller shallow UXO's.

Figure 76 New Dielectric-Loaded Horn Antenna with Smaller Footprint

Currently there are three main goals to be addressed. The first is to confirm the assumptions made about the sources of false alarms and non-detections based on the comparison of processed results and the ground truth data. The second goal is to use the new antennas to demonstrate the reduction of false alarms and non-detections. The third goal is to find the sources of the remaining false alarms that are unclear. A list of tasks is presented below which will achieve these goals.

1. False alarm evaluation (OSU/ESL Backyard)

The assumptions about the sources of false alarms will be tested by recreating the situations in which the false alarms occurred. There will be an investigation of the false alarm source where there is a non-linear target buried underneath one arm of the antenna (i.e. offset situation), as discussed in Section 7.3.2 part A. This will be accomplished by burying a sphere in the sandbox and taking measurements with the HFB antenna with one arm over the target. Then the same sphere will be measured with the new small footprint antenna to demonstrate the improved discrimination.

The false alarm source attributed to non-linear objects with a linear edge, see Figure 65, will be investigated next. This source of false alarms was discussed in Section 7.3.2 part B. Tests will use a square metal plate with proportions so that when seen from above it appears to be a thin bar. The inclination angle of the plate will also be varied from 0 to 90 degrees. The plate will be measured with the HFB antenna and with the new side-looking antenna from offset positions. These measurements will be analyzed to demonstrate the improvement of the discrimination capability for this type of false alarm source.

Other false alarm sources such as a soda can, cluster of nails, a paint can, and orthogonal pipes will also be investigated.

2. Dropped UXO-like targets evaluation (OSU/ESL Backyard)

The assumptions about the sources of dropped UXO's will be tested by recreating the situations in which the dropped targets occur. There will be an investigation of the non-detection source where there is a linear target buried with an inclination angle greater than 45 degrees, as discussed in Section 7.3.1 part

C. This will be accomplished by burying an aluminum bar in the sandbox at inclination angles varying from 0 to 90 degrees and taking measurements with the HFB antenna. Then the same bar will be measured with the new side-looking antenna to determine whether there is any improvement.

3. Demonstration of new antennas (Tyndall ?)

The new antennas can be used to measure a small set of troublesome targets at the Tyndall site to demonstrate the improved detection rate and decreased false alarm rate.

4. Unknown false alarm sources (Tyndall)

The new antennas can be used to investigate the unknown false alarm sources. Some sites will be excavated to determine whether there are unknown multiple targets present.

8 References

[1] C-C. Chen, "Buried UXO Classification Using the Polarization and Resonance Signatures", *US UXO Forum, Atlanta, Georgia, May 1999*.

[2] C.-C. Chen and L. Peters Jr., "Buried Unexploded Ordnance Identification via Complex Natural Resonances", *IEEE Transactions on Antenna and Propagations*, Vol. 42, pp. 1645-1654, Nov. 1997.

[3] C.E. Baum, "The SEM Representation of Scattering From Perfectly Conducting Targets in Simple Lossy Media," *Phillips Laboratory Interaction Note 492*, Apr. 1993.

[4] C.-C. Chen, "A New Ground Penetrating Radar Antenna Design -- The Horn-Fed Bowtie (HFB)", *Proceeding of Antenna Measurement Techniques Association* (AMTA) Symposium, October 1997, pp.67.

[5] K. O'Neill, "Discrimination of UXO in Soil Using Broadband Polarimetric GPR Backscatter," *IEEE Trans. Geosci. Rem. Sens.*, in press, 2000.

[6] J.D. Young, "Radar Imaging from Ramp Response Signatures", *IEEE Transactions on Antenna and Propagations*, Vol. 24, pp. 1645-1654, May 1976.

[7] S. Nag and L. Peters Jr., "Radar Images of Penetrable Targets Generated from Ramp Profile Functions", *IEEE Trans. Geosci. Rem. Sens.*, accepted for publication.

Appendix A: Output Data Format

A.1 Raw Data File

The data for system-calibrated frequency-domain radar data was stored in ASCII-format files called "aydddaa.cdt", where "a" is from A to Z for file ordering. The letter "y" indicates the last digit of the year. For example, "0" means the year of 2000. The three-digit number, "ddd" , indicates the Julian date when the data was stored. Each file contains a two-dimensional data taken at one target location. The first frequency (10 MHz) data was stored in the first row, the second frequency (12 MHz) data was stored in the second row,…, etc. Each column stores the frequency, co-polarization and cross-polarization data in a format shown below. For each radar file, '*.cdt", there is an associated comment file called "*.txt" to store the system information, comments and processed results. All of these files will be available in a CD-ROM after this submission of this report.

Frequency (MHz)	$Re(S_{11})$	$Im(S_{11})$	$Re(S_{21})$	$Im(S_{21})$	$Re(S_{22})$	$Im(S_{22})$

"Re()" and "Im()" indicate the real and imaginary parts, respectively (combined, these provide the amplitude and phase).

A.2 Processed Data File: "tarproc#.dat"

The processed data were recorded into a text file in the format of the following example.

X	Y	P	F	EL N	DE	ET L (m)	ET O (degree)	DE P (m)
3	6	1		0.8	0.7	0.6	50	0.3
1	2	2		0.2	0.1	0.3	75	0.2
:	:	:		:	:	:	:	:

In this example, the first row indicates the target location is at the Lower Pad (P=1), 3rd column from West boundary and 6th row from South boundary. The estimated linearity factor (ELF), angle density, target length (ETL), target orientation (ETO) and target depth (DEP) are also included. The target in the second row is located at Upper Pad (P=2). When multiple-position data are available for a target, # =1 indicates that the largest-ELF-value position was chosen and #=2 indicates that the largest-(ELF+DEN)-value position was chosen to base the results on.

A.3 Level-One UXO Classification MATLAB Routine: "uxosel1.m"

This routine first reads in the processed data from the file – "tarproc.dat". Then the user will be asked to enter the desired threshold level for a chosen parameter, which will determine the UXO-like/non-UXO decision. Currently, this parameter could be ELF or ELF&DEN.

Choosing ELF as the parameter means that *only* the ELF value will be used as the decision criterion (Only those targets that have ELF values greater then the user-entered threshold are selected as UXO-like objects). It is noted that the ELF value ranges from 0 to 1. The larger the ELF value, the better the linearity of the target geometry. UXO-like objects may also be selected based on the combination of ELF and DEN. A straight line defined by the user-entered threshold (from 0 to 2), is used to separate UXO-like objects from false alarms. This is demonstrated in Figure 15, discussed below, where dots represent the estimated ELF and DEN combination for each target. Ideally, UXO-like targets should cluster near the upper-right corner where both ELF and DEN are close to one. On the other hand, false alarms should cluster near the lower-left corner where low ELF and low DEN are observed. The threshold entered by the user defines the distance between the origin and the intersection points on the axes; equivalently, it determines how far the dashed decision line is shifted, without change in slope, between the lower left corner and upper right corner. If the line is located very close to the upper right corner, then points corresponding to essentially all targets would lie below the line and be classified as non-UXO. If the line were shifted to a position very close to the lower left corner (origin), then essentially all target points would lie above it and be considered to correspond to UXO-like objects.

The information for selected UXO-like objects is stored in a text file called "**uxolist1.dat**" in the same format as the "**tarproc#.dat**" file discussed in the previous section. This file can then be used in the Level Two UXO classification.

A.4 Level One UXO Classification MATLAB Routine: "uxosel2.m"

Among the UXO-like objects selected based on geometrical linearity during the Level One UXO selection process, the user can specify specific criteria for choosing a class of UXO. For example one might know that the site was used as a practice range for a certain class of ordnance with a standard length. Or ordnance at a shallow depth may have particular cleanup priority. Thus the additional criteria type can be either length (ETL) or depth (DEP). The user will be prompted to choose the criteria type, enter the desired value and error bound. All UXO-like objects that meet this second criteria will be selected and stored in a text file called "**uxolist2.dat**" in the same format as the "**tarproc#.dat**" file.

A.5 Comment Text File

The comment text files contain information about measurement conditions (i.e. position, direction, etc.) and any comments the user entered during the measurements. Comment files with an extra letter on the end of the names are the processed comment files. These files contain all the information about measurement, as before, but also contain information about the processing of the file. For example, the comment file a0014gbu.txt is printed below:

14-Jan-2000/Target #: 101/No Target File: a0014fz.cdt/Antenna Orientation: 194/Antenna Position: xoffset: 0.0000/yoffset: 10.0000/Relative Permittivity: 4/User Comments: UE3@@@********/$ETO/3/ -1.0000/ 179.0000/ 0.7471/ELF/2/ 0.7726/ 0.0213/CNR/2/ 0.0913/ 0.2046/ETL/1/ 0.3666/SNR/1/**

49.7574/TCP/2/ 12.3932/ 0.5861/timerange1/ 17.3146/timerange2/ 24.4088/timepeakmax/ 12.3932/waveformselection/ 3.0000/FELF/ 0.8443/$$

This is a typical comment file after processing. The letter 'u' on the end of the file name denotes that a user specified center frequency band-pass filter was used before the processing of the file. A letter 'f' on the end would denote that the full 800 MHz bandwidth was used in processing that file, while a letter 'l' and 'h' denotes that a low-pass and a high-pass filter was used, respectively.

One can see that all of the processed parameters (i.e. ETO, ETL, ELF, etc.) for this target are store in the file. There are also four other parameters (timerange1, timerange2, timepeakmax, and waveformselection) stored in the file which provide information about the late-time region selected to do processing on. These parameters allow for the automatic re-processing of the data, if necessary.

Appendix B: Tyndall AFB UXO Site Target Information

A demonstration site was setup in Tyndall AFB, FL for UXO characterization test using GPR signatures. This site contains two 100-cell grids designated as "Upper Pad" and "Lower Pad". The upper pad has a maximum depth of two meters. The lower pad has a maximum depth of one meter. Due to the orientation requirement, large target items are buried in upper pad. Smaller items were buried at both pads. In general, the average depth of the targets is greater in the upper pad than that in the lower pad.

Each grid cell is 5mx5m. Each cell contains at most one target located at a known location (not necessarily centered). The Lower Pad has a depth of approximately 0.6 meter above water table. The Upper Pad has a depth of approximately 1.6 meter above water table. The soil type of both grids is white sand whose relative permittivity and conductivity are approximately 3~5 and 0.001~0.005 S/m. All targets buried are metallic and were buried at various depths and orientations. A detail list of these targets is provided in Table 8. Other than several calibration targets such as conducting spheres, pipes and rebars, information for each target was unknown to the measurement team. These targets were buried in cells indicated by red dots shown in Figure 77 and Figure 78.

Table 8 Table of Targets Buried at Tyndall Site

No.	Type	Depth (m)	ϕ	θ	Length (m)	Max Dia. (m)	UXO-Like
1	105mm Inert	0.20	0	0	0.35	0.105	Y
2	105mm Inert	0.20	0	45	0.35	0.105	Y
3	105mm Inert	0.20	0	90	0.35	0.105	Y
4	105mm Inert	0.40	0	0	0.35	0.105	Y
5	105mm Inert	0.24	0	30	0.35	0.105	Y
6	105mm Inert	0.40	45	0	0.35	0.105	Y
7	105mm Inert Heat	0.34	45	60	0.35	0.105	Y
8	105mm Inert Heat	0.43	0	0	0.35	0.105	Y
9	105mm Inert Sabot	0.60	0	30	0.64	0.105	Y
10	105mm Inert Sabot	0.86	0	30	0.64	0.105	Y
11	105mm Inert	0.62	0	30	0.35	0.105	Y
12	105mm Inert	0.60	0	30	0.35	0.105	Y
13	105mm Inert	0.50	0	30	0.35	0.105	Y
14	105mm Inert	0.55	0	30	0.35	0.105	Y
15	105mm Inert	0.73	45	60	0.35	0.105	Y
16	105mm Inert	0.62	90	45	0.35	0.105	Y
17	105mm Inert	0.68	0	0	0.35	0.105	Y
18	105mm Inert Heat	0.57	45	0	0.35	0.105	Y
19	105mm Inert Heat	0.80	45	90	0.35	0.105	Y
20	105mm Inert Sabot	0.81	0	0	0.64	0.105	Y
21	105mm Inert Sabot	0.68	45	45	0.64	0.105	Y
22	60mm Mortar	0.70	0	0	0.23	0.060	Y
23	60mm Mortar	0.75	30	45	0.23	0.060	Y
24	60mm Mortar	0.54	45	90	0.23	0.060	Y
25	60mm Mortar	0.40	30	0	0.23	0.060	Y
26	60mm Mortar	0.33	0	45	0.23	0.060	Y
27	20mm Projectile	0.63	0	0	0.15	0.020	Y
28	MK82 500lb	1.00	0	90	1.20	0.350	Y
29	MK82 500lb	1.40	35	0	1.20	0.350	Y
30	75mm hep Projectile	0.50	0	0	0.30	0.075	Y
31	90mm Projectile	0.11	0	0	0.30	0.090	Y
32	4.2" Mortar	0.30	45	45	0.11	0.106	Y
33	50 mm Russian Mortar	0.23	0	0	0.27	0.050	Y

34	3 “ AA Projectile	0.21	0	0	0.30	0.076	Y
35	BDU33 (Tail only)	0.50	0	0	0.40	0.106	Y
36	BDU33 (Bent Tail)	0.36	0	0	0.60	0.106	Y
37	BDU33 (Bent Tail)	0.40	0	0	0.60	0.106	Y
38	BDU33 (No Tail)	0.40	45	45	0.25	0.106	Y
39	BDU33	0.80	0	60	0.60	0.106	Y
40	BDU33	0.58	45	0	0.60	0.106	Y
41	BDU33	0.42	30	30	0.60	0.106	Y
42	BDU33	0.70	90	0	0.60	0.106	Y
43	155mm	1.40	60	30	0.86	0.155	Y
44	RR Tie	0.92	0	45	0.86	0.155	Y
45	55gal Drum	1.85	0	0	0.91	0.610	N
46	55gal Drum	1.46	19.5	45	0.91	0.610	N
47	2000lb	1.40	30	30	2.70		Y
48	8" Shell	0.90	0	15	1.00	0.203	Y
49	8" Shell	0.80	60	30	1.00	0.203	Y
50	8" Shell	1.43	24.8	30	1.00	0.203	Y
51	81mm Mortar	0.80	15	0	0.50	0.081	Y
52	81mm Mortar	1.00	0	30	0.50	0.081	Y
53	Fragment	0.06	0	0	0.05	0.006	N
54	Fragment	0.11	0	0	0.05	0.006	N
55	Fragment	0.06	45	0	0.05	0.006	N
56	Fragment	0.10	90	0	0.05	0.006	N
57	Fragment	0.33	0	0	0.05	0.006	N
58	Fragment	0.30	45	0	0.05	0.006	N
59	Fragment	0.33	90	0	0.05	0.006	N
60	Fragment	0.17	0	0	0.05	0.006	N
61	Fragment	0.30	45	0	0.05	0.006	N
62	Fragment	0.30	90	0	0.05	0.006	N
63	Alum. Barb Wire	0.10	0	0	0.40		N
64	Alum. Barb Wire	0.12	0	0	0.40		N
65	Alum. Barb Wire	0.43	0	0	0.40		N
66	Alum. Barb Wire	0.40	0	0	0.40		N
67	Alum. Barb Wire	0.50	0	0	0.40		N
68	Steel Plate	0.17	0	0	0.30	0.00635	N
69	Steel Plate	0.30	45	0	0.30	0.0127	N
70	Steel Plate	0.32	0	0	0.30	0.00635	N
71	Steel Plate	0.58	45	0	0.30	0.0127	N
72	Steel Plate	0.51	0	0	0.30	0.00635	N
73	Steel Plate	0.23	45	0	0.30	0.0127	N
74	Cal. Metal Pipe*	0.30	0	0	0.30	0.0254	Y
75	Cal. Metal Pipe*	1.10	0	0	0.60	0.0254	Y
76	Cal. Metal Pipe*	1.50	0	0	0.90	0.0254	Y
77	Cal. Metal Pipe*	0.12	0	0	0.30	0.0254	Y
78	Cal. Metal Pipe*	0.26	0	0	0.60	0.0254	Y
79	Cal. Metal Pipe*	0.43	0	0	0.90	0.0254	Y
80	Clusters of nails	0.10	0	0	0.08	0.1523	N
81	Clusters of nails	0.57	0	0	0.08	0.1522	N
82	55 Gal Lid	0.20	0	0	0.00	0.6399	N
83	55 Gal Lid	0.40	0	0	0.00	0.6399	N
84	55 Gal Lid	0.70	90	0	0.00	0.6399	N
85	Pipes Diverge	0.20	0	0	0.91	0.0762	Y
86	Pipes Diverge	0.34	0	0	0.50	0.051	Y
87	Pipes Diverge	0.45	0	0	0.64	0.0254	Y
88	Pipes Diverge	0.55	0	0	0.64	0.019	Y
89	Pipes Ortho	0.44	0	0	1.82	0.102, 0.089	Y
90	Pipes Ortho	0.46	0	0	0.00		Y
91	Rebar 90° Arc Mid	0.53	0	0	0.30	0.019	N
92	Rebar 90° Arc End	0.40	0	0	1.22	0.019	N
93	Pipes Ortho Attac	0.65	0	0	0.00		N
94	Pipes Ortho Attac	1.00	0	0	0.00		N
95	Paint Can (Open)	0.12	45	45	0.00		N
96	Paint Can (Top On)	0.45	0	0	0.00		N
97	Metal Box	0.70	0	0	0.43	0.13	Y

98	Metal Box	0.99	0	0	0.43	0.13	Y
99	Rebar–strt + bent	0.58	0	0	0.30		N
100	Rebar 90° Mid Arc	1.60	0	0	0.30	0.019	N
101	RR Tie	1.66	0	290	1.00	0.100	Y
102	160mm Mortar	1.20	60	270	1.09		Y
103	Frag (Exploded)	0.21	15	260	0.91		Y
104	Tire Rim	0.70	0	0	0.00	0.330	N
105	Base Plate (Fuse)	0.48	30	90	0.00	0.300	N
106	Tine (Steel Plate)	0.79	90	0	0.48	0.019	N
107	5” Gun Round	1.40	80	0	0.91	0.127	Y
108	Tire Rim	0.66	90	0	0.00	0.330	N
109	Angle Iron	0.92	0	0	0.30	0.00635	Y
110	Angle Iron	0.38	0	90	0.30	0.00635	Y
111	Soda Can	0.40	0	0	0.13	0.0762	N
112	Soda Can	0.41	0	90	0.13	0.0762	N
113	Soda Can Crushed	0.50	0	0	0.00		N
114	Soda Can Stacked	0.20	0	90	0.13	0.0762	N
115	Pipe Att End (90°)	0.77	100	30	0.46	0.019	N
116	Pipe Att End (90°)	0.74	100	150	0.46	0.019	N
117	Metal Box Open	0.65	20	60	0.46	0.00635	Y
118	Metal Box Closed	1.00	0	0	0.40	0.400	N
119	Exploded Scrap (2)	0.52	0	0	0.25	0.00318	N
120	Bomb Parts	0.20	0	0	0.46	0.00635	N
121	Panel Large	0.78	0	45	0.60	0.00635	N
122	Scrap & Wire	0.99	45	60	1.00		N
123	Exploded scrap	0.40	90	30	0.00		N
124	Panel Medium	0.30	0	90	0.46	0.00635	N
125	Looped Pipe	0.50	120	45	0.41	0.019	N
126	Exploded Tube	0.50	30	60	0.51	0.0762	Y
127	Mine AT	0.06	0	0		0.33	N
128	Steel Plate Stacked	0.30	0	0	0.30	0.00634	N
129	60mm Mortar	0.10	0	0	0.23	0.060	Y
130	Angle Iron (2)	0.15	0	0	0.30	0.00635	Y
131	Scrap Crushed	0.21	0	0	0.48	0.00635	N
132	Rim	0.30	45	0	0.00	0.330	N
133	Plate & 105mm Sb	0.20	30	0	0.35	0.00635 0.105	Y
134	Plate	0.34	90	0	0.30	0.00635	N
135	Rebar	1.00	90	0	0.91	0.019	Y
136	Paint Can Open D	0.33	45	0	0.00		N
137	Rebar 90° Arc Mid	0.16	30	90	0.30	0.019	N
138	BDU Bar Fin	0.12	45	45	3.60	0.0508	Y
139	Crushed Box	0.33	40	100	0.46	0.150	Y
140	Angle Iron (2)	0.33	10	0	0.30	0.00635	Y
141	Mine AT	0.14	0	0		0.33	N
142	60mm Mortar	0.36	45	45	0.23	0.060	Y
143	Soda Can	0.10	45	45	0.13	0.0762	N
144	60mm Mortar	0.30	0	0	0.23	0.060	Y
145	60mm Mortar	0.30	30	45	0.23	0.060	Y
146	60mm Mortar	0.33	0	10	0.23	0.060	Y
147	Scrap Tin Folded	0.16	90	0	0.30	0.100	N
148	Sphere	0.50	0	0	0.15		N
149	Sphere	0.30	0	0	0.15		N
150	UXO	0.50	45	0	0.60		Y
151	Pipe	0.50	45	0	0.60		Y
152	Rebar	0.50	90	0	0.50		Y
153	Rebar	0.50	0	150	1.02		Y

ϕ: elevation angle, 90 is pointing straight down

θ: azimuth angle from north


GROUND SURFACE
DEPTH
ϕ
NORTH
θ
EAST
LOOKING DOWN INTO THE GROUND

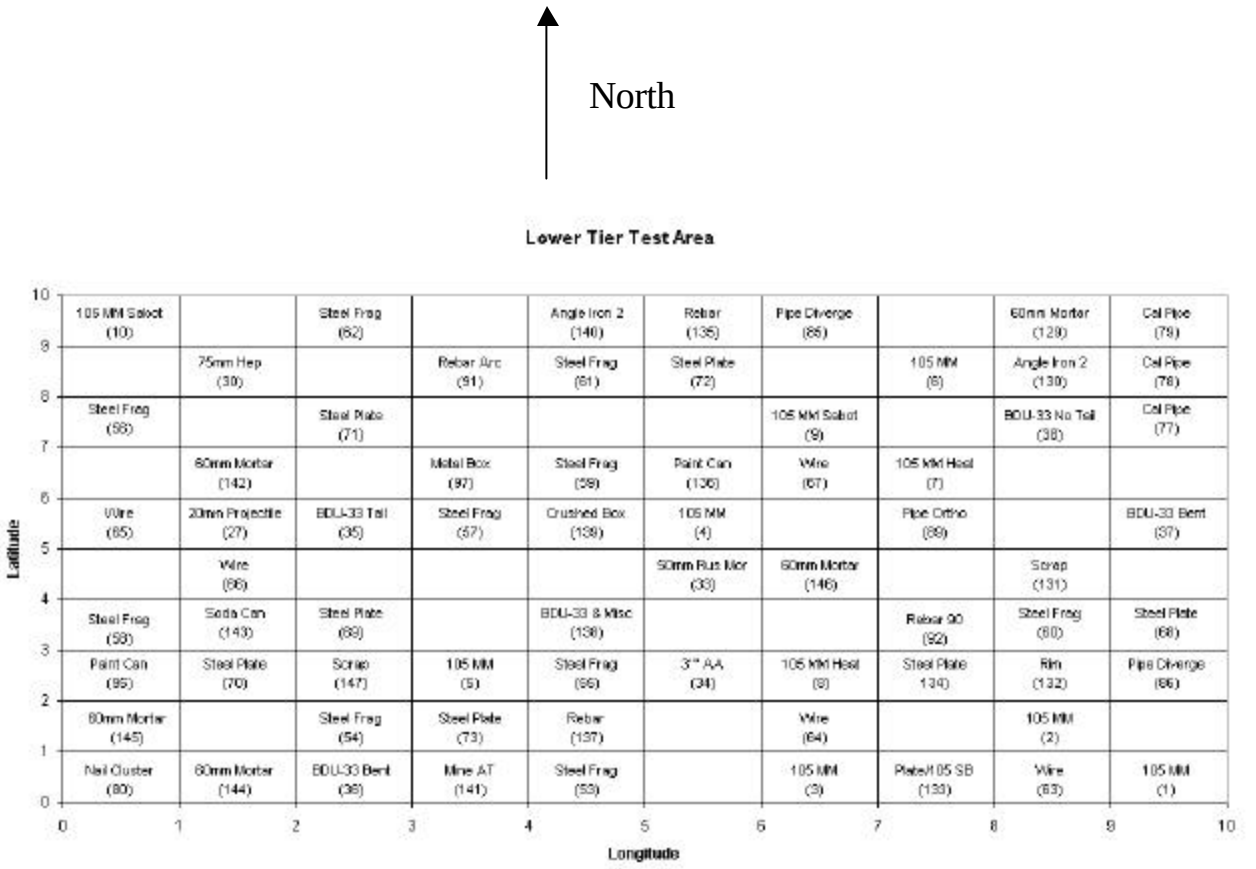

Figure 77 Ground Truth for Lower Pad

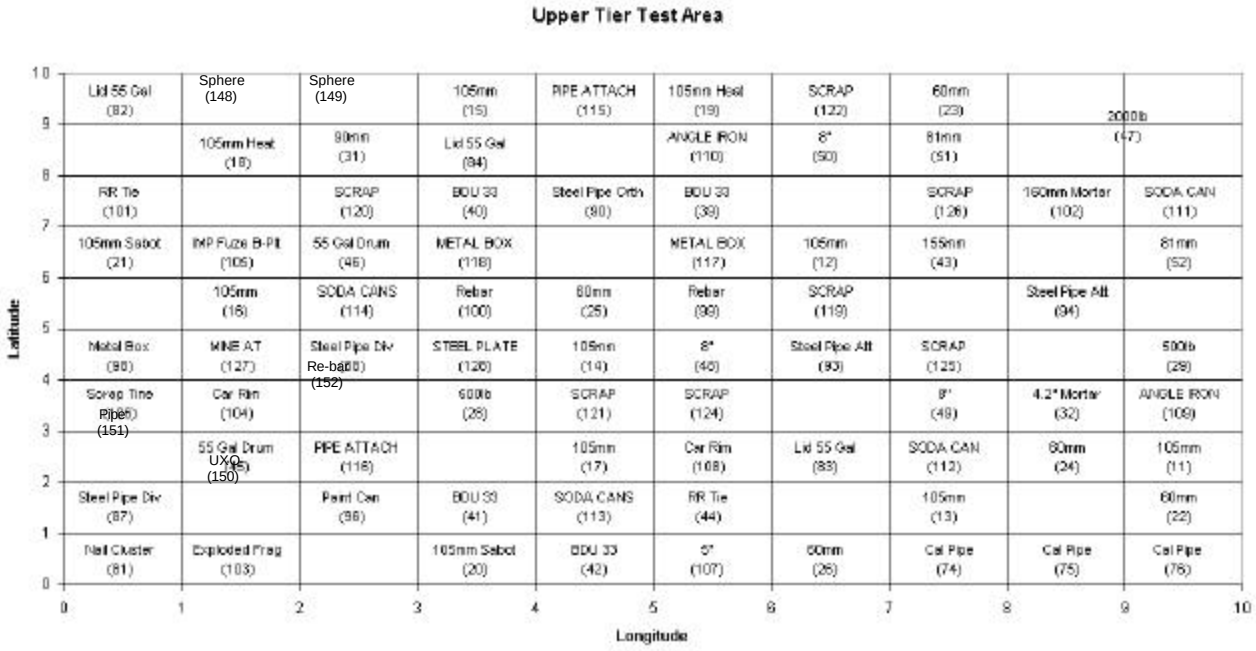

Figure 78 Ground Truth for Upper Pad

Appendix C: Tyndall Site Soil Characteristics

C.1 Electrical Property

The soil electrical property – permittivity and conductivity at 40 MHz and 60 MHz were measured at different depths using the OSU/ESL soil probe as shown in Figure 80 and 17. The results are shown from Figure 82 to Figure 91. In the Lower Pad the water table was observed at approximately 25-inch depth. This would be 61 inches in the Upper Pad.

Figure 79 Subsurface inhomogeneity

Figure 80 OSU/ESL soil probe for permittivity and conductivity measurement at 40 MHz and 60 MHz.

Figure 81 OSU/ESL soil probe inserted the ground to measure soil electrical property at different depths.

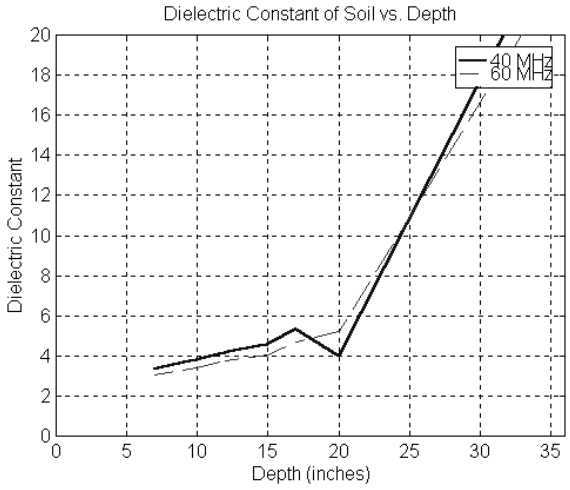

Figure 82 Measured relative soil permittivity on 1/11/2000 at lower pad.

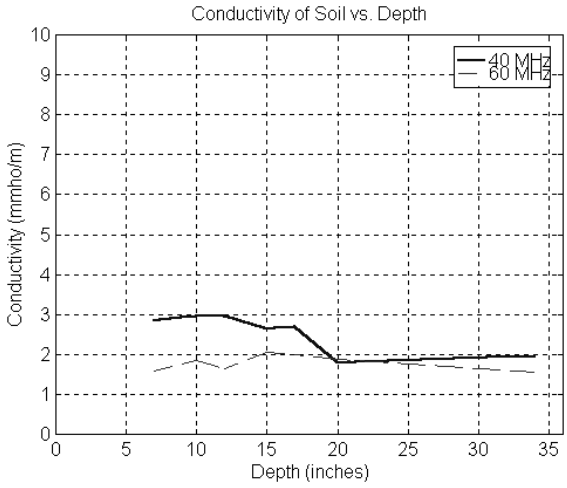

Figure 83 Measured relative soil conductivity on 1/11/2000 at lower pad.

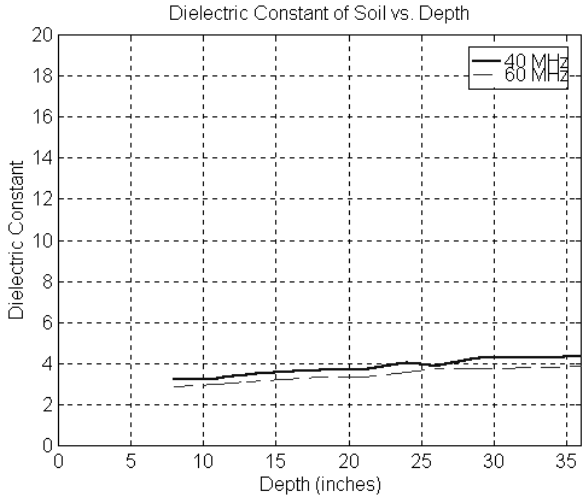

Figure 84 Measured relative soil permittivity on 1/14/2000 at the Upper Pad.

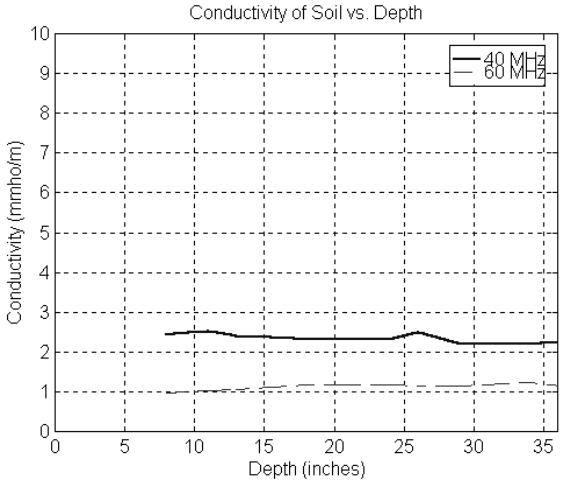

Figure 85 Measured relative soil conductivity on 1/14/2000 at the Upper Pad.

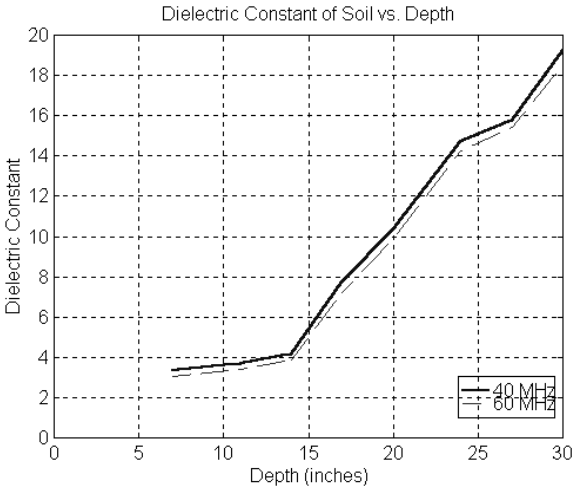

Figure 86 Measured relative soil permittivity on 1/20/2000 at Lower Pad.

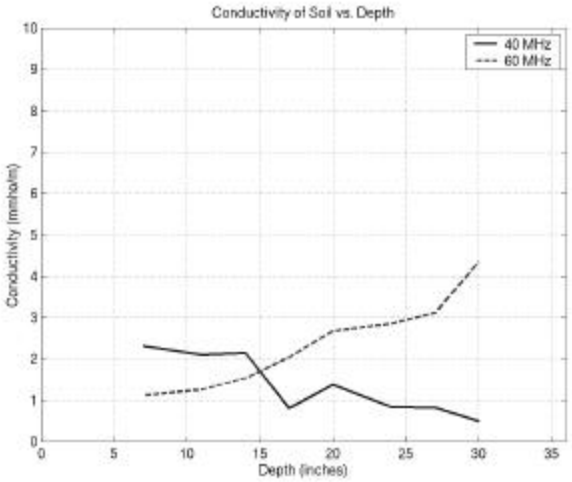

Figure 87 Measured relative soil conductivity on 1/20/2000 at the Lower Pad.

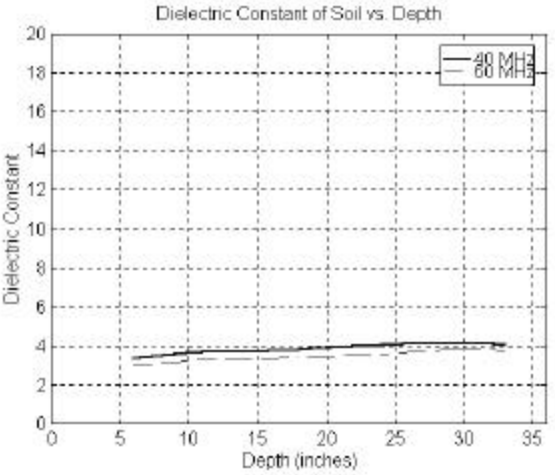

Figure 88 Measured relative soil permittivity on 1/20/2000 at the Upper Pad.

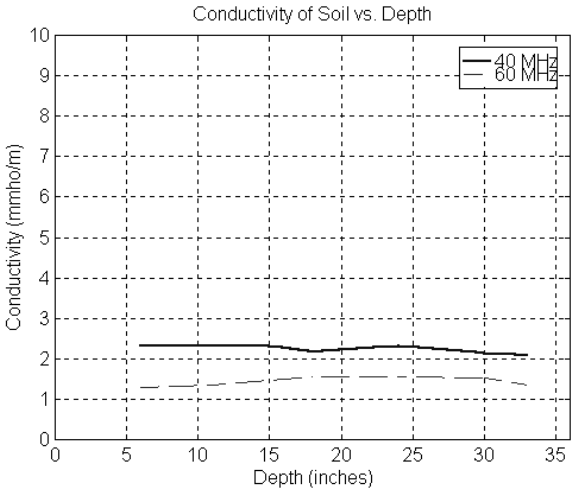

Figure 89 Measured relative soil conductivity on 1/20/2000 at the Upper Pad.

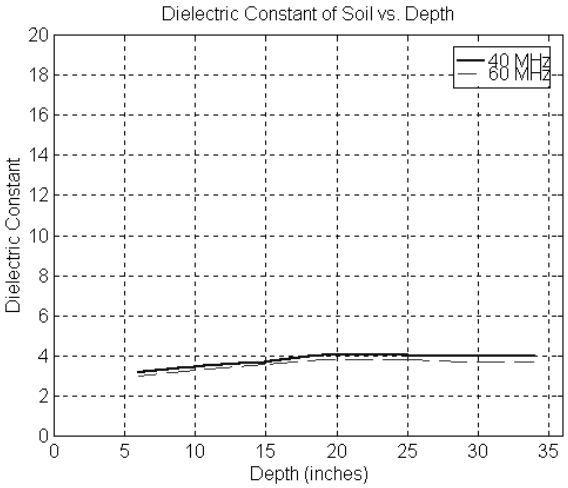

Figure 90 Measured relative soil permittivity on 1/21/2000 at the Upper Pad.

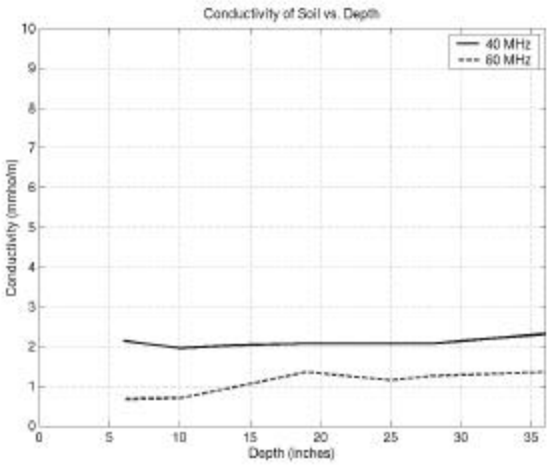

Figure 91 Measured relative soil conductivity on 1/21/2000 at the Upper Pad.

C.2 Moisture Content (CRREL)

Soil samples were collected at various depths, location on different days during the 01/10/2000 ~ 01/20/2000 period of radar measurement at Tyndall AFB UXO Site . The moisture content of each sample was then determined at CRREL by measuring the weight difference before and after the drying process. The results are shown in Table 9.

Table 9 Moisture contents of soil samples collected at the Tyndall AFB UXO site.

Date	Location	Time	Sample Depth (in)	Wet Wt. (g)	Dry Wt. (g)	Water (g)	Moisture Content (%)	Depth (in)	Moisture Content (%)
1/21/00	Up Pad Ctr	1414	0-6	177.43	173.23	4.20	2.42%	3	2.4
			6-10	119.38	116.30	3.08	2.65%	8	2.6
			10-14	147.08	143.08	4.00	2.80%	12	2.8
			14-19	178.35	172.42	5.93	3.44%	21.5	3.4
			19-25	194.34	187.40	6.94	3.70%	22	3.7
			25-28	183.09	176.21	6.88	3.90%	26.5	3.9
			28-36	273.65	263.70	9.95	3.77%	32	3.8
1/19/00	L Pad Ctr	730	0-6	159.17	155.83	3.34	2.14%	3	2.1
			6-11	232.94	226.06	6.88	3.04%	8.5	3.0
			11-14	152.54	146.56	5.98	4.08%	12.5	4.1
			14-18	252.26	235.66	16.60	7.04%	16	7.0
			18-21	265.84	243.24	22.60	9.29%	19.5	9.3
			21-24	416.79	343.52	73.27	21.33%	22.5	21.3
			24-29	278.78	229.52	49.26	21.46%	26.5	21.5
			29-32	402.15	312.37	89.78	28.74%	30.5	28.7
1/19/00	Up Pad Ctr	1513	0-6	152.89	148.62	4.27	2.87%	3	2.9
			6-19	182.65	176.87	5.78	3.27%	12.5	3.3
			19-23	196.19	189.08	7.11	3.76%	21	3.8
			23-28	190.18	182.95	7.23	3.95%	25.5	4.0
			28-36	223.46	214.30	9.16	4.27%	32	4.3
1/11/00	L Pad		Dug Hole	97.54	89.63	7.91	8.83%		
			0-7	90.65	88.33	2.32	2.63%	3.5	2.6

			7-10	96.23	92.55	3.68	3.98%	8.5	4.0
			10-12	75.42	72.44	2.98	4.11%	11	4.1
			12	60.88	58.41	2.47	4.23%	12	4.2
			12-15	76.22	72.76	3.46	4.76%	13.5	4.8
			15-17	97.65	91.35	6.30	6.90%	16	6.9
			17-18	102.26	96.45	5.81	6.02%	17.5	6.0
			18-20	267.74	254.84	12.90	5.06%	19	5.1
1/12/00	L Pad Ctr	1530	0-6	66.64	65.11	1.53	2.35%	3	2.3
			6-9	61.64	60.15	1.49	2.48%	7.5	2.5
			9-12	91.62	88.06	3.56	4.04%	10.5	4.0
			12-15	62.86	59.98	2.88	4.80%	13.5	4.8
			15-18	94.39	87.60	6.79	7.75%	16.5	7.8
			18-21	292.64	253.37	39.27	15.50%	19.5	15.5
			21-24	150.34	123.32	27.02	21.91%	22.5	21.9
			24-26	148.85	120.93	27.92	23.09%	25	23.1
			26-27	258.32	212.74	45.58	21.43%	26.5	21.4
1/14/00	Up Pad Ctr	730	6	101.69	98.79	2.90	2.94%	3	2.9
			9-12	115.63	112.06	3.57	3.19%	10.5	3.2
			12-14	150.95	145.63	5.32	3.65%	13	3.7
			14-17	139.57	135.09	4.48	3.32%	15.5	3.3
			17-21	206.03	197.97	8.06	4.07%	19	4.1
			21-24	203.42	196.35	7.07	3.60%	22.5	3.6
			24-27	187.68	181.10	6.58	3.63%	25.5	3.6
			27-30	194.64	187.35	7.29	3.89%	28.5	3.9
1/18/00	Up Pad Ctr	1640	0-6	176.97	173.35	3.62	2.09%	3	2.1
			6-12	171.13	167.32	3.81	2.28%	9	2.3
			12-16	161.05	156.18	4.87	3.12%	14	3.1
			16-21	218.72	210.83	7.89	3.74%	18.5	3.7
			21-26	276.05	265.80	10.25	3.86%	23.5	3.9
			26-31	158.25	152.25	6.00	3.94%	28.5	3.9